THE UNIVERSITY OF CHICAGO

ENGINEERING LYMPH NODE-TARGETING INVERSE VACCINES FOR THE PREVENTION AND TREATMENT OF AUTOIMMUNITY AND FOOD ALLERGIES

A DISSERTATION SUBMITTED TO

THE FACULTY OF THE PRITZKER SCHOOL OF MOLECULAR ENGINEERING

IN CANDIDACY FOR THE DEGREE OF

DOCTOR OF PHILOSOPHY

BY

CHITAVI DEVI MAULLOO

CHICAGO, ILLINOIS

JUNE 2021

TABLE OF CONTENTS

List of Abbreviations (in alphabetical order)

β2m: Beta-2 microglobulin

BEC: Blood Endothelial Cell

CTLA-4 : Cytotoxic T Lymphocyte Antigen 4

DC: Dendritic Cell

FDC: Follicular Dendritic Cell

FRC: Fibroblast Reticular Cell

GalNAc: N-Acetyl Galactosamine (Gal)

GluNAc: N-Acetyl Glucosamine (GluNAc)

LAG-3: Lymphocyte- Activating Gene 3

LN-LEC: Lymph Node Lymphatic Endothelial Cell

MAC: Macrophage

Man: Mannose

PD-1/ PD-L1: Programmed Death 1/ Programmed Death Ligand 1

SCS: Subcapsular Sinus

TCR: T Cell Receptor

Tim-3: T cell immunoglobulin and mucin domain-containing protein 3

WT: Wild-type

List of Figures

List of Tables

ACKNOWLEDGEMENTS

I dedicate this dissertation to my parents, Bharatee and Hoolash Maulloo, who have always believed in me and encouraged me to pursue my passion even though this meant moving 9000 miles away from home, to my aunts, Amrita and Sheela Maulloo, who provided unconditional support and advice throughout the years, shaping me into the strong confident woman I grew into, and to the remainder of my family and friends who have helped me stay sane in various ways throughout this roller-coaster of a journey. I am grateful to my advisors, Jeff Hubbell and Melody Swartz, for giving me the opportunity to further their science and explore my interests in science and commercialization, and to my lab members for valuable help, advice, mentoring and friendships. I especially thank my fellow co-authors, especially Scott Wilson, Shijie Cao and Elyse Watkins, without whom the published work would not have been possible. I am grateful to Kevin Miao for outstanding help with graphic design, large data analysis and general advice. I thank the University of Chicago facility personnel in flow cytometry (David LeClerc, Mike Olson), imaging, microscopy and animal care (Ani Solanki) for their dedication to training, instrument support and relieving much work burden over the years. I thank the Chicago latin dancing scene for creating my most cherished friendships in graduate school. Last, but not the least, I thank my committee for their patience and helpful feedback.

Chapter 1

Lymph node-targeted synthetically glycosylated antigen leads to antigen-specific immunological tolerance.

Abstract

Inverse vaccines that tolerogenically target antigens to antigen-presenting cells (APCs) offer promise in prevention of immunity to allergens and protein drugs and treatment of autoimmunity. We have previously shown that targeting hepatic APCs through intravenous injection of synthetically glycosylated antigen leads to effective induction of antigen-specific immunological tolerance. Here, we demonstrate that targeting these glycoconjugates to lymph node (LN) APCs under homeostatic conditions leads to local and increased accumulation in the LNs compared to unmodified antigen and induces a tolerogenic state both locally and systemically. Subcutaneous administration directs the polymeric glycoconjugate to the draining LN, where the glycoconjugated antigen generates robust antigen-specific $CD4^+$ and $CD8^+$ T cell tolerance and hypo-responsiveness to antigenic challenge via a number of mechanisms, including clonal deletion, anergy of activated T cells, and expansion of regulatory T cells. Lag-3 up-regulation on $CD4^+$ and $CD8^+$ T cells represents an essential mechanism of suppression. Additionally, presentation of antigen released from the glycoconjugate to naïve T cells is mediated mainly by LN-resident $CD8^+$ and $CD11b^+$ dendritic cells. Thus, here we demonstrate that antigen targeting via synthetic glycosylation to impart affinity for APC scavenger receptors generates tolerance when LN dendritic cells are the cellular target, not only when hepatic APCs are as in our previous work.

Keywords: inverse vaccine, subcutaneous, lymph node, synthetically glycosylated, antigen, glycoconjugate, tolerance, scavenger receptor, antigen-presenting cells.

Introduction

Current treatments for allergic and autoimmune diseases are non-curative and rely on broad nonspecific immunosuppression, risking a number off-target effects, complications, and opportunistic infections that limit the long-term use of these strategies (*1*–*3*). As the underlying mechanisms of immune suppression and the identities of the disease-causing autoantigens and allergens are being increasingly unraveled, antigen-specific therapies are being put through the clinical developmental pipeline to a greater extent (*4*–*7*). For instance, in the context of food allergy, the first peanut antigen-specific prescription oral immunotherapy was approved in early 2020, paving the way for more antigen-targeted therapies to also hit the market soon. Even though this is a revolutionary first step, more work needs to be done to improve the efficacy and safety profile of tolerance therapies, both in autoimmunity and allergy.

Several strategies to induce a more directed antigen-specific immune response are under investigation (*8*). When dealing with unmodified antigen alone, as most current therapies use, the route of administration can be used to modulate the response. For example, the subcutaneous route has been explored clinically for reasons such as ease of administration and higher patient compliance (*9*–*11*), and may be particularly desirable to treat allergic patients with considerable levels of antigen-specific circulating IgE antibodies (*12*). Another validated approach is to direct antigen to APCs for preferential uptake without activation and subsequent tolerogenic education of naïve T cells. A number of distinct strategies have been employed to skew the behavior of APCs

from inflammatory to tolerogenic (*13*), for example, by targeting antigen to these cell types through surface modifications of antigen-encapsulated particles (*14–16*).

Antigen glycosylation consists of one of these surface modifications that has been leveraged as an immune-modulatory tool in the context of both vaccination and tolerance (*17*). Since glycan binding to carbohydrate-binding receptors is a low-affinity event, multivalency of glycosylation has been shown to be beneficial in the optimal engagement of these receptors (*18*). The covalent attachment of carbohydrate structures from pathogens or cancer cells to immunogenic proteins has been explored to improve the efficacy of activating or tolerogenic vaccines (*19*). Moreover, antigens modified with glycosylation repeats have been used to target a number of lectin receptors such as the asialoglycoprotein receptor (*20*), DC-SIGN (*21*), MARCO receptor (*22*), and LSECtin (*23*).

We have shown in prior work that antigens decorated with synthetic glycopolymers of N-acetyl glucosamine (p(GluNAc)) or N-acetyl galactosamine, after intravenous (i.v.) injection, promiscuously target various subsets of hepatic APCs, resulting in antigen-specific tolerance (*24*, *25*). Here, we extend this concept to demonstrate that a peripheral subcutaneous (s.c.) method of administering p(GluNAc)-conjugated antigen to target resident APCs in the draining lymph nodes (dLNs) represents a viable strategy to induce antigen-specific tolerance. We show that antigen-p(GluNAc) is retained to a higher extent in the dLNs, improving uptake by APCs and promoting antigen presentation so as to generate a pool of long-lived anergic antigen-specific $CD4^+$ and $CD8^+$ T cells in addition to regulatory T (Treg) cells that attenuate effector T cell responses and maintain tolerance in the face of an inflammatory antigenic challenge.

We also explore differences in immunological mechanisms between tolerization via the LN, accessed via s.c. administration, and liver, via i.v. administration, with synthetically glycosylated antigen. Thus, we present a subcutaneous biocompatible inverse vaccine platform that is promising for blunting the response to antigens, such as primary autoantigens or allergens, paving the way for a new class of antigen-specific therapies, with implications in a clinically relevant route of administration that offers more advantages over an i.v. mode in specific contexts, such as in food allergy treatment.

Results

Antigen-p(GluNAc) conjugate injected subcutaneously accumulates in the draining lymph nodes where it targets various subsets of antigen presenting cells

Our previous work describes the synthesis of antigen-glycopolymer conjugates composed of synthetic polymers formulated from N-acetylglucosamine-decorated monomers conjugated to protein or peptide antigens via a self-immolative linker that cleaves in response to intracellular stimuli (*24*) (**Fig. 1A**). When injected i.v., our antigen-N-acetylglucosamine glycopolymer (p(GluNAc)) conjugates accumulate in the liver and are taken up by hepatic APCs. Upon delivery to hepatic APCs, our self-immolative linker is cleaved from the antigen, which releases the conjugated antigen in its unmodified form to allow efficient antigen processing and presentation by hepatic APCs (*24*). Here, we explore the nature of the response to LN APCs.

We first determined whether s.c. injected glyco-polymerized antigen, in this case OVA-p(GluNAc), is specifically retained in the draining LNs (dLN), which we expected due to

their optimal size and molecular weight (~100 kDa) for lymphatic uptake (*26*, *27*). Indeed, we were able to detect OVA-p(GluNAc) in the draining axillary and popliteal LNs (dLNs), using whole-organ fluorescence imaging, only when injected s.c. in the hocks but not after an i.v. injection (**Fig. 1B, C**). Conversely, OVA-p(GluNAc) was only detected in the liver when injected i.v. but not s.c. (**Fig. 1B, C**). We also verified that no antigen remained at the site of immunization 72 h after injection (**Fig. S1A**). This demonstrates the versatility and unique trafficking profile of our synthetically glycosylated antigen platform depending on the injection route.

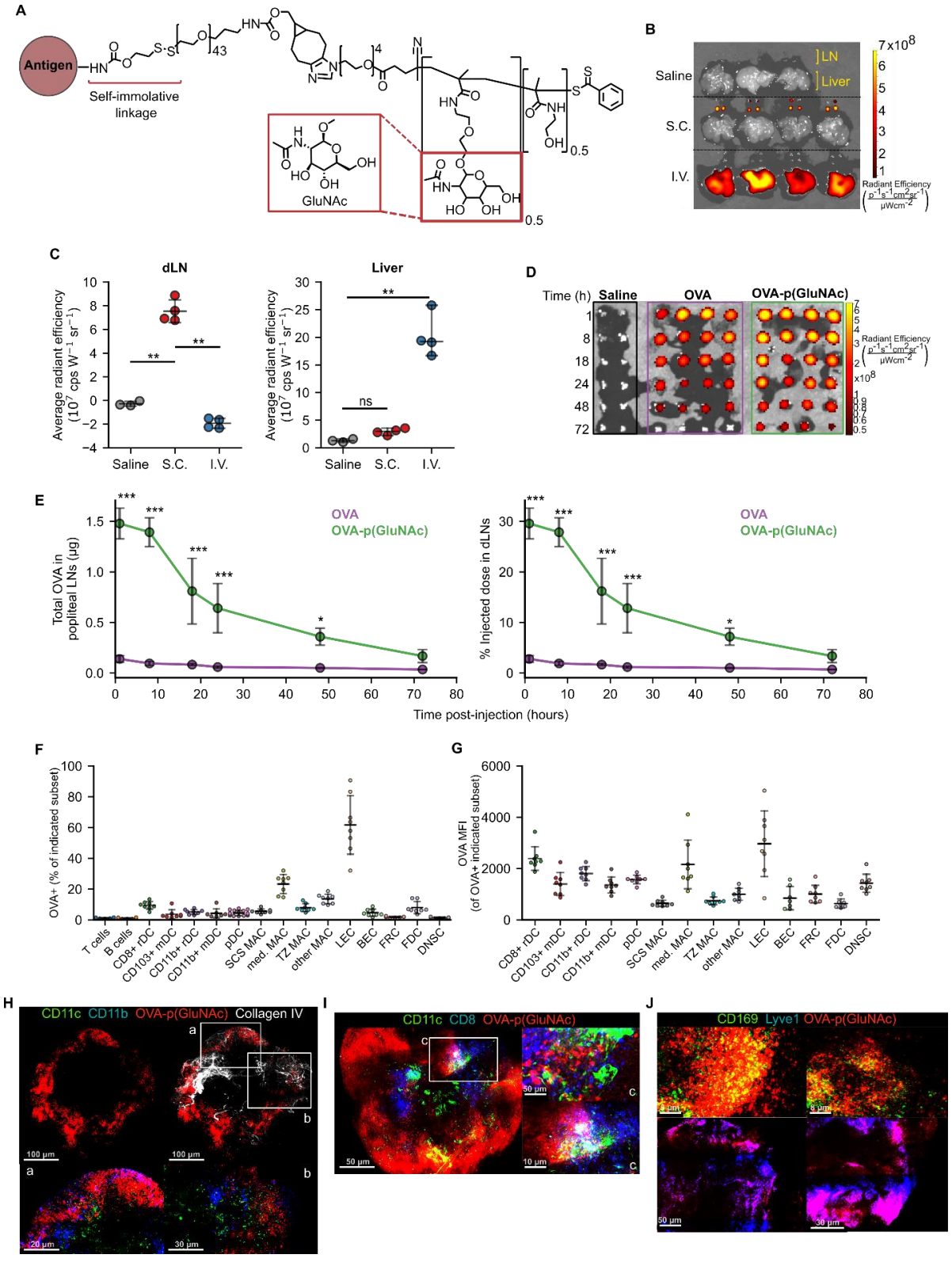

Fig. 1. Antigen-p(GluNAc) conjugate injected s.c. accumulates in the dLNs where it targets various subsets of APCs. (A) Structure of p(GluNAc) conjugated to an antigen lysyl side chain

Fig. 1. *Antigen-p(GluNAc) conjugate injected s.c. accumulates in the dLNs where it targets various subsets of APCs (continued)* amine via a self-immolative linker. (B-C) Accumulation of OVA_{647} or OVA_{647}-p(GluNAc) in the dLNs and livers 15 h after s.c. or i.v. injection. (B) Representative NIR images of dLNs and liver. (C) Average NIR intensities of dLNs and livers. (D-E) Mice were injected with saline or 5 μg of OVA_{647} or OVA_{647}-p(GluNAc) s.c. and the draining popliteal LNs were isolated and imaged at various timepoints between 1-72 h post-injection n (dLN)= 2 for saline and 4 for OVA_{647} or OVA_{647}-p(GluNAc) at each timepoint. (D) Representative NIR images of dLNs. (E) Quantification of OVA accumulation in dLNs, expressed as μg (left) or % of initial injected dose (right). (F-G) Flow cytometry analysis of LN cells that took up OVA_{647}-p(GluNAc) 15 h after s.c. injection of 20 μg of OVA_{647}-p(GluNAc). DC: dendritic cell; pDC: plasmacytoid dendritic cell; MAC: macrophage; SCS: subcapsular sinus; med: medullary; TZ MAC: T cell zone macrophage; LEC: lymphatic endothelial cell ($CD45^-CD31^+gp38^+$); BEC: blood endothelial cell ($CD45^-CD31^+gp38^-$); FRC: fibroblastic reticular cell ($CD45^-CD31^+gp38^-CD21/35^-$); FDC: follicular dendritic cell ($CD45^-CD31^+gp38^-CD21/35^+$); DNSC: double negative stromal cell ($CD45^-CD31^-gp38^-$). (F) Percent of each cell subset that is OVA^+. (G) OVA_{647} MFI of each OVA^+ cell subset. (H-J) Representative whole mount confocal images of immunostained dLNs after s.c. injection of OVA_{647}-p(GluNAc) (red). (H) LNs stained versus CD11c (green), CD11b (blue) and Collagen IV (white), 8 h post-injection (p.i.). $CD11c^+CD11b^+$ DCs are shown in aqua and co-localized OVA-p(GluNAc) is shown in magenta. Scale bar ranges from 20-100 μm and is indicated in each panel. (I) LNs stained versus CD11c (green) and CD8 (blue) 18 h p.i. $CD11c^+CD8^+$ double positive DCs are shown in aqua and co-localized OVA-p(GluNAc) is shown in magenta. Scale bar ranges from 5-50 μm and is indicated in each panel. (J) LNs stained versus CD169 (green, top) and Lyve1 (blue, bottom). Co-localized OVA-p(GluNAc) with $CD169^+$ macrophages is shown in yellow (top), and OVA-p(GluNAc) co-localized with the lymphatics is shown in magenta (bottom). Scale bar ranges from 5-50 μm and is indicated in each panel. Data represent mean ± SD. *$p \leq 0.05$, **$p \leq 0.01$, ***$p \leq 0.001$ by one-way ANOVA using Tukey's post hoc test in C, and two-way ANOVA using Sidak's post hoc test in E.

Following s.c. injection of an equivalent antigen dose and visualization of the fluorescence in the dLNs at different timepoints after injection, we found that OVA-p(GluNAc) localizes to the dLNs dramatically better than unconjugated OVA. (**Fig. 1D**). The higher accumulation of OVA-p(GluNAc) is expressed in two ways: as absolute protein content calculated from a dose-radiant efficiency standard curve, and as a percent of the initially injected antigen dose per hock of 5 μg (**Fig. 1E**). We detected a 17-fold difference in antigen accumulated (maximum at time = 8 h), and a 10-fold difference in the area under the curve, demonstrating that antigen conjugation to p(GluNAc) increases the retention in the dLNs, and thus, potentially increasing the bioavailability of antigen to APCs (**Fig. 1E**). Increased antigen retention in the first few

days of immunization is especially important under unadjuvanted conditions where antigen dose and availability need to trump transient TCR-pMHC interactions for fruitful T cell stimulation to occur (*28*, *29*).

After confirming that antigen-p(GluNAc) accumulated in the dLN, we verified whether antigen was taken up by APCs in the LN microenvironment. We conducted a biodistribution experiment in which we assessed the types of APCs that took up antigen-p(GluNAc) and the extent to which they did 15 h after s.c. injection. OVA-p(GluNAc) was taken up by different APC types, reported as % OVA^+ within each APC subset (**Fig. 1F**) or mean fluorescence intensity (MFI) of OVA^+ cells **(Fig. 1G**). These APCs included various subsets of macrophages, dendritic cells and lymphatic endothelial cells (LECs) that efficiently take up antigen due to their strategic location within the LN, their phagocytic ability and expression of scavenger receptors (*30*–*34*). Using multi-parameter flow cytometry, we elucidated the contribution of specific APC subsets that took up antigen after administration of OVA-p(GluNAc). Among these were APCs found at and surveilling the subcapsular sinus such as LECs (37), $CD169^+$ subcapsular sinus macrophages (*38*) and $CD11b^+$ resident DC2s (*30*) as well as APCs that are more deeply located in the medullary or cortical regions of the LN, such as the $CD169^+$ medullary macrophages, cross-presenting resident $CD8^+$ DC1s (*36*)(*37*) and T cell zone $CX3CR1^+Mertk^+$ macrophages (*34*). These results confirm that antigen-p(GluNAc) can traffic and be taken up by APCs located at different locations within the LN for subsequent processing and presentation (**Fig. 1F, G**).

To obtain a visual confirmation for our flow cytometry results, we isolated popliteal LNs from mice that had been injected s.c. in the hind hocks with fluorescently-labeled OVA_{647}-p(GluNAc) and imaged whole mounts on a confocal microscope. We stained APCs using a combination of CD11c and CD11b for non-cross presenting DC2s (**Fig. 1H**), or CD11c and CD8 for resident cross-presenting DCs (**Fig. 1I**), or CD169 for subcapsular sinus and medullary macrophages **(Fig. 1J**). We also stained for the basement membrane and lymphatics using antibodies to collagen IV and Lyve1 respectively (**Fig. 1H, J**). OVA-p(GluNAc) was found to promiscuously co-localize with all the APC subsets imaged and mentioned above, consistent with our flow cytometry results and indicating that the mechanism of action is not preferential targeting of specific APC subsets but increased antigen uptake by LN APCs in general.

Uptake of synthetically glycosylated antigen by APCs is mediated through the carbohydrate binding domain of various C type lectin and scavenger receptors and can be inhibited by the addition of free sugars in media (*24*). We analyzed the immgen database (http://www.immgen.org/) for the expression of several scavenger and lectin receptors involved in the uptake of carbohydrates, including GluNAc-terminated residues, among APCs targeted by OVA-p(GluNAc), and found that they were broadly expressed, but to different extents on these cell types (**Fig. S1B**). We identified Asgr1 and 2 to be only minor players in LN APCs compared to hepatic APCs (*38*). Clec4g (LSECtin) was found to be highly expressed exclusively on LECs, justifying their high uptake of OVA-p(GluNAc) and their similarity in scavenging profile to liver sinusoidal endothelial cells (*23*, *39*). Other receptors found highly expressed by the hematopoietic

APCs were DEC-205 (Ly75), commonly used as an antigen target for the induction of tolerance (*14*, *40*) and Clec9a, primarily used as apoptotic scavenger receptor by cross-presenting DCs (*41*). LECs and macrophages share MARCO expression that has been used for antigen targeting in tolerance induction (*22*, *42*). The mannose receptor (Mrc1), which can promiscuously bind GluNAc glycosylated antigen, was also highly expressed on LECs (*43*). This analysis also revealed shared receptors between LECs and macrophages, which reflects their synergy in scavenging in the LN subcapsular sinus, similar to the parallels between sinusoidal endothelial cells and Kupffer cells in the liver (*44*). Thus, by virtue of size, retention, expression of C-type lectin and scavenger receptors, synthetically glycosylated antigen is ideally poised for uptake by LN APCs to orchestrate downstream immune responses.

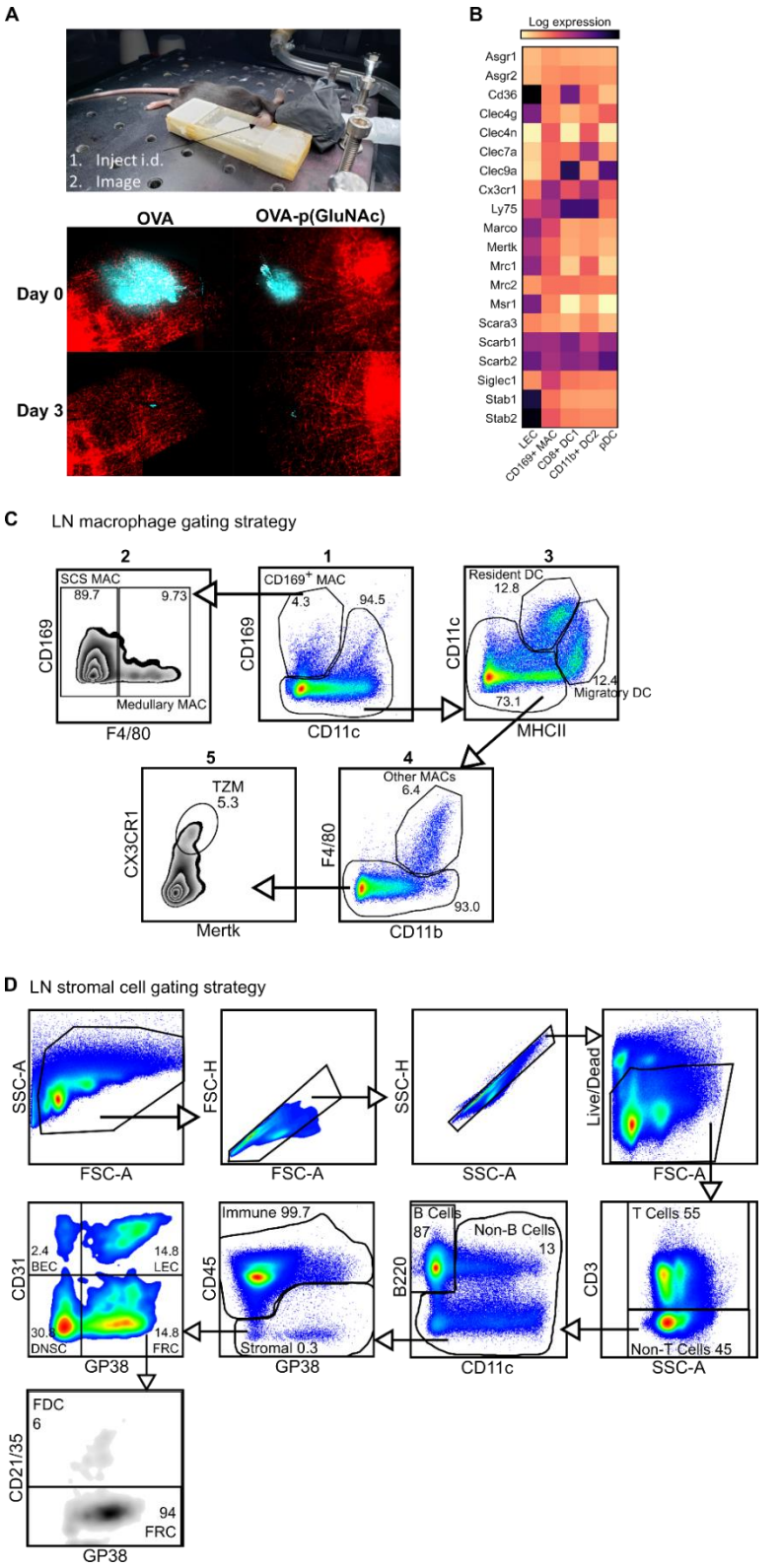

Fig. S1. Characterization of lymphatic drainage from the s.c. injection site, LN APC subsets and expression of GluNAc-binding receptor candidates on these subsets. (A) ProxTom (Prox1-

Fig. S1. *Characterization of lymphatic drainage from the s.c. injection site, LN APC subsets and expression of GluNAc-binding receptor candidates on these subsets (continued)* tdTomato) mice were injected in the ear dermis with OVA_{647} or OVA_{647}-p(GluNAc). The ear dermis around the site of injection was imaged on the day of injection (day 0) and 3 days post-injection using *in vivo* fluorescence microscopy. Lymphatics are shown in red, and OVA antigen is displayed in cyan. (B) Heatmap showing the comparative expression of different classes of carbohydrate-binding and scavenger receptors on LECs, $CD169^+$ macrophages, $CD8^+$ DC1s, $CD11b^+$ DC2s and plasmacytoid DCs in the s.c. LNs of wild-type male C57BL/6 mice. Data analyzed from the immgen database (http://www.immgen.org/). (C) Representative flow cytometry plots showing the gating strategy used for LN macrophage subsets. (D) Representative flow cytometry plots showing the gating strategy used for LN stromal cell subsets.

Antigen-p(GluNAc) leads to antigen-specific $CD4^+$ and $CD8^+$ T cell tolerance, induction of regulatory subsets and hypo-responsiveness upon antigenic challenge

We used the OTI/II ovalbumin (OVA)-reactive transgenic T cell receptor (TCR) model to assess the impact of s.c. administration of OVA-p(GluNAc) on the immune response. We adoptively transferred naïve $CD45.1^+$ OTI $CD8^+$ and OTII $CD4^+$ T cells into mice one day before they were injected s.c. with OVA-p(GluNAc) or saline as unimmunized control, and compared that to i.v. administered OVA-p(GluNAc), as we have published (*24*). We first determined the optimal dose at which OVA-p(GluNAc) was tolerogenic through the s.c. route. We also compared the effect of immunizing mice one vs. two times with the same molecule. We challenged mice with OVA and LPS 9 days following injection (for mice that received one dose) or 9 days following the second dose (for mice that received two doses) and assessed the OVA-specific immune response 5 days after challenge (**Fig. 2A**). We observed a strong dose-dependent response in inhibiting OVA-specific $CD8^+$ T cell proliferation in the dLNs (**Fig. 2B**). In mice that received one dose, significantly fewer OTI cells were recovered from the challenge site dLNs of mice that received a mid (5 μg) or higher (20 μg) dose, but not a low (1 μg) dose. The same dose-

dependent reduction in OTI was observed in mice that received two doses, with lowest OTI recovery in the mice that received the highest dose (2 x 20 μg), indicating that clonal deletion was more effective with a higher dose of antigen (**Fig. 2B**). These results were consistent with OTI numbers recovered from the spleen, showing that even though T cell education takes place locally in the s.c. dLNs, a systemic tolerogenic response is generated (**Fig. S2A**). Furthermore, it was necessary to increase the s.c. dose in order to match the tolerogenic behavior observed with one dose of an i.v. injection, suggesting that a higher threshold to suppression exists in the LN and peripheral lymphatics compared to the liver and also that antigen dose is an important modulating factor (*45*–*47*).

We then focused on the OTI and OTII cell phenotypes in experiments performed at the optimized dose of 20 μg s.c. and in the prime-boost regimen that generated the most effective OTI deletion, and assessed the tolerogenic responses induced by OVA-p(GluNAc) compared to unconjugated OVA. In this context, tolerance induction is characterized by an abrogated T-cell response to antigenic challenge and an enrichment of antigen-specific Treg cells. Five days post-challenge on day 22, s.c. prophylactic tolerization with OVA or OVA-p(GluNAc) both resulted in a significant reduction in OTI proliferation in the dLNs compared to untreated saline controls (**Fig. 2C**). This result was comparable to that obtained in the spleen (**Fig. S2B**). Even though OVA-p(GluNAc) did not lead to a significantly lower OTI recovery compared to unmodified OVA, it induced a number of tolerogenic signatures distinct from OVA-educated T cells. OTI cells primed with OVA-p(GluNAc) expressed significantly higher levels of co-inhibitory receptors, including PD-1 and Lag-3, compared with OVA (**Fig.**

2D, E). OTI cells from the OVA-p(GluNAc) group also highly expressed Tim-3, another co-inhibitory marker of exhaustion (**Fig. 2F**). OVA-p(GluNAc) also induced a sizeable subset of OTI cells that co-express PD-1 and Tim-3 (**Fig. S2C**), known to mark terminally exhausted cells in the context of tumors and chronic viral infections (*48*). Additionally, OTI cells from both the OVA and OVA-p(GluNAc) groups had significantly down-regulated the surface expression of their TCR, indicative of a self-inhibitory and anergic response (**Fig. 2G**). Upon restimulation of OTI cells isolated from OVA-p(GluNAc)-treated mice with their cognate peptide $OVA_{257-264}$ peptide *ex vivo*, a similar fraction produced the pro-inflammatory cytokine IFNγ (**Fig. S2D**) but to a significantly lower extent illustrated by a 2-fold reduction in IFNγ MFI of the secretors (**Fig. 2H**). OTI cells from the OVA-p(GluNAc) group secreted significantly higher levels of IL-10, an immunosuppressive cytokine known to play important roles in the induction and maintenance of tolerance (**Fig. 2I**) (*49*).

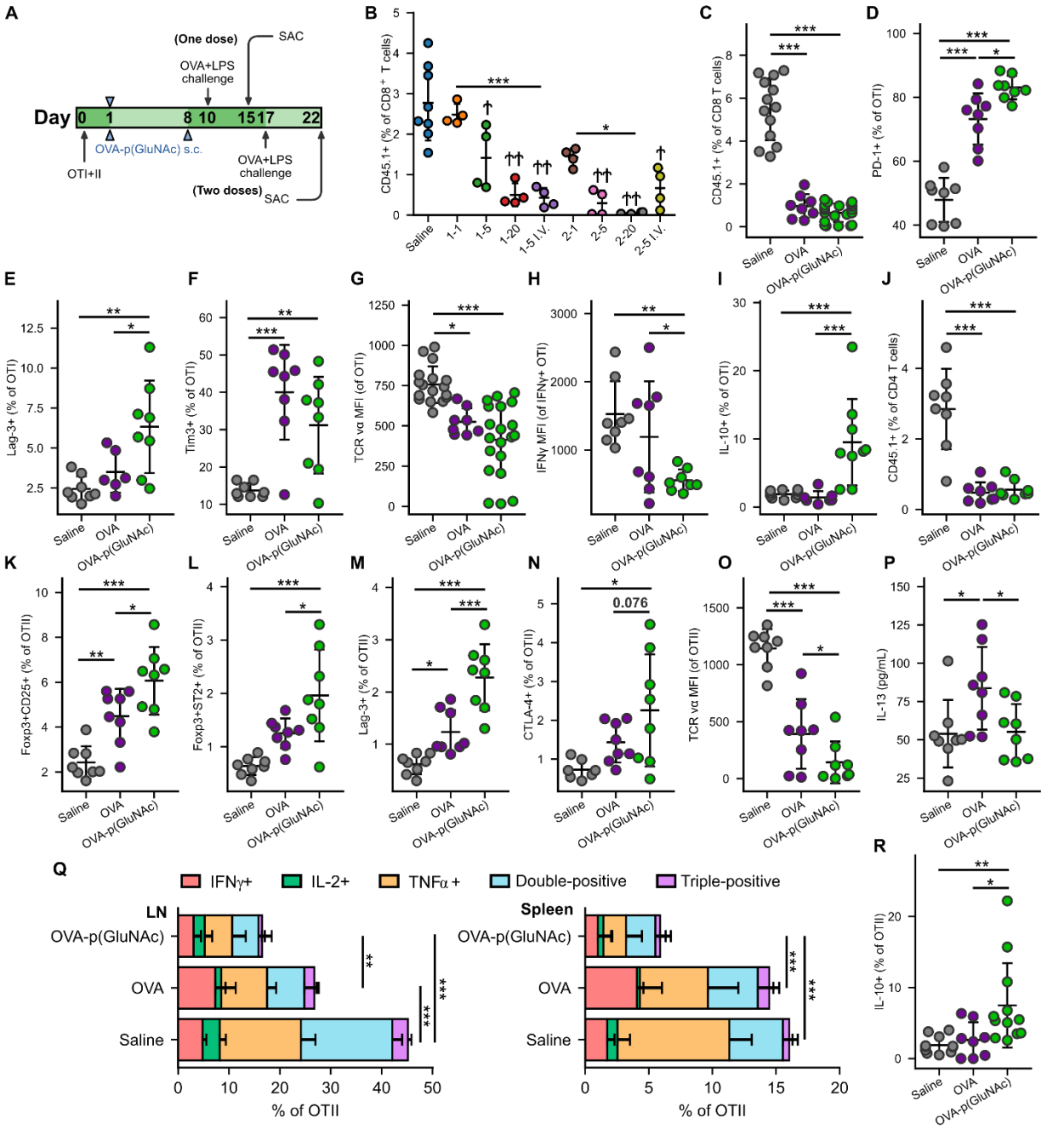

Fig. 2. Antigen-p(GluNAc) leads to antigen-specific CD4+ and CD8+ T cell tolerance, induction of regulatory subsets and hypo-responsiveness upon antigenic challenge. (A) Experimental timeline of the dose-efficacy study, n=4. CD45.2$^+$ mice that had received an adoptive transfer of both OTI (CD45.1$^+$CD3$^+$CD8$^+$) and OTII (CD45.1$^+$CD3$^+$CD4$^+$) T cells via i.v. injection, were treated with saline or a low, mid or high dose of OVA-p(GluNAc) s.c. in all four hocks or i.v. in the tail vein (as benchmark) either once on day 1 or twice on days 1 and 8. 9 days following the last dose, on day 10 (for the groups that received one dose) or on day 17 (for the groups that received two doses), all mice were administered an OVA+LPS challenge s.c., and 5 days later, the dLNs and

Fig. 2. *Antigen-p(GluNAc) leads to antigen-specific CD4+ and CD8+ T cell tolerance, induction of regulatory subsets and hypo-responsiveness upon antigenic challenge (continued)* spleen were examined for an OVA-specific response. Stars above horizontal bars represent p values with respect to the i.v. groups (*p ≤ 0.05, **p ≤ 0.01, ***p ≤ 0.001) and † indicate p values with respect to the saline group († p ≤ 0.05, †† p ≤ 0.01). (B) OTI $CD8^+$ T cells recovered from dLNs at time of sacrifice. Plot legends are as follows: 1-1 (1 μg s.c., once), 15 (5 μg s.c., once), 1-20 (20 μg s.c., once), 1-5 i.v. (5 μg i.v., once), 2-1 (1 μg s.c., twice), 2-5 (5 μg s.c., twice), 2-20 (20 μg s.c., twice) and 2-5 i.v. (5 μg i.v., twice). (C-R) Data are representative of three pooled experiments performed at the optimal high 20 μg dose of OVA as unconjugated OVA or OVA-p(GluNAc) injected twice on days 1 and 8, followed by an OVA+LPS challenge on day 17 and sacrifice on day 22, n=8-20. (C) OTI $CD8^+$ T cells recovered from dLNs. (D) PD-1^+ OTI $CD8^+$ T cells in dLNs. (E) Lag-3^+ OTI $CD8^+$ T cells in spleen. (F) Tim-3^+ OTI $CD8^+$ T cells in spleen. (G) MFI of the TCR on OTI $CD8^+$ T cells in dLNs. (H) IFNγ MFI of IFNγ secreting OTI cells after a 6-h ex vivo restimulation with $OVA_{257-264}$ peptide. (I) IL-10 producing OTI $CD8^+$ T cells after a 6-h ex vivo restimulation with $OVA_{257-264}$ peptide. (K) OTII $CD4^+$ T cells recovered from dLNs. (L) $Foxp3^+CD25^+$ OTII $CD4^+$ Tregs induced in dLNs. (M) $Foxp3^+ST2^+$ OTII $CD4^+$ Tregs induced in dLNs. (N) $Lag3^+$ OTII $CD4^+$ T cells in dLNs. (O) CTLA-4^+ OTII $CD4^+$ T cells in dLNs. (P) MFI of the TCR on OTII $CD4^+$ T cells in dLNs. (P) IL-13 levels in the supernatant of LN cells restimulated with 100 μg/mL OVA protein for 4 days, measured by LegendPlex assay. (Q) OTII $CD4^+$ T cells from the dLNs (left) or spleen (right) that secreted IFNγ, IL-2, TNFα, or a combination of two or all three cytokines after a 6-h ex vivo restimulation with $OVA_{323-339}$ peptide. (R) IL-10 producing OTII $CD4^+$ T cells after a 6-h ex vivo restimulation with $OVA_{323-339}$ peptide. Data represent mean ± SD. *p ≤ 0.05, **p ≤ 0.01, ***p ≤ 0.001 by one-way ANOVA using Tukey's post hoc test.

We observed similar tolerogenic effects exerted in the OTII compartment. Upon antigenic challenge, fewer OTII cells were recovered from the dLNs in both the OVA and OVA-p(GluNAc) treated mice compared to untreated saline controls (**Fig. 2J**). The OVA-p(GluNAc) treatment induced significantly higher $CD4^+$ antigen-specific $Foxp3^+CD25^+$ Tregs (**Fig. 2K**), as well as $Foxp3^+ST2^+$ Tregs (**Fig. 2L**), both with major roles in tolerance (*50*). The OTII cells tolerized with OVA-p(GluNAc) more highly expressed co-inhibitory molecules such as Lag-3 (**Fig. 2M**) and CTLA-4 (**Fig. 2N**) and also down-regulated their TCR **(Fig. 2O**). Next, we evaluated the effector function of the OTII cells upon *ex vivo* antigen reencounter, and detected cytokines either (1) produced by cells isolated from dLNs and spleen using flow cytometry after a 6-hour culture with their cognate $OVA_{323-339}$ peptide, or (2) secreted into the culture supernatant using the LegendPlex assay after a 3-day culture with full OVA protein. LN cells from OVA-

p(GluNAc)-treated mice had significantly reduced IL-13 production into the supernatant, suggesting that this treatment can also be useful in suppressing Th2-mediated reactions such as allergies (**Fig. 2P**). There were also lower levels of Th17 cytokines, IL-17 and IL-22 secreted (**Fig. S2E, F**). Furthermore, OTII cells from both the LN and spleen produced markedly lower levels of Th1 pro-inflammatory cytokines such as IFNγ, IL-2 and TNFα, indicating a severe ablation of their effector response (**Fig. 2Q**). OVA-p(GluNAc) successfully suppressed the presence of polyfunctional $CD4^+$ T cells, measured by their ability to produce more than one cytokine, pointing to a severe dysfunctional state (*51*). The OTII cells also produced higher IL-10 levels (**Fig. 2R**). Thus, we successfully demonstrated that s.c. treatment with p(GluNAc) conjugated antigen generates robust antigen-specific tolerance, characterized by deletion, upregulation of surface co-inhibitory molecules, induction of both $CD25^+$ (IL-2 receptor) and $ST2^+$ (IL-33 receptor) Tregs, and an abrogation of broad-spectrum effector cytokines upon antigenic challenge.

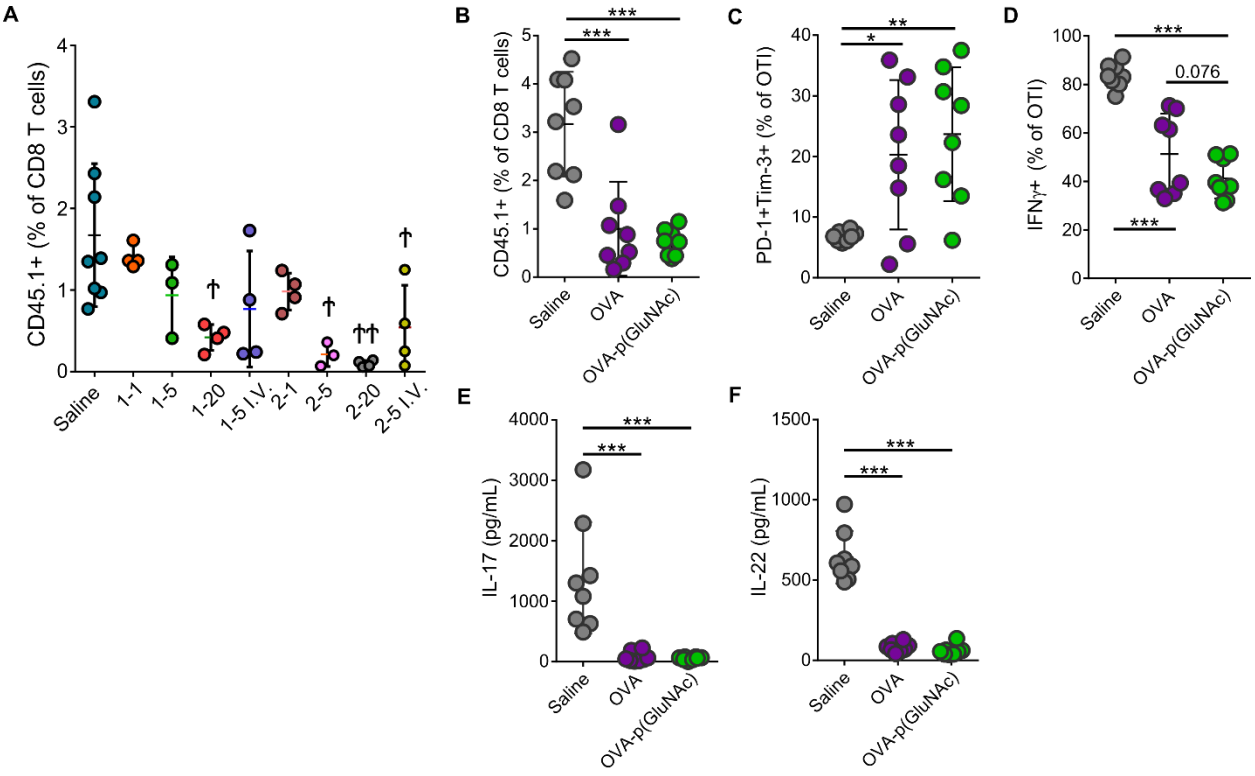

Fig. S2.1. Antigen-p(GluNAc) leads to antigen-specific CD4$^+$ and CD8$^+$ T cell tolerance in the spleen in addition to dLNs, and suppresses Th17 responses. (A) Experimental set-up described in Fig. 2A. % OTI cells recovered from the spleen at time of sacrifice. Plot legends are as follows: 1-1 (1 µg s.c., once), 15 (5 µg s.c., once), 1-20 (20 µg s.c., once), 1-5 i.v. (5 µg i.v., once), 2-1 (1 µg s.c., twice), 2-5 (5 µg s.c., twice), 2-20 (20 µg s.c., twice) and 2-5 i.v. (5 µg i.v., twice). (B) % OTI cells recovered from the spleen at day 22. (C) % PD-1$^+$Tim-3$^+$ (terminally exhausted) OTI cells in the spleen at day 22. (D) % IFNγ secreting OTI cells after a 6-h ex vivo restimulation with $OVA_{257-264}$ peptide. (E) IL-17 levels in the supernatant of LN cells restimulated with 100 µg/mL OVA protein for 4 days, measured by LegendPlex^{TM} assay. (F) IL-22 levels in the supernatant of LN cells restimulated with 100 µg/mL OVA protein for 4 days, measured by LegendPlex assay. Data represent mean ± SD. Statistical differences were determined by one-way ANOVA using Tukey's post hoc test (*p ≤ 0.05, **p ≤ 0.01, ***p ≤ 0.001).

Here, we present extended data showing how the OTI CD8$^+$ T cell phenotype is modulated by dose, beyond just proliferation upon challenge and recovery. In addition to saline and the i.v. injected doses, we used mice injected s.c. with 20 µg of OVA-p(GluNAc) injected two weeks prior to the adoptive transfer to compare with the archiving context that we have explored in chapter 3 of this thesis (**Fig S2.2A**). As described above, mice were immunized one day following the OTI/OTII adoptive

transfer (except in the archiving control where they were dosed two weeks before transfer), and were challenged with OVA and LPS nine days post-immunization, and were sacrificed five days post-challenge to evaluate the OTI $CD8^+$ T cell response (**Fig S2.2A**). We first measured the extent to which the CFSE-labeled OTI $CD8^+$ T cells proliferated in the blood three days following adoptive transfer. There was a dose-dependent proliferation where the OTI cells proliferated to increasing degrees with increasing s.c. dose, and proliferated the most at the highest dose of 20 μg (**Fig S2.2B**). This proliferation was higher than that observed with the i.v. control; the archiving control induced lowest proliferation levels in accordance with what we have observed in the past in this model (**Fig S2.2B**). Consistent with the skewed central memory $CD8^+$ T cell phenotype that we have observed with archived OVA-p(GluNAc), we saw the highest upregulation in central memory phenotype with the highest s.c. dose, also in a dose-dependent manner (**Fig S2.2C**). In fact, the central memory phenotype observed with the higher tolerogenic dose of 20 μg was even higher than that previously observed with archived OVA-p(GluNAc) (**Fig S2.2C**). At day 14 post-challenge, we obtained a significant dose-dependent deletion of OTI $CD8^+$ T cells in the dLNs, with progressively fewer OTI cells recovered with increasing immunizations dose (**Fig S2.2D**). Though not as striking, the trend was similar in OTI $CD8^+$ T cell numbers recovered from the spleen (**Fig S2.2E**). PD-1 was induced and maintained on OTI $CD8^+$ T cells in a dose-dependent fashion and the higher 20 μg was required to match the i.v. control (**Fig S2.2F**). Tim-3 was also induced to high levels with the 20 μg s.c. dose, comparable to the i.v. group (**Fig S2.2G**). The T cell receptor on OTI $CD8^+$ T cells was down-regulated also in a dose-dependent fashion both in the LN (**Fig S2.2H, left**) and spleen (**Fig**

S2.2H, right)(*47*). The ability of OTI CD8$^+$ T cells to secrete inflammatory cytokines in response to challenge was severely abrogated and, in a dose-dependent manner. We were able to show loss in function of cytotoxic CD8$^+$ T cells in terms of the number of IFNγ$^+$ cells detected from the LN (**Fig S2.2I, left**) and spleen (**Fig S2.2I, right**) as well as in the number of IL-2$^+$ cells detected from the LN (**Fig S2.2J, left**) and spleen (**Fig S2.2J, right**). Even though the numbers of cytokine$^+$ cells might appear skewed from the already low numbers of cells recovered, their inherent ability to secrete those cytokines was significantly affected when we measured cytokine$^+$ as a % of total OTI CD8$^+$ T cells (**Fig S2.2K, L**). Furthermore, OTI CD8$^+$ T cells from mice treated with the 20 μg s.c. dose had an enhanced ability to produce the anti-inflammatory cytokine IL-10 in response to challenge in a dose-dependent fashion in the LNs and more in a digital fashion at the high dose in the spleen (**Fig S2.2M**). Higher IL-10 production also appeared to be specific to the s.c. approach as we failed to observed IL-10$^+$ OTI CD8$^+$ T or OTII CD4$^+$ T cells with i.v. administration of OVA-p(GluNAc) (**Fig S2.2M**). Of note, OTII CD4$^+$ T cells did not give useful results due to a reliably low number of cells recovered at the time of sacrifice. These data show that it is possible to induce robust CD8$^+$ T cell tolerance by targeting glyco-modified antigen to the LN, and that a higher dose in required to achieve systemic tolerance comparable to the published liver-targeting strategy.

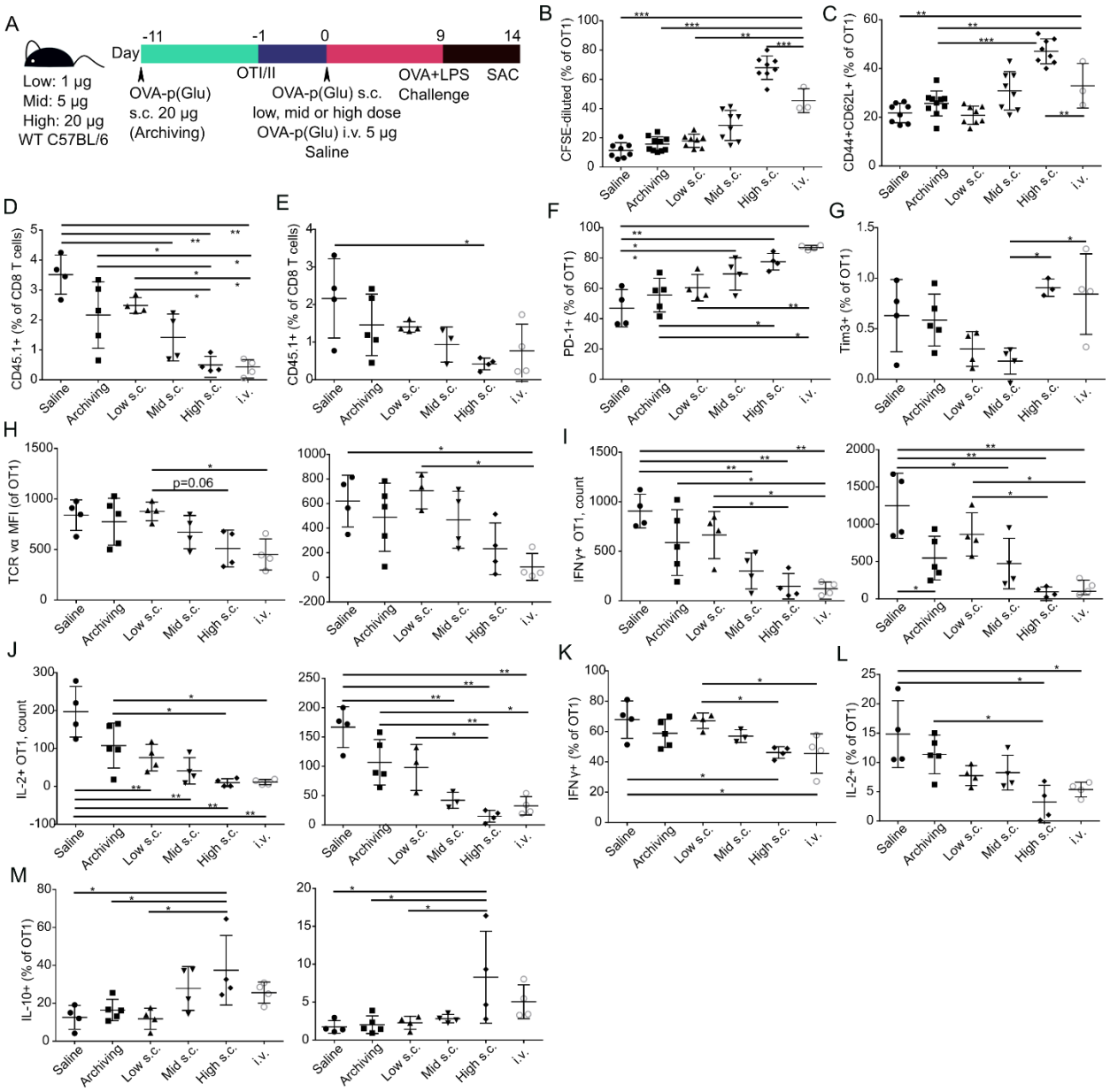

Fig S2.2. Antigen-p(GluNAc) administered once s.c. tolerogenically induces a more suppressed CD8$^+$ T cell phenotype, comparable to i.v. administration, and higher than when archived. A) Experimental timeline of dose-efficacy study, n=4. All mice were immunized once s.c. in all hocks. The archiving control mice were immunized 11 days before adoptive transfer. The remainder of the mice were immunized one day after adoptive transfer following the dose regimen. All mice were challenged with OVA and LPS on day 9, followed by an assessment of the OTI/OTII phenotype on day 14. (B-C) The phenotype of the OTI in blood was characterized on day 3. (B) OTI that have diluted CFSE, i.e., proliferated in blood. (C) OTI that are central memory (CD44$^+$CD62L$^+$). (D-M) The phenotype of OTI from dLNs and spleen of mice at the time of sacrifice at day 14. (D) OTI in LNs. (E) OTI in spleen. (F) % PD-1$^+$ OTI in LNs. (G) % Tim-3$^+$ OTI in LNs. (H) MFI of the T Cell Receptor (TCR) vα on OTI in LNs (left) and spleen (right). (I-M) Cytokine production by OTI upon restimulation with $OVA_{257-264}$. (I) Number of IFNγ$^+$ OTI in LNs (left) and spleen (right). (J) Number of IL-2$^+$ OTI in LNs (left) and spleen (right). (K) % IFNγ$^+$ OTI

Fig S2.2*. Antigen-p(GluNAc) administered once s.c. tolerogenically induces a more suppressed CD8⁺ T cell phenotype, comparable to i.v. administration, and higher than when archived. (continued)* in LNs. (L) % IL-2⁺ OTI in LNs. (M) % IL-10⁺ OTI in LNs (left) and spleen (right). Statistical differences were determined by one-way ANOVA using Tukey's post hoc test (*p ≤ 0.05, **p ≤ 0.01, ***p ≤ 0.005).

We next investigated whether the tolerogenic and hypo-responsive $CD8^+$ T cell response observed with one dose of glycoconjugated antigen can be enhanced with two doses in a prime-boost regimen, due to higher antigen availability and priming that such a regimen can impose(*52*). We followed the same schedule, groups and controls as before and the only difference was that mice were immunized twice spaced one week apart with the same molecule (except for the archiving control that only received one injection of OVA-p(GluNAc)) (**Fig S2.3A**). We obtained an even more effective deletion and significantly suppressed OTI recovery upon challenge with the highest 20 ug s.c. dose in both the LNs (**Fig S2.3B, left**) and spleen (**Fig S2.3B, right**) in a dose-dependent fashion as observed before. The i.v. control did not give the best performance in this regimen, most likely because the mice were immunized one week apart as opposed to four days apart, which was the optimized schedule with this molecule through the i.v. route (*24*). OTI cells from the high group were most suppressed in their ability to proliferate as they expressed lower levels of the Ki67 nuclear protein, which also changed in a dose-dependent manner (**Fig S2.3C**). OTI cells expressed high PD-1 levels only in the mid and high dose groups, which matched that in the i.v. group (**Fig S2.3D**). Expression of co-inhibitory marker Tim-3 was notably restricted to the high s.c. group both in the LN (**Fig S2.3E, left**) and right (**Fig S2.3E, right**). Lag-3 expression was highest in the high s.c. group in the LN (F, left) but was elevated in both the mid and high s.c. groups in the spleen (**Fig S2.3F, right**). TCR

expression on OTI $CD8^+$ T cells suffered the highest down-regulation in the high s.c. group, both in the LN (**Fig S2.3G, left**) and spleen (**Fig S2.3G, right**), which was not observed as a feature of the archiving or i.v. control groups. This indicates that the $CD8^+$ T cells had undergone durable suppression as they were unable to engage with peptide-loaded MHC on APCs. The two-dose regimen also resulted in a deeper suppression of IFNγ and IL-2 cytokines upon restimulation, especially in the high group (**Fig S2.3H, I**). Not only did the immunization with 2x high OVA-p(GluNAc) lead to abrogated production of the cytokines from a lower % $cytokine^+$ cells (**Fig S2.3H**), but also led to lower overall numbers of the cytokine+ cells (**Fig S2.3I**). Since this prime-boost regiment resulted in more effective $CD8^+$T cell hypo-responsiveness, characterized by highest deletion, up-regulation of co-inhibitory markers and abrogation of type 1 cytokine production, we adopted this optimized schedule for all following experiments with s.c. p(GluNAc) immunization.

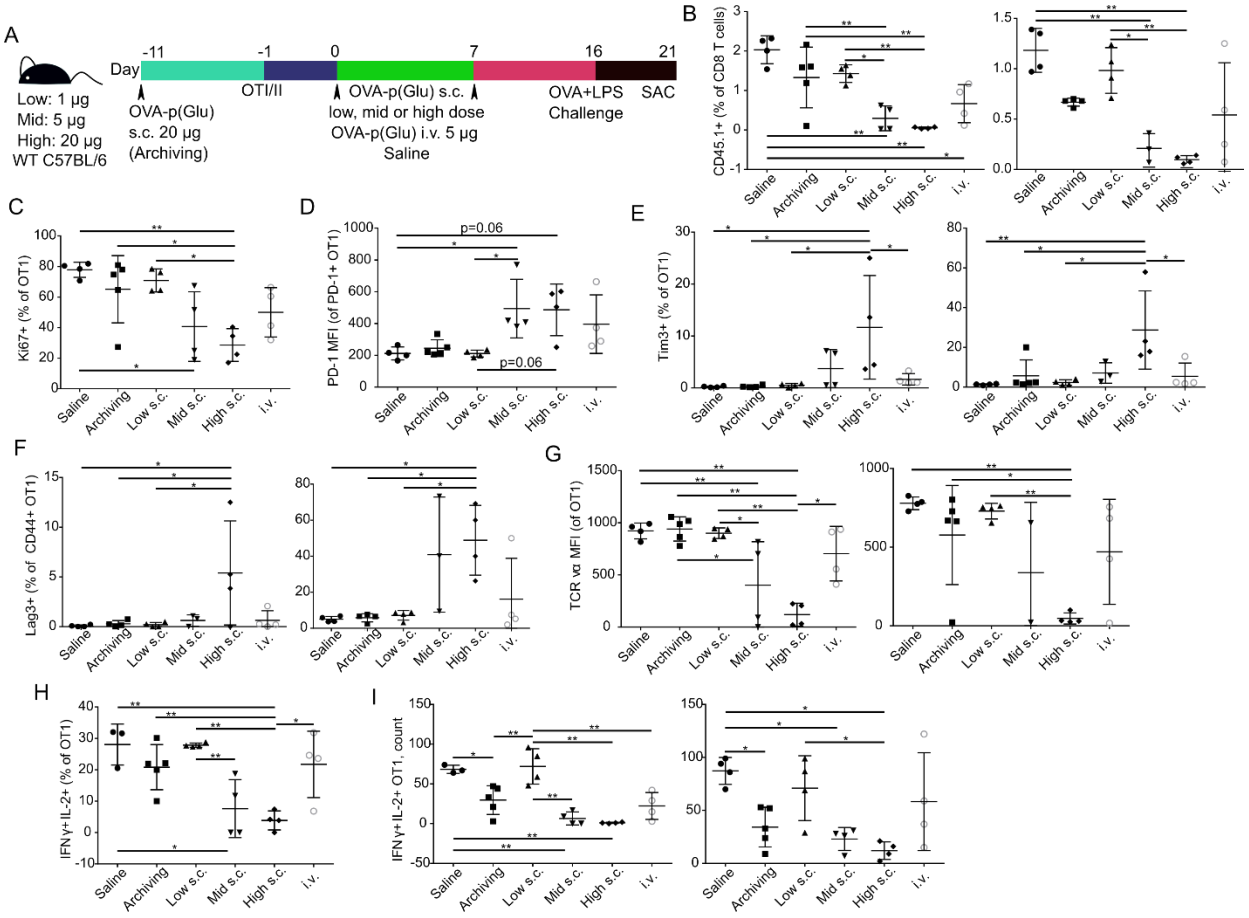

Fig S2.3. LN-targeted hypo-responsiveness with glyco-conjugated antigen can be improved through multiple doses in a prime-boost regimen. (A) Experimental timeline for the dose-efficacy study, n=4. All mice (except for the archiving control) were immunized twice s.c. in the hocks according to the dose regiment, and were challenged with OVA and LPS on day 16, followed by an assessment of the T cell phenotype at day 21. (B) OTI recovered in the LNs (left) and spleen (right) at day 21. (C) Ki67$^+$, i.e., proliferative OTI CD8$^+$ T cells in LNs. (D) MFI of PD-1 on PD-1$^+$ OTI CD8$^+$ T cells in LNs. (E) Tim-3$^+$ OTI CD8$^+$ T cells in LNs (left) and spleen (right). (F) Lag-3$^+$ on activated (CD44$^+$) OTI CD8$^+$ T cells in LNs (left) and spleen (right). (G) MFI of TCR Vα on OTI CD8$^+$ T cells in LNs (left) and spleen (right). (H) OTI CD8$^+$ T cells that secreted IFNγ and IL-2 upon restimulation with $OVA_{257-264}$. (I) Number of OTI CD8$^+$ T cells that secreted IFNγ and IL-2 upon restimulation with $OVA_{257-264}$. Statistical differences were determined by one-way ANOVA using Tukey's post hoc test (*p ≤ 0.05, **p ≤ 0.01, ***p ≤ 0.005).

LN-targeted antigen-p(GluNAc) conjugate induces tolerogenic memory via CD8$^+$ regulatory subsets that can suppress adoptively transferred effector CD4$^+$ T cells

We sought to further evaluate the mechanisms of action of LN-targeted OVA-p(GluNAc) by assessing suppressive populations induced in the long-term at steady-state (without an antigenic challenge), especially in the antigen-specific CD8$^+$ T cell compartment. We treated mice s.c. with either unconjugated OVA or OVA-p(GluNAc), and evaluated the OTI phenotype in the dLNs and spleen one month following the booster injection (**Fig. 3A**). At day 38, we observed a significantly lower recovery of OTI cells from the dLNs of OVA-p(GluNAc)-treated mice, indicating that the activated antigen-specific CD8$^+$ T cells were deleted, resulting in a smaller pool of circulating cells (**Fig. 3B**). We confirmed that OVA-p(GluNAc) treatment leads to a substantial initial proliferation of OTI cells, measured by CFSE dilution of circulating OTI in blood 3 days post-injection (**Fig. S3.1**), establishing that the deletion observed with s.c. OVA-p(GluNAc) was not due to incomplete priming by LN APCs but rather abortive proliferation, similar to the mechanism observed with liver-targeted OVA-p(GluNAc) (*24*). Thus, p(GluNAc) conjugation enhanced clonal deletion as its tolerogenic mechanism, a phenomenon observed not only in adoptively transferred T cells but also in endogenous autoimmune disease models (*53*)(*54*).

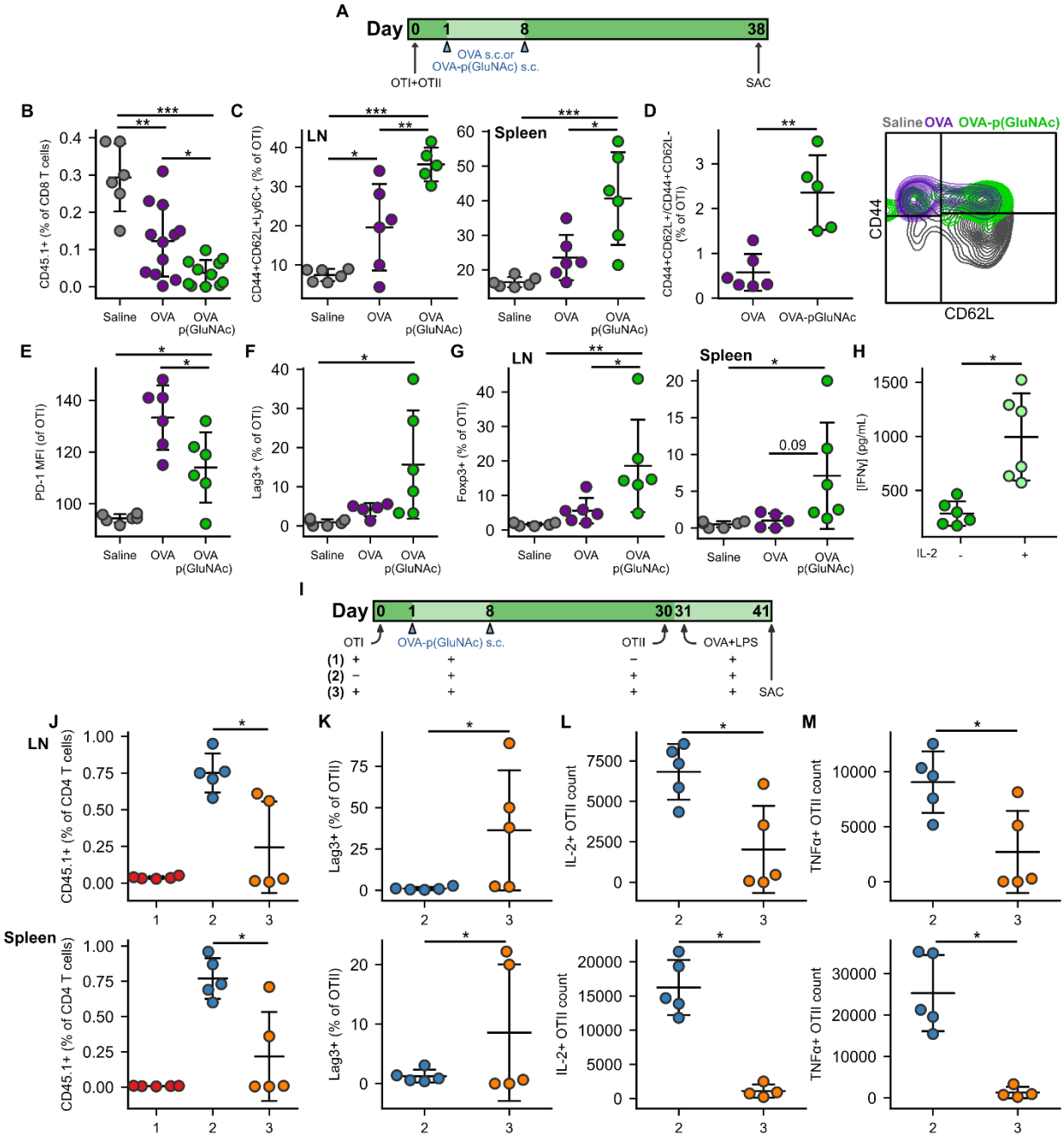

Fig. 3. LN-targeted antigen-p(GluNAc) conjugate induces tolerogenic memory via CD8$^+$ regulatory subsets that can suppress adoptively transferred effector CD4$^+$ T cells. (A) CD45.2$^+$ mice that had received an adoptive transfer of 1x10^6 of both OTI (CD45.1$^+$CD3$^+$CD8$^+$) and OTII (CD45.1$^+$CD3$^+$CD4$^+$) T cells via i.v. injection, were treated s.c. in all four hocks on days 1 and 8 with saline, or 20 µg of OVA or OVA-p(GluNAc) (5 µg per hock). On day 38, all mice were sacrificed and the dLNs and spleen were analyzed for OTI and OTII T cell phenotype. (B) OTI CD8$^+$ T cells recovered from dLNs. (C) Central memory OTI CD8$^+$ T cells in dLNs (left) and spleen (right). (D) Ratio of central memory to effector memory OTI CD8$^+$ T cells (left) and representative flow cytometry contour plot of the memory subsets (right) induced in the spleen. (E) PD-1 MFI on OTI CD8$^+$ T cells in dLNs. (F) Lag-3$^+$ OTI CD8$^+$ T cells in dLNs. (G) Foxp3$^+$ OTI CD8$^+$ T cells in

Fig. 3. *LN-targeted antigen-p(GluNAc) conjugate induces tolerogenic memory via CD8$^+$ regulatory subsets that can suppress adoptively transferred effector CD4$^+$ T cells (continued)* dLNs (left) and spleen (right). (H) Splenocytes from the OVA-p(GluNAc) group were restimulated with 100 µg/mL OVA in culture media alone or supplemented with 200 Units/mL (~12 ng/mL) exogenous IL-2, and IFNγ levels were measured in the supernatant 3 days later by ELISA. (I) CD45.2$^+$ mice received a first adoptive transfer of 1x10^6 OTI CD8$^+$ T cells (groups 1,3) or no cells (group 2), followed by two s.c. OVA-p(GluNAc) treatments on days 1 and 8 for all groups. On day 30, mice from groups 2 and 3 received a second adoptive transfer of 5x10^5 OTII CD4$^+$ T cells. All mice were administered an OVA+LPS challenge on day 31, and 10 days later, the dLNs and spleen were examined for the OTII CD4$^+$ T cell response. (J) OTII CD4$^+$ T cells recovered from dLNs (top) and spleen (bottom). (K) Lag-3$^+$ OTII CD4$^+$ T cells in dLNs (top) and spleen (bottom). (L) Numbers of IL-2 producing OTII cells in dLNs (top) or spleen (bottom) after a 6-h ex vivo restimulation with $OVA_{323-339}$ peptide. (M) Numbers of TNFα secreting OTII CD4$^+$ T cells in dLNs (top) or spleen (bottom) after a 6-h ex vivo restimulation with $OVA_{323-339}$ peptide. Data are pooled from two independent experiments (n= 5-12), and represent the mean ± SD. *p ≤ 0.05, **p ≤ 0.01, ***p ≤ 0.001 by one-way ANOVA using Tukey's post hoc test in B, C, E-G, unpaired Student's T test in D and H, and the Mann Whitney U test in J-M.

Furthermore, we investigated whether the ability to induce tolerance through the s.c. route was unique to p(GluNAc) and whether it could be applied to the other glycopolymer (p(Gal) and p(Man)) antigen conjugates as well. We followed the optimized immunization schedule where we adoptively transferred OTI CD8$^+$ and OTII CD4$^+$ T cells into WT mice, and immunized them with 20 µg of OVA conjugated to p(GluNAc), p(Man) or p(Gal), followed by a boost one week later at the same dose. Nine days later, the mice were administered an OVA and LPS challenge and the T cell phenotype was evaluated after five days. We bled the mice three days after the first dose and found that the OTI CD8$^+$ T cells massively proliferated, with the highest proliferation seen with OVA-p(Man) (~90%) and lowest with OVA-p(Gal) (~60%). OTI CD8$^+$ T cells stimulated with OVA-p(GluNAc) led to an intermediate proliferative state (~ 75%) (**Fig. S3.1A**). OTII CD4$^+$ T cells also highly proliferated in response to the immunization, with maximum expansion seen with OVA-p(Man) and OVA-p(Gal) (~95%) and lowest with OVA-p(GluNAc) (65%) (**Fig. S3.1B**). The OTI CD8$^+$ T cells had

experienced antigen and adopted an activated phenotype from the up-regulation of the surface CD44 marker (**Fig. S3.1C**). Similarly, OTII CD4$^+$ T cells were also antigen-experienced from elevated CD44 expression (**Fig. S3.1D**). Thus, LN-targeted synthetically glycosylated antigen, in general, leads to fruitful T cell priming following immunization, with highest OTI CD8$^+$ T cell proliferation seen with OVA-p(Man) and highest OTII CD4$^+$ T proliferation seen with OVA-p(Man) and OVA-p(Gal). OVA-p(GluNAc) also leads to significantly high proliferation levels, though not to the same extent as the other two glycopolymers.

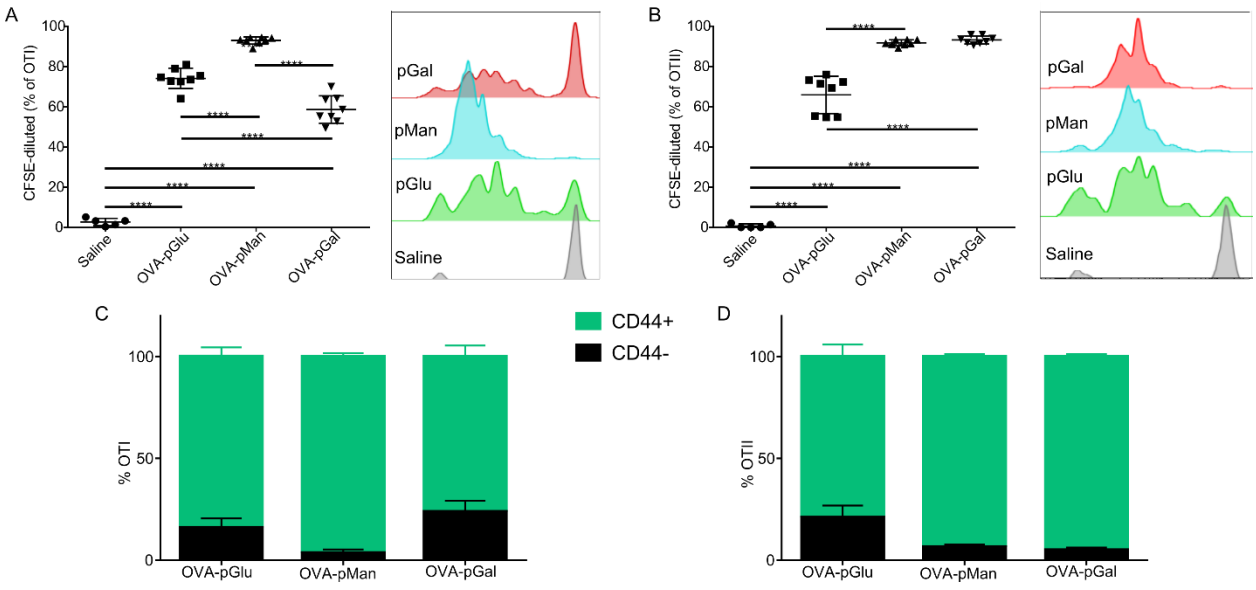

Fig. S3.1. LN-targeted glyco-conjugated antigen results in massive initial proliferation of naïve antigen-specific CD4$^+$ and CD8$^+$ T cells. Mice received an adoptive transfer of OTI/OTII T cells and one day later, were immunized s.c. in all hocks with 20 ug of OVA-p(GluNAc), OVA-p(Man) or OVA-p(Gal), or saline as control, and the phenotype of the T cells was evaluated 3 days post-immunization in the blood. (A) OTI CD8$^+$ T cells that proliferated i.e., diluted CFSE quantified (left) and shown in histograms (right). (B) OTII CD4$^+$ T cells that proliferated i.e., diluted CFSE quantified (left) and shown in histograms (right). (C) OTI CD8$^+$ T cells that are CD44$^+$ or CD44$^-$. (D) OTII CD4$^+$ T cells that are CD44$^+$ or CD44$^-$. Statistical differences were determined by one-way ANOVA using Tukey's post hoc test (A-B) and Mann-Whitney t test (C-D) (*p ≤ 0.05, **p ≤ 0.01, ***p ≤ 0.005).

Phenotype	LN	pGlu	pMan	pGal	Spleen	pGlu	pMan	pGal
OT1#		☻				☻		
OT2#	No diff				No diff			
OT1-TCR↓		☻				☻	☻	
OT2-TCR↓	No diff				No diff			
OT1-CD44↓		☻						☻
OT2-CD44↓	No diff							☻
OT1-PD1+		☻				☻		
OT2-PD1+			☻		No diff			
OT1-Lag3+		☻		☻				☻
OT1-Tim3+	No diff					☻		☻
OT1-Prolif↓			☻				☻	
OT2-Prolif↓			☻				☻	
OT1-Tox+				☻	No diff			

Key:
↓ Down-regulation
↑ Up-regulation
☻ Best at, does not mean only one that can do it

Phenotype	LN	pGlu	pMan	pGal	Spleen	pGlu	pMan	pGal
OT1 Foxp3+ CD8 Treg			☻					☻
OT2 Conv Treg	No diff				No diff			
OT2-Tbet ↓				☻	No diff			
OT2-Roryt↓	No diff							☻
OT2-Tim3+↓	No diff					☻		
OT1-IFNγ↓		☻				☻		☻
OT1-IL-2↓			☻				☻	
OT1-IFNγ+IL-2↓		☻	☻				☻	
OT1-IL-10↑	No diff					☻		
OT2-IFNγ↓		☻		☻	No diff			
OT2-IL-2↓			☻				☻	☻
OT2-IL-10↑			☻			☻		
OT2-IL-17↓		☻		☻	No diff			
IL-5 (ELISA)↓		☻	☻		No diff			

Table 1. Comparing the T cell tolerogenic response across glycoconjugates in response to inverse vaccination with p(Sugar)-antigen, at time of sac.

Antigen challenge with LPS resulted in a significant suppression of OTI $CD8^+$ T cells in all groups compared to saline in both the dLNs (**Fig. S3.3A, left**) and spleen (**Fig. S3.3A, right**). OVA-p(GluNAc) generated significantly better CD8+ T cell suppression compared to p(Gal) and p(Man) (**Fig. S3.3A**). We did not observe any OTII deletion in response to challenge, suggesting that this LN targeting strategy generated a tolerogenic effect specific to CD8+ T cells (**Fig. S3.3B**). Next, we focused on glycopolymer-specific signatures of tolerance induced in this experiment. p(GluNAc) resulted in the highest down-regulation of the TCR in the LNs and spleen (**Fig. S3.3C**).

OTI cells educated with p(GluNAc) were also most significantly suppressed in their ability to differentiate into effectors upon challenge in the LNs and spleen (**Fig. S3.3D**). OTI cells in the p(GluNAc) group also expressed highest PD-1 levels in the LN, which was accentuated in the spleen (**Fig. S3.3E**). Furthermore, p(GluNAc) resulted in the highest up-regulation of other co-inhibitory molecules including Lag-3 on LN OTI cells (**Fig. S3.3F**) and Tim-3 on splenic OTII cells (**Fig. S3.3G**). p(Man), on the other hand, was most effective at reducing proliferation of OTI and OTII cells from % cells that expressed Ki67 in the both the LNs and spleen (**Fig. S3.3H, I**). p(Man) also resulted in the highest induction of Foxp3-expressing $CD8^+$ regulatory T cells in the LN though this responsibility was shared by all glycopolymer groups in the spleen (**Fig. S3.3J**). Interestingly, p(Man) also showed some indication of immunogenicity from the highest proportion of effector OTI cells induced post-challenge (**Fig. S3.3K**). Overall, all groups resulted in abrogation of type 1 cytokine production in OTI cells upon restimulation with the cognate peptide. IFNγ production was equally suppressed (**Fig. S3.3L**). IL-2 was most highly suppressed with p(Man) (**Fig. S3.3M**). Besides a reduction in the ability of OTI cells to produce the cytokines, reduction in total counts of all cytokine producers was also significant both in the LNs and spleen (**Fig. S3.3N**). p(GluNAc) resulted in the highest IL-10 secretion from OTI cells, indicative of dominant suppressive mechanisms (**Fig. S3.3O**). Even though OTII cells were not suppressed in numbers, they were suppressed functionally as they had a diminished ability to produce IFNγ (**Fig. S3.3P**) and IL-2 both in the LNs and spleen (**Fig. S3.3Q**). In conclusion, antigen-p(GluNAc)/(Gal)/(Man) all were tolerogenic when targeted to the LNs (**table 1**).

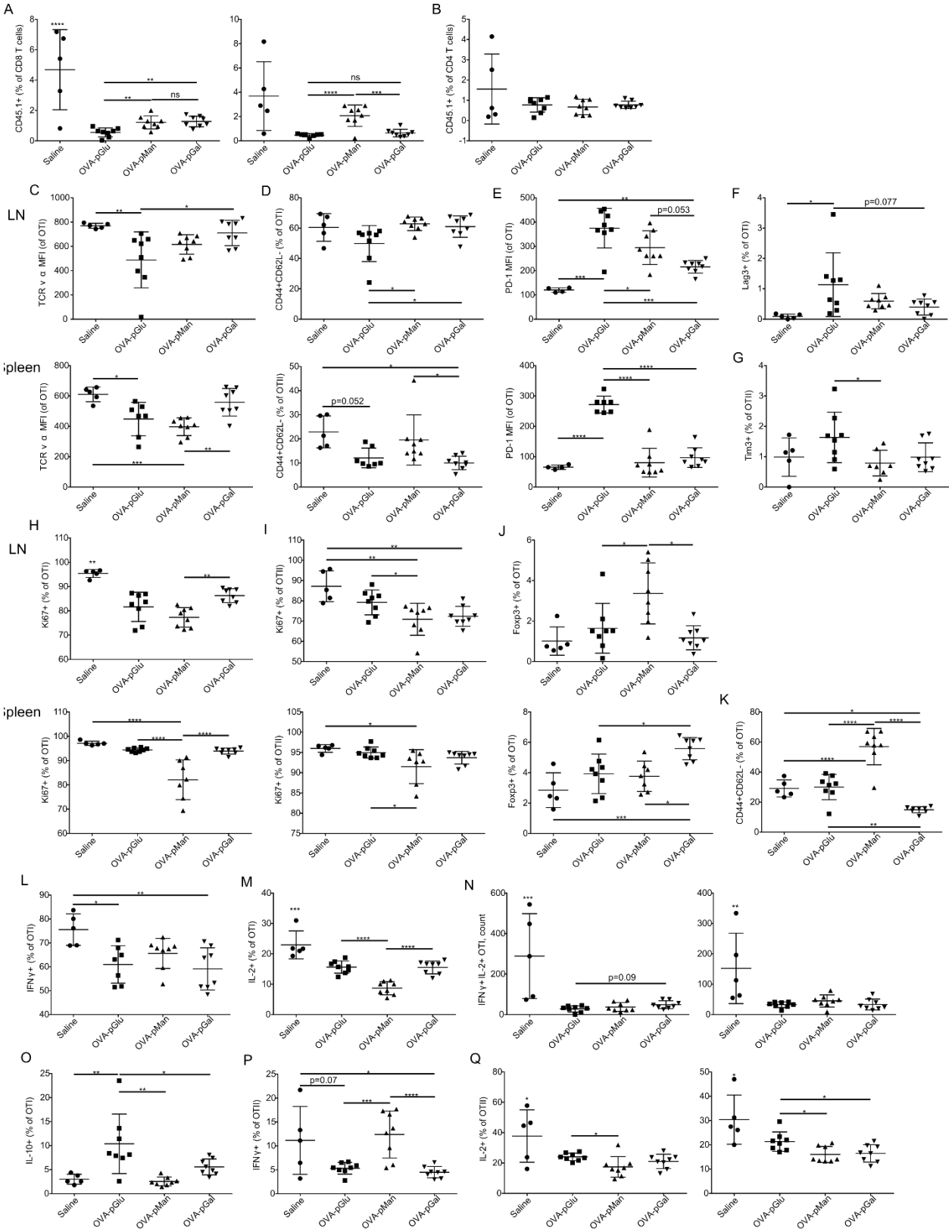

Fig. S3.2. LN-targeted glyco-conjugated antigen results in robust $CD8^+$ T cell suppression, with tolerogenic signatures unique to each glycopolymer. This is a continuation of the experiment **Fig.**

S3.2. *LN-targeted glyco-conjugated antigen results in robust CD8$^+$ T cell suppression, with tolerogenic signatures unique to each glycopolymer (continued)* described two figures before, n=8. Mice received two doses of each OVA-glycopolymer conjugate on days 0 and 7, before receiving a challenge of OVA and LPS on day 16. The T cell phenotype was assessed at day 21. (A) OTI CD8$^+$ T cells in LNs (left) and spleen (right). (B) OTII CD4$^+$ T cells in LNs. (C-E) The OTI CD8$^+$ T cell phenotype is shown in LNs (top) and spleen bottom). (C) MFI of TCR Vα. (D) Effector (CD44$^+$CD62L$^-$) OTI CD8$^+$ T cells in LNs (top) and spleen (bottom). (E) PD-1 MFI of OTI CD8$^+$ T cells. (F) LAG-3$^+$ OTI CD8$^+$ T cells in LNs. (G) Tim-3+ OTII CD4$^+$ T cells. (H-J) The OTI CD8$^+$ T cell phenotype is shown in LNs (top) and spleen (bottom). (H) Ki67$^+$ i.e., proliferating OTI CD8$^+$ T cells. (I) Ki67$^+$ i.e., proliferating OTII CD4$^+$ T cells. (J) Foxp3$^+$ OTI CD8$^+$ T cells. (K) Effector (CD44$^+$CD62L$^-$) OTI CD8$^+$ T cells in spleen. (L) IFNγ$^+$ OTI CD8$^+$ T cells. (M) IL-2$^+$ OTI CD8$^+$ T cells. (N) Number of IFNγ$^+$IL-2$^+$ OTI in LNs (left) and spleen (right). (O) IL-10$^+$ OTI CD8$^+$ T cells in spleen. (P) IFNγ$^+$ OTII CD4$^+$ T cells. (Q) IL-2$^+$ OTII CD4$^+$ T cells in LNs (left) and spleen (right). Statistical differences were determined by one-way ANOVA using Tukey's post hoc test (*$p \leq 0.05$, **$p \leq 0.01$, ***$p \leq 0.005$).

We next investigated whether a circulating antigen-specific regulatory memory was preferentially induced in CD8$^+$ T cells educated by p(GluNAc) conjugated antigen, compared to free antigen, in the dLNs. Surviving OTI cells educated by OVA-p(GluNAc) exhibited a central memory phenotype characterized by high expression of CD44, CD62L and Ly6C in the dLNs (**Fig. 3C, left**). OTI cells from the spleen also shared this phenotype, further validating that local antigen education in the dLNs is able to generate a circulating central memory T cell pool poised for immune suppression (**Fig. 3C, right**) (*70*)(*55*). Not only did OVA-p(GluNAc) lead to more central memory CD8$^+$ T cells overall but the proportion of central memory cells (CD44$^+$CD62L$^+$) compared with effector memory cells (CD44$^+$CD62L$^-$) was significantly higher (**Fig. 3D**).

In contrast to what we observed after challenge, OTI cells in the OVA-p(GluNAc) group had a lower PD-1 expression at steady-state (**Fig. 3E**), possibly because of the absence of chronic inflammatory stimuli and feedback networks that are usually needed to maintain high PD-1 expression and an exhausted state (*56*). Contrarily to PD-1, Lag-3

was expressed at high levels on OTI (**Fig. 3F**), indicating that other mechanisms exist to maintain its expression even in the absence of residual antigen or chronic inflammation, which might be through interaction with scavenger receptor LSECtin (Clec4g) expressed on LECs (*57*).

Importantly, we noticed a significant induction in $CD8^+$ regulatory T cells that were $Foxp3^+$ both in the dLNs and spleen of mice that had been treated with OVA-p(GluNAc) (**Fig. 3G**). Along with antigen-specific $CD4^+$ Tregs, these could also be the source of the heightened IL-10 levels secreted upon antigenic challenge (**Fig. 2I**). Foxp3-expressing $CD8^+$ Tregs have been reported to be important suppressive players in autoimmune disease such as type 1 diabetes and especially in the context of transplantation where donor cells continue to express MHCI for long time periods following the graft (*58*, *59*). The anergic T cells were rescued in their ability to produce IFNγ by the addition of exogenous IL-2 in the restimulation culture supernatant (**Fig. 3H**) (*60*). Since this was an ELISA measurement, it was not possible to point out the identities of the T cells that were most responsible for this reversal in effector function, but it is most likely due to both $CD4^+$ and $CD8^+$ T cells. A similar restoration or increase in cytokine production was observed when cells from the saline and OVA groups were also restimulated in the presence of additional IL-2 (**Fig. S3.2B**). Nonetheless, tolerance induced by s.c. antigen-p(GluNAc) is long-lasting, as evidenced by the resistance to antigenic challenge three months following the tolerization dose (**Fig. S3.2C**).

We next asked whether the antigen-specific $CD8^+$ Tregs induced by OVA-p(GluNAc) were capable of suppressing antigen-specific effector $CD4^+$ T cells. We set up three groups to answer this question. Group (1) received a first adoptive transfer of OTI cells, followed by the OVA-p(GluNAc) tolerizing treatment and antigenic challenge but not the second OTII adoptive transfer (positive control for tolerance). Group (2) did not receive a first adoptive transfer of OTI cells but received the OVA-p(GluNAc) treatment, followed by a second adoptive transfer of OTII cells and challenge (negative control for tolerance). Experimental group (3) received both the first and second adoptive transfers, including OVA-p(GluNAc) treatments and the antigenic challenge. The purpose of the challenge following the second adoptive transfer was to activate the naïve $CD4^+$ T cells into an effector phenotype. Moreover, we chose to wait an additional 10 days prior to sacrificing the mice to give the OTI $CD8^+$ Tregs enough time to encounter the effector OTII cells in the face of a potentially overwhelming LPS-induced inflammatory environment (**Fig. 3I**). We found that OTII cells from group (3) were significantly suppressed compared to OTII cells from group (2) at day 41. OTII cells from the dLNs and spleen of group (3) were recovered in smaller numbers (**Fig. 3J**), more highly expressed Lag-3 (**Fig. 3K**), and were impaired in their ability to produce IL-2 and TNFα cytokines upon restimulation with their cognate peptide (**Fig. 3L, M**). This shows that antigen-specific $CD8^+$ Tregs induced with p(GluNAc)-conjugated antigen are long-lived and able to suppress antigen-specific effector $CD4^+$ T cells, signifying that this strategy may be effective in treating autoimmune disorders or allergies in a therapeutic setting.

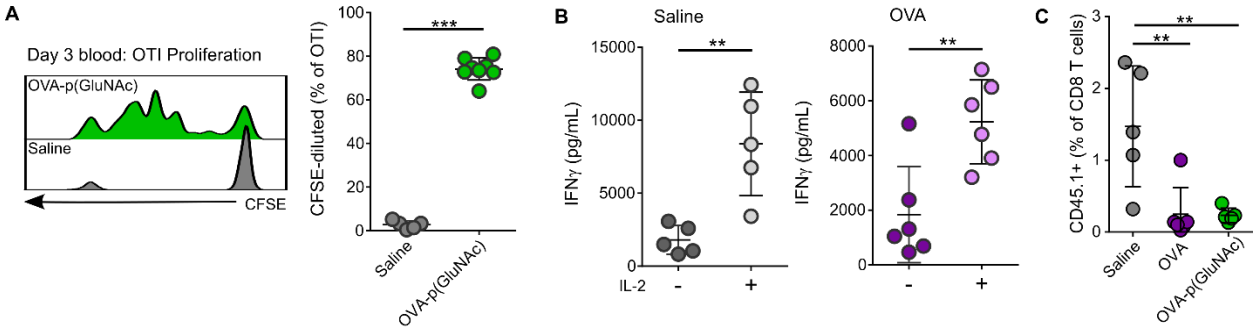

Fig. S3.3. LN-targeted antigen-p(GluNAc) induces extensive initial proliferation of $CD8^+$ T cells and subsequent long-lived tolerogenic memory in the face of an inflammatory challenge. (A) (Left) Representative flow cytometry histograms of the CFSE dilution (proliferation) undergone by OTI cells in the blood of wild-type mice 3 days post-s.c. injection with saline or OVA-p(GluNAc). (Right) Quantitative analysis of the OTI proliferation. (B) Experimental set-up described in Fig. 3A. Splenocytes from the saline or OVA group were restimulated with 100 µg/mL OVA in culture media alone or supplemented with 200 Units/mL (~12 ng/mL) exogenous IL-2, and levels of IFNγ were measured in the supernatant 3 days later by ELISA. (C) Mice were immunized as described in Fig. 3A, received an OVA+LPS challenge 3 months following the second dose, and were sacrificed 5 days post-challenge. % OTI cells recovered from dLNs. Statistical differences were determined by unpaired Student's T test in A, B, and one-way ANOVA using Tukey's post hoc test in C (*$p \leq 0.05$, **$p \leq 0.01$, ***$p \leq 0.001$).

Inhibition of LAG-3 signaling completely reverses CD4⁺ and CD8⁺ T cell tolerance induced by LN-targeted OVA-p(GluNAc)

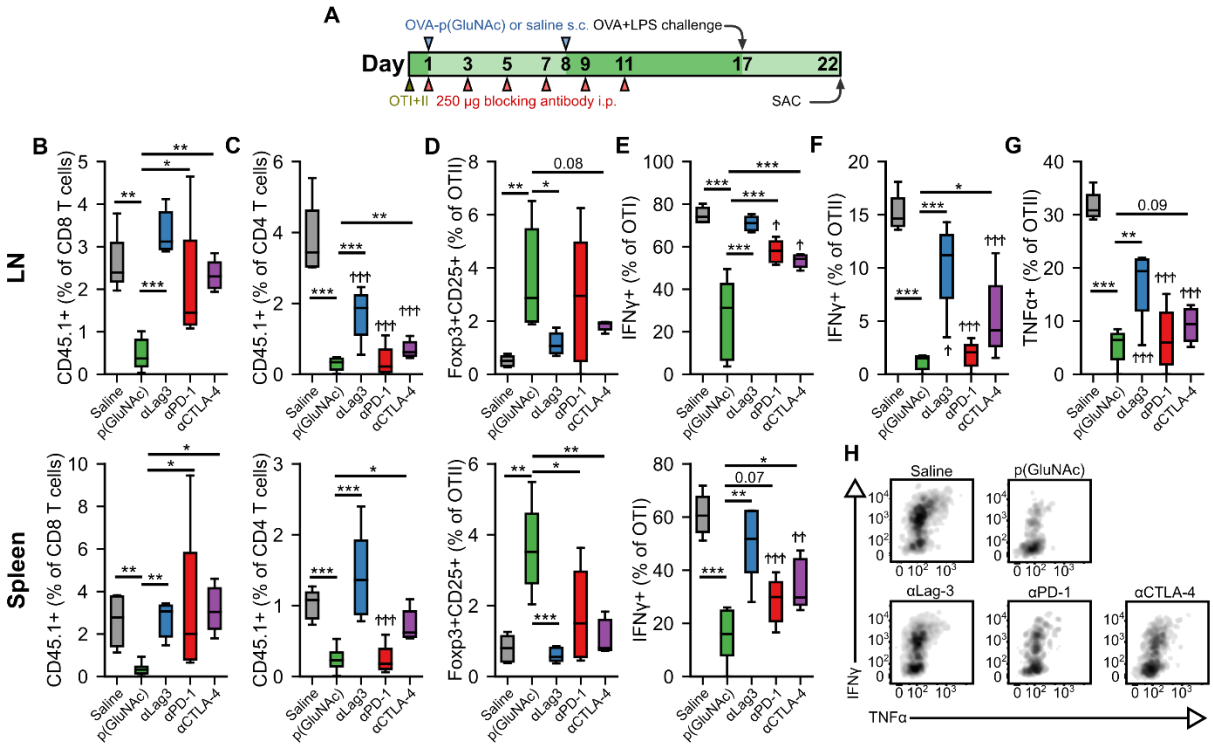

Fig. 4. Inhibition of LAG-3 signaling completely reverses CD4⁺ and CD8⁺ T cell tolerance induced by LN-targeted OVA-p(GluNAc). (A-F) CD45.2⁺ mice that had received an adoptive transfer of $1x10^6$ of both OTI ($CD45.1^+CD3^+CD8^+$) and OTII ($CD45.1^+CD3^+CD4^+$) T cells via i.v. injection, were treated on days 1 and 8 with saline, or 20 µg of OVA-p(GluNAc) s.c. in all four hocks (5 µg per hock). On days 1, 3, 5, 7, 9 and 11, mice were also treated with 250 µg of either αLag-3, αPD-1 or αCTLA-4. On day 17, mice were given a s.c. OVA+LPS challenge, and were sacrificed 5 days later to evaluate the OTI and OTII T cell phenotype in the dLNs and spleen. (B) OTI $CD8^+$ T cells recovered from dLNs (top) and spleen (bottom). (C) OTII $CD4^+$ T cells recovered from dLNs (top) and spleen (bottom). (D) Antigen-specific OTII $CD4^+$ Tregs in dLNs (top) and spleen (bottom). (E) IFNγ secreting OTI $CD4^+$ T cells after a 6-h ex vivo restimulation with $OVA_{257-264}$ peptide from dLNs (top) and spleen (bottom). (F) IFNγ producing OTII $CD4^+$ T cells after a 6-h ex vivo restimulation with $OVA_{323-339}$ peptide. (G) TNFα secreting OTII $CD4^+$ T cells after a 6-h ex vivo restimulation with $OVA_{323-339}$ peptide. (H) Representative flow cytometry plots depicting $IFNγ^+$ and $TNFα^+$ OTI $CD8^+$ T cells from dLNs after a 6-h ex vivo restimulation with $OVA_{257-264}$ peptide. Data are pooled from two independent experiments (n= 5-10), and box-and-whisker plots represent the median, first and third quartiles. Statistical differences were determined by one-way ANOVA using Dunnett's post hoc test. Stars above horizontal bars represent p values with respect to the OVA-p(GluNAc) group (*p ≤ 0.05, **p ≤ 0.01, ***p ≤ 0.001) and † indicate p values with respect to the saline group († p ≤ 0.05, †† p ≤ 0.01, ††† p ≤ 0.001).

We have demonstrated that OTI and OTII cells engage the co-inhibitory module by up-regulating several surface immunosuppressive molecules, including PD-1 and Lag-3. We thus sought to investigate the role of these co-inhibitory signaling pathways in the tolerogenic mechanism of action of LN-targeted antigen-p(GluNAc) glycoconjugates. We set up a tolerance experiment as described above, but where we administered, during the OVA-p(GluNAc) priming window, i.p. injections of 250 µg blocking antibody against either Lag-3, PD-1 or CTLA-4, or no antibody for a total of 6 injections (**Fig. 4A**). We challenged the mice with OVA and LPS 6 days following the last dose of blocking antibody and assessed the impact on the OTI and OTII response 5 days after challenge. The antigen-specific $CD8^+$ T cell deletional tolerance established with OVA-p(GluNAc) was completely ablated to the non-tolerized saline levels when Lag-3, PD-1 or CTLA-4 was blocked, measured in both the dLNs and spleen, though a slightly larger effect was observed with Lag-3 neutralization (**Fig. 4B**). Deletional tolerance was also reversed in the OTII compartment but not to levels seen in the saline-treated mice, except with αLag-3 and αCTLA-4 in the spleen (**Fig. 4C**). Antigen-specific $CD4^+$ Treg induction was also abrogated and diminished back to saline levels, especially with Lag-3 neutralization (**Fig. 4D**). Upon restimulation with $OVA_{257-264}$ peptide, IFNγ production by OTI cells was completely rescued with αLag-3 but only partially with αPD-1 and αCTLA-4 (**Fig. 4E**). Similar trends were observed in IFNγ and TNFα production in the OTII compartment, albeit not to equivalent levels as with OTI (**Fig. 4F-H**). OTII cytokine impairment was not rescued in the spleen, indicating that there is more of a $CD4^+$ T cell local effect in the dLNs (**Fig. S4A, B**). Therefore, these inhibitory signaling pathways investigated have a larger and more important effect in the dLNs and in the antigen-

specific CD8⁺ T cell compartment, suggesting a greater dependence for CD8⁺ T cell tolerance, and also that other axes of tolerance induced by LN-targeted antigen-p(GluNAc) glycoconjugates contribute to CD4⁺ T cell tolerance.

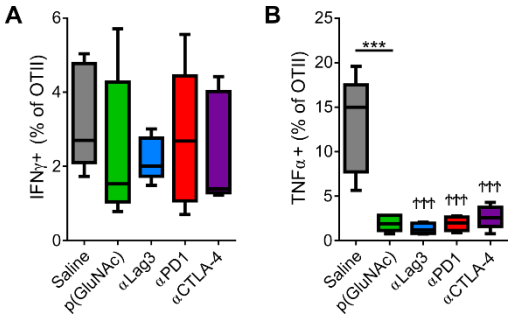

Fig. S4. Antigen-specific CD4⁺ T cell effector function is conserved in the spleen of mice treated with s.c. antigen-p(GluNAc) and antibodies blocking LAG-3, PD-1 and CTLA-4. (A) Experimental set-up described in Fig. 4A. % IFNγ producing splenic OTII cells after a 6-h ex vivo restimulation with $OVA_{323-339}$ peptide. (B) % TNFα secreting splenic OTII cells after a 6-h ex vivo restimulation with $OVA_{323-339}$ peptide. Box-and-whisker plots represent the median, first and third quartiles. Statistical differences were determined by one-way ANOVA using Dunnett's post hoc test. Stars above horizontal bars represent p values with respect to the OVA-p(GluNAc) group (*p ≤ 0.05, **p ≤ 0.01, ***p ≤ 0.001) and † indicate p values with respect to the saline group († p ≤ 0.05, †† p ≤ 0.01, ††† p ≤ 0.001).

OVA-p(GluNAc) presentation to CD4⁺ T cells and cross-presentation to CD8⁺ T cells is mediated by dendritic cells and is independent of intrinsic pathways of presentation

The biodistribution experiment described in Fig. 1 showed that several professional and semi-professional APCs were responsible for antigen-p(GluNAc) uptake in the dLNs but their contribution to antigen presentation to naïve CD4⁺ and CD8⁺ T cells in the dLNs remained to be elucidated. To tease out the contribution of specific APC subsets to antigen presentation, we evaluated the proliferation of OTI and OTII cells 3 days post-s.c. immunization in transgenic mice that lacked the APC subsets of interest or in wild type C57BL/6 mice where those APC subsets were depleted using monoclonal

antibodies. We first focused our attention on macrophages, which we showed are major uptakers (**Fig. 1I**). We compared the initial proliferative response of OTI and OTII cells in wild type mice that received 250 µg of anti-CFS1R depleting antibody or isotype control s.c. on days 0, 3, 6 and 9. These mice received an adoptive transfer of CSFE-labeled OTI and OTII cells on day 7 and 20 µg OVA-p(GluNAc) s.c. on day 8. They were also administered daily i.p. injections of FTY-720 inhibitor to trap the T cells in the LNs in order to maximize exposure of the T cells to peptide-bearing MHC expressing APCs (**Fig. 5A**). A problem with antibody depletion such as with anti-CSF1R is the systemic dissemination associated with i.v. or i.p. injections of the antibody (*61*). In order to limit macrophage depletion to the dLNs, we administered the antibody s.c. in the hocks in the same way that we immunized the animals. We found that, compared with clodronate depletion, this local antibody injection successfully depleted macrophage populations of interest, namely $CD169^+$ SCS and medullary macrophages as well as more deeply located TZMs, in LNs only but left splenic macrophages intact (**Fig. S5A**). We observed massive but similar OTI and OTII proliferation in both the αCSF1R-treated and isotype-treated mice, indicating that LN macrophages are dispensable to the priming of $CD4^+$ and $CD8^+$ T cells in response to s.c. administered antigen-p(GluNAc) (**Fig. 5B**).

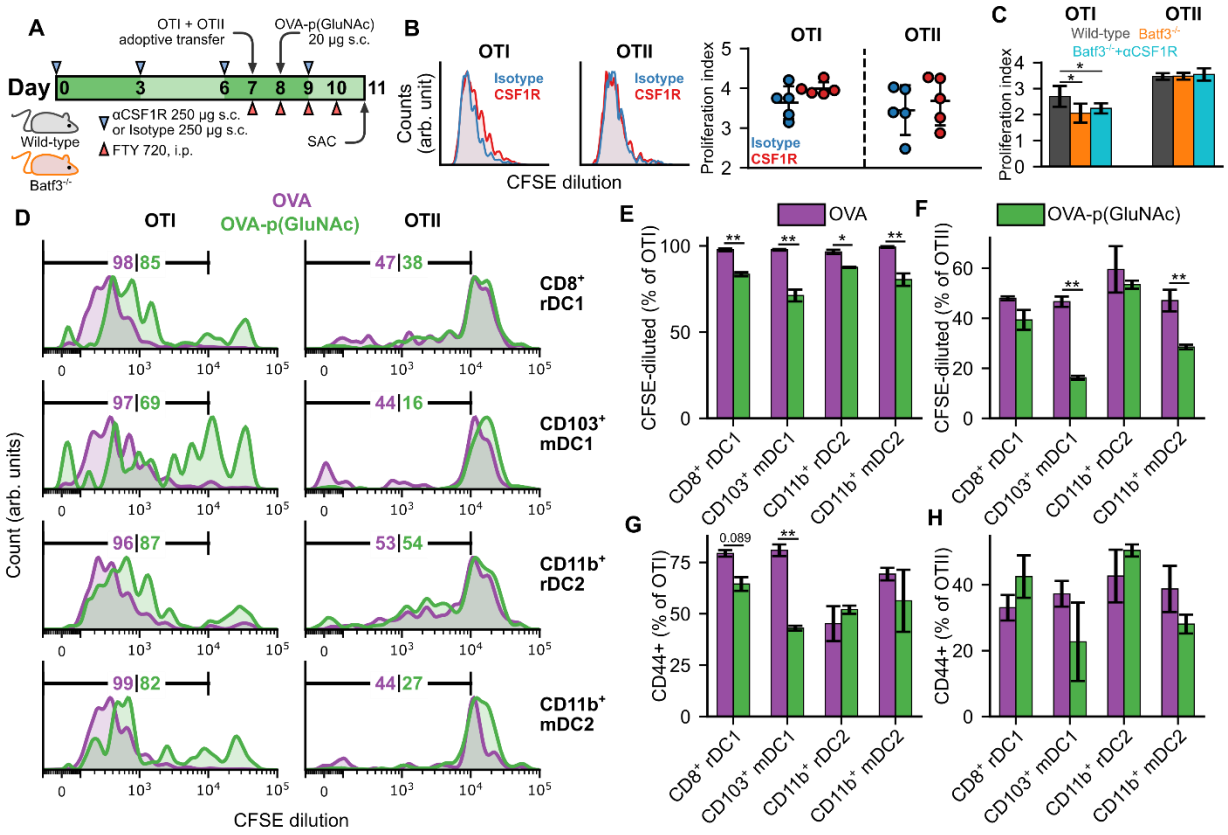

Fig. 5. OVA-p(GluNAc) presentation to CD4$^+$ T cells and cross-presentation to CD8$^+$ T cells is mediated by dendritic cells and is independent of intrinsic pathways of presentation. (A) CD45.2$^+$ mice of wild-type (WT) or Batf3$^{-/-}$ genotype were treated s.c. in all four hocks with 250 µg of αCSF1R or an isotype IgG2a control on days 0, 3, 6 and 9. On day 7, mice received an adoptive transfer of CFSE-labeled OTI CD8$^+$ T and OTII CD4$^+$ T cells via i.v. injection, followed by a s.c. administration of 20 µg OVA-p(GluNAc) on day 8, and daily i.p. injections of FTY 720 inhibitor starting on day 7. On day 11, mice were sacrificed and the dLNs and spleen were examined for OTI and OTII proliferation. (B) (Left) Representative flow cytometry histograms of the CFSE dilution undergone by OTI CD8$^+$ T (left) and OTII CD4$^+$ T (right) cells in the dLNs of WT mice in the isotype control (blue) and αCSF1R (red) conditions. (Right) Quantitative analysis of the OTI and OTII T cell proliferation index in dLNs of WT mice treated as described above. (C) Quantitative analysis of the OTI and OTII T cell proliferation index in dLNs of Batf3$^{-/-}$ mice and WT mice treated as described above. (D-H) DCs were FACS sorted from s.c. LNs (axillary, brachial, inguinal, popliteal, cervical) of WT mice into four populations: CD8$^+$ resident (CD8$^+$ rDC1), CD103$^+$ migratory (CD103$^+$ mDC1), CD11b$^+$ resident (CD11b$^+$ rDC2) and CD11b$^+$ migratory (CD11b$^+$ mDC2), and stimulated in vitro in a 1:1 ratio with CFSE-labeled OTI CD8$^+$ T and OTII CD4$^+$ T cells in the presence of 2 µM of OVA or OVA-p(GluNAc). 3 days later, the OTI and OTII T cells were analyzed for proliferation and activation (CD44$^+$). (D) Representative flow cytometry histograms of the CFSE dilution (numbers indicate percent proliferated) undergone by OTI CD8$^+$ T (left) and OTII CD4$^+$ T (right) cells induced by each DC subset in the OVA (purple) and OVA-p(GluNAc) (green) groups. (E) Quantitative analysis of the OTI CD8$^+$ T proliferation. (F) Quantitative analysis of the OTII CD4$^+$ T proliferation. (G) CD44$^+$ OTI CD8$^+$ T cells. (H) CD44$^+$ OTII CD4$^+$ T cells. The graphs show means ± SD, n= 5. *p ≤ 0.05, **p ≤ 0.01 by two-way ANOVA using Sidak's post hoc test in B, E-H and two-way ANOVA using Tukey's post hoc test in C.

To determine the contribution of another major uptaker, cross-presenting DCs, to s.c. OVA-p(GluNAc) immunization, we used Batf3$^{-/-}$ mice that lack cross-presenting CD8^{+} DCs (*62*). These Batf3$^{-/-}$ mice are on a C57BL/6 background and we verified that there were minimal residual DCs in the LNs of these mice due to compensatory Batf1 expression (**Fig. S5B**). We followed the same schedule as described above (**Fig. 5A**). OTI cells proliferated significantly less in the Batf3$^{-/-}$ mice compared to wild type mice, showing that these DCs play an important role in the cross-presentation of OVA-p(GluNAc); OTII cells were unaffected as anticipated (**Fig. 5C**). To confirm that macrophages were not involved, we further depleted these subsets through s.c. αCSF1R antibody injections in Batf3$^{-/-}$ mice according to the above-described schedule (**Fig. 5A**) and observed no further change in proliferation of OTI cells (**Fig. 5C**). Even though we identified that cross-presenting DCs were important, they are evidently not the only APC involved since we obtained non-negligible residual OTI proliferation in the Batf3$^{-/-}$ mice (**Fig. 5C**).

Because we still saw substantial OTI proliferation in Batf3$^{-/-}$ mice, we turned to FACS sorting and *ex vivo* antigen priming to identify the important DC players. We isolated the subcutaneous LNs (axillary, brachial, inguinal, popliteal, cervical) from wild-type mice and sorted the LN digests into four populations: CD8^{+} resident (CD11c^{+}MHCII^{int}CD8^{+}CD11b^{-}, denoted as CD8^{+} rDC1), CD103^{+} migratory (CD11c^{+}MHCII^{high}CD103^{+}CD11b^{-}, denoted as CD103^{+} mDC1), CD11b^{+} resident (CD11c^{+} MHCII^{int}CD8^{-}CD11b^{+}, denoted as CD11b^{+} rDC2) and CD11b^{+} migratory

(CD11c^{+}MHCII^{high}CD103^{-}CD11b^{+}, denoted as CD11b^{+} mDC2). We then stimulated each population *in vitro* in a 1:1 ratio with CFSE-labeled OTI and OTII cells in the presence of 2 μM of unmodified OVA or OVA-p(GluNAc). 3 days later, the OTI and OTII cells were analyzed for proliferation and activation (antigen experience), measured by dilution of the CFSE dye and CD44 expression, respectively. We made four main observations: (1) OVA-p(GluNAc) presentation elicited mainly a CD8^{+} T cell response (i.e. proliferation and activation), (2) presentation was not limited to cross-presenting DC1s but DC2s were also important, (3) LN-resident subsets were more important than migratory populations for both DC1s and DC2s and, (4) OVA-p(GluNAc) generally resulted in a lower OTI and OTII proliferation and activation compared to unmodified OVA, indicative of an early tolerogenic skewing of T cell fate (**Fig. 5D-H**). We also assessed the ability of LECs (the other major uptaker) to present OVA-p(GluNAc), and, while they did, they did so to a lower extent compared to DCs (**Fig. S5C**). Thus, we established that DCs, alongside being good uptakers, are also the main LN APC involved in presenting s.c. administered antigen-p(GluNAc) to naïve CD4^{+} and CD8^{+} T cells.

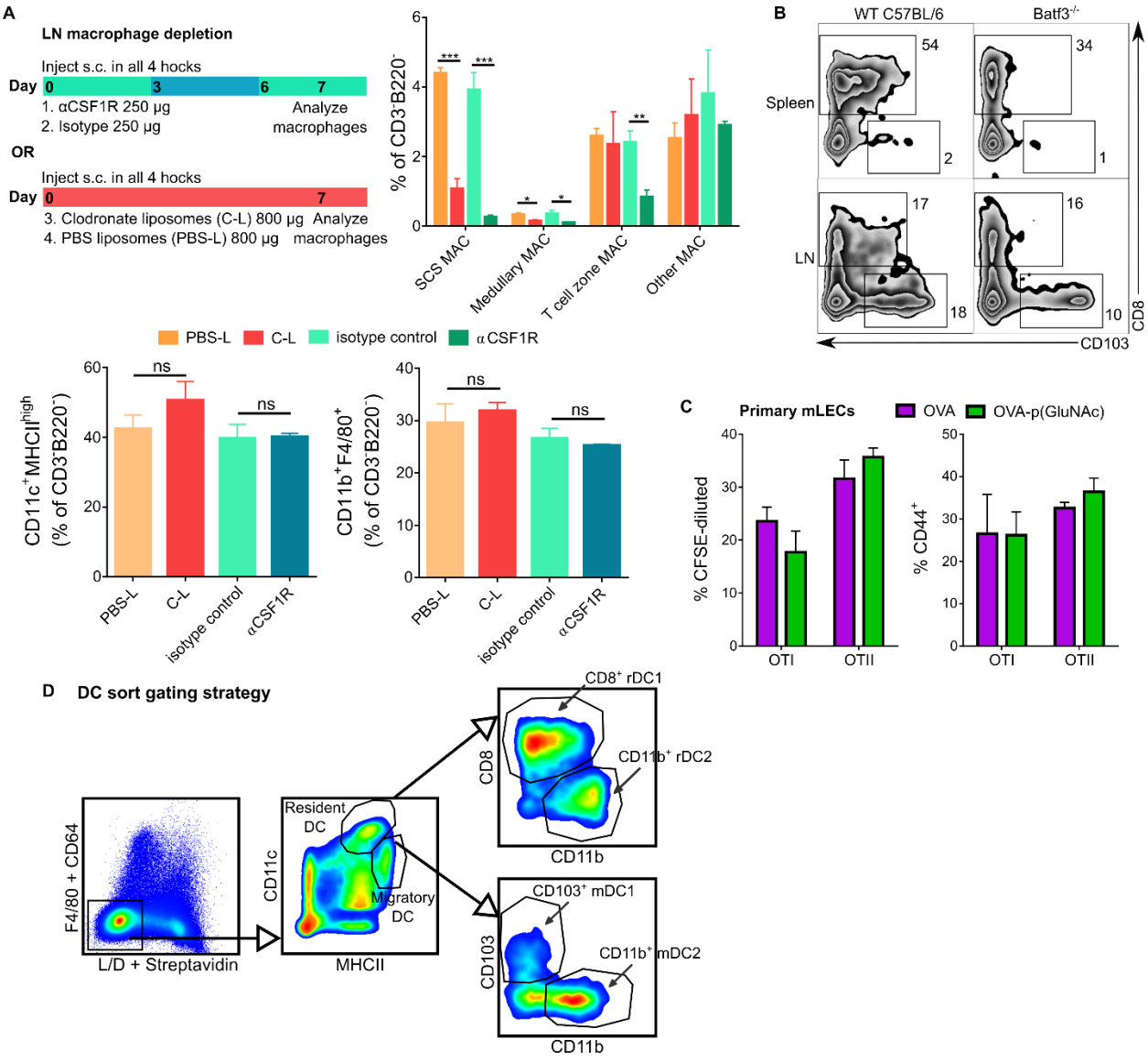

Fig. S5. Macrophage subsets are effectively depleted in the dLNs of mice injected s.c. with αCSF1R, and are not responsible for antigen-p(GluNAc) priming to naïve T cells. (A) (Top left) Wild-type mice were treated s.c. in all four hocks with 250 µg of αCSF1R or an isotype IgG2a control on days 0 and 3, or alternatively, with 800 µg of clodronate or PBS-loaded liposomes on day 0. On day 7, mice were sacrificed and the dLNs and spleen were examined for the presence of macrophage subsets and DCs. (Top right) % macrophages in each subset in the dLNs. (Bottom left) % DCs in the dLNs. (Bottom right) % splenic macrophages. (B) Representative flow cytometry plots showing the reduction, but not complete absence, of $CD8^+$ rDC1 and $CD103^+$ mDC1 in the s.c. LN and spleen of $Batf3^{-/-}$ mice. (C) LN-LECs were isolated from wild-type mice and expanded ex vivo before they were stimulated in a 1:1 ratio with CFSE-labeled OTI and OTII cells in the presence of 2 µM of unmodified OVA or OVA-p(GluNAc). 3 days later, the OTI and OTII cells were analyzed for proliferation and activation ($CD44^+$). Quantitative analysis of the OTI and OTII proliferation (left) and activation quantified by % $CD44^+$ (right) in the conditions described above. (D) Representative flow cytometry plots showing the gating strategy used for sorting LNs into the four DC populations described in Fig.

Fig. S5. Macrophage subsets are effectively depleted in the dLNs of mice injected s.c. with αCSF1R, and are not responsible for antigen-p(GluNAc) priming to naïve T cells (continued) 5E-I. The graphs show means ± SD. Statistical differences were determined by two-way ANOVA using Tukey's post hoc test in A (top right) and one-way ANOVA using Tukey's post hoc test in A (bottom) and C (*p ≤ 0.05, **p ≤ 0.01).

To test the efficacy of prophylactic LN-targeted synthetically glycosylated antigen in an autoimmune disease model, we turned to the spontaneous non-obese diabetic (NOD) mouse model. This is a difficult model to achieve prophylactic or therapeutic efficacy in because, similar to the disease condition in humans, it is associated with a considerable polyspecific T cell response as the pancreatic β islet cell destruction is mediated by $CD4^+$ and $CD8^+$ T cells targeting several antigens presented by different MHC molecules (*63*)(*64*)(*65*). The polyspecificity of the response is also accompanied by a range of TCR avidities that are correlated with pathogenic potential of specific clones (*66*). There is a big gender discrepancy in the spontaneous development of T1D in these mice, where despite having higher susceptibility to onset, females still develop glycemia at a rate of at 80-90% at most with an earlier onset at about 12 weeks of age (*67*). For prophylactic efficacy, it is crucial to treat female NOD mice before this onset window such that auto-reactive clones already present in the prediabetic mice can be suppressed in their effector and islet destruction function (*66*).

We picked the β insulin antigen for conjugating to our glycopolymers, specifically the 9-23 epitope on the protein. In prediabetic NOD mice, 50% of the T-cell clones established from islet-infiltrating lymphocytes were insulin-specific and the majority of these clones recognized the insulin B:9-23 (ins_{9-23}) epitope (*68*). Ins_{9-23} bound to MHCII (I-Ag7) has been shown to be recognized by $CD4^+$ T cells in the NOD mice (*69*). This

peptide sequence has also been shown to stimulate $CD8^+$ T cells in the context of MHCI HLA molecules to varying levels of avidity (*70*)(*71*).

$Ins_{9\text{-}23}$ needed to be modified with cysteine sequence (GGSGCRG) for successful conjugation to p(GluNAc) and p(Gal). This is contrast with full length proteins that are conjugated to the glycopolymers via their free amines in a more straightforward fashion (*24*). These conjugates yielded a molecular weight of 50- 150 kDa, that can be purified from unconjugated peptide using size exclusion chromatography as described before; pooled fractions ran on an SDS-page gel are shown (**Fig. 6A**). Young four-week-old female NOD mice were prophylactically treated s.c. with a total of four doses of insB, $ins_{9\text{-}23}$-p(GluNAc), $ins_{9\text{-}23}$-pGal or saline every two weeks until they reached 10 weeks of age, and glycemia levels were monitored for up to 20 weeks through tail bleeds. Mice that reached 250 mg/dL units for three consecutive days were euthanized. There was overall no significant difference in onset of glycemia between the saline-treated mice and the ins-treated groups (**Fig. 6B**). Only ~60% mice in the intreated group spontaneously developed diabetes, which makes interpretation of a prophylactic benefit in this experiment difficult since it is hard to know if the mice that never became glycemic never became so because of the model or because the treatment was successful in preventing the onset (**Fig. 6C**). In the earlier weeks before week 17, we observed that $ins_{9\text{-}23}$-p(GluNAc) treated mice experienced a significant delay in onset by three weeks compared with $ins_{9\text{-}23}$ treated mice (**Fig. 6D**). This effect was however not lasting since more mice in the $ins_{9\text{-}23}$-p(GluNAc) group eventually became glycemic, leading differences between groups to disappear. This could be due to our prior findings that LN-targeted antigen glyco-conjugate does not result in as effective as a $CD4^+$ T cell

suppression compared with the CD8⁺ T cell compartment, accounting for the low prophylactic efficacy of s.c. glyco-modified antigen in the NOD model of type 1 diabetes.

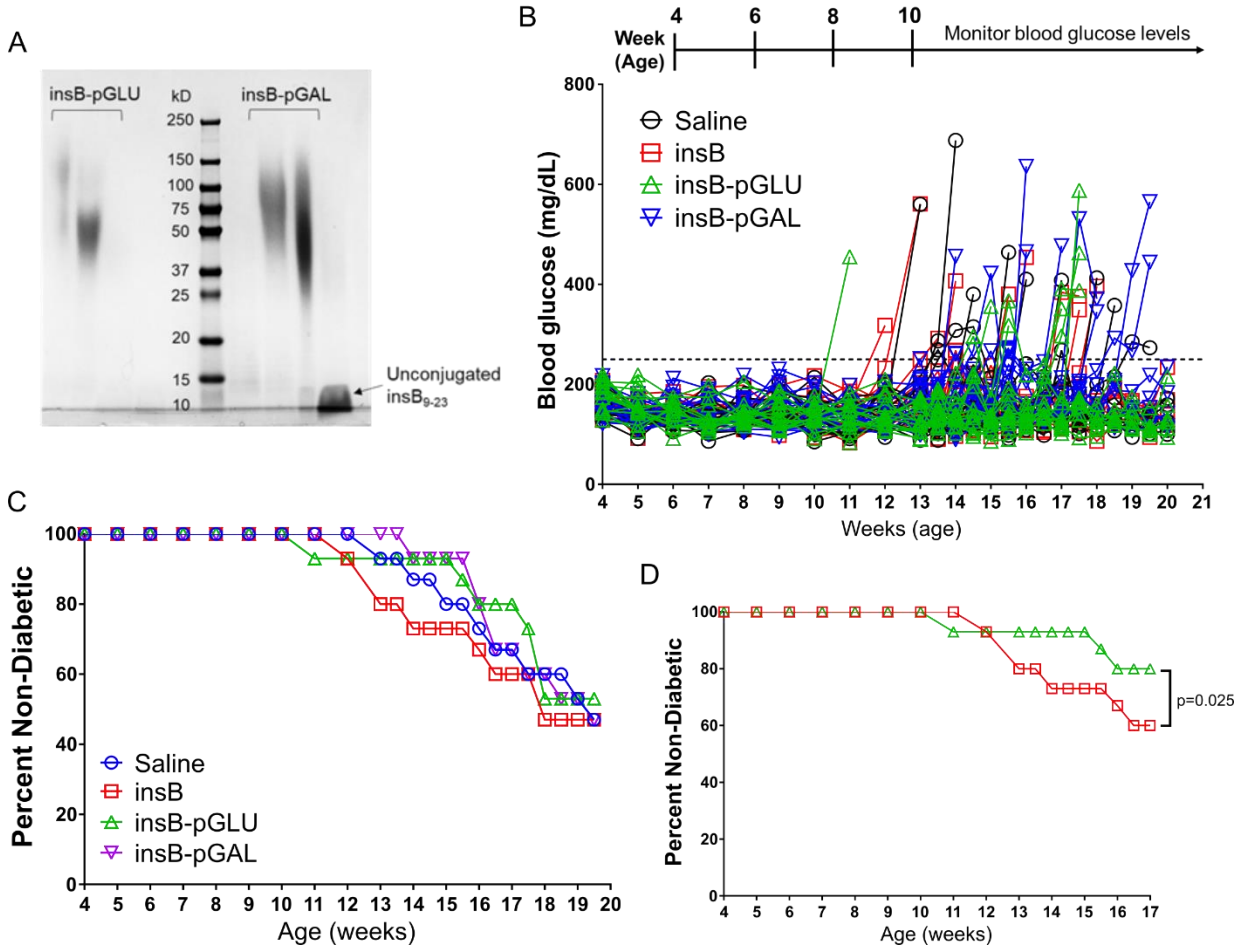

Fig. 6. LN-targeted glyco-conjugated antigen modestly delays the onset of type 1 diabetes in the spontaneous NOD mouse model. (A) Non-reducing SDS-page gel showing the position of the pooled size exclusion peaks of insB-p(GluNAc) and ins-pGal w.r.t unconjugated peptide. Both lanes for each conjugate were further pooled and concentrated for concentration measurement and further use. (B-D) NOD mice were immunized s.c. in all hocks with 0.5 ug of unconjugated insB, insB-p(GluNAc) or ins-pGal or saline as control starting at week 4 of age, for every two weeks until they reached week 10 in age. They were monitored for glycemia once to twice a week until they all reached week 20 in age. (B) Blood (GluNAc)cose levels in blood in mg/dL. Mice were euthanized when the level was 250 or above for three consecutive days. (C) % non-diabetic mice. (D) % non-diabetic mice in insB and ins-p(GluNAc) groups only until week 17. Statistical differences were determined by one-way ANOVA using Tukey's post hoc test (*p ≤ 0.05, **p ≤ 0.01, ***p ≤ 0.005).

Discussion

Our previous work has demonstrated that synthetically glycosylated antigen may be useful as an inverse vaccine platform for inducing antigen-specific tolerance (*24*). The versatility and mild conditions of the antigen conjugation chemistry to our glycopolymer ensure that the strategy can be universally applied to any antigen that contains a native or engineered primary amine. A synthetically-glycosylated inverse vaccine has now entered phase I clinical trials for inducing tolerance in the context of celiac disease (ClinicalTrials.gov Identifier: NCT04248855). Although our previous work investigated targeting hepatic APCs (*24*), in this study we investigate tolerance induction mediated by targeting LN-resident APCs accessed through s.c. injection.

LNs are the site of tightly orchestrated responses that can be guided toward immunity or tolerance, depending on context (*72*). Similar to the liver, antigen dose and frequency, formulation and co-formulation with modulatory signals, as well as specific APC players determine the immunological response (*73*). Here, we focus on understanding the mechanisms of action of synthetically glycosylated inverse vaccines on LN-resident APCs, and to what extent dose and dose frequency may need to be adapted to achieve tolerance. Delivering the antigen conjugated to a glycopolymer may be beneficial for lymphatic absorption and channeling to LN-resident APCs and then for uptake via binding to their scavenger receptors to promote tolerance.

When delivered s.c., antigen conjugated to p(GluNAc), in this case OVA-p(GluNAc), rapidly drains and accumulates in the dLNs, to a significantly higher extent than unmodified OVA, which is consistent with particle filtration dynamics in the dLNs. Glyco-polymerization alters the physicochemical properties of the antigen in important ways: the molecular weight is increased by 30-70 kDa, resulting in a net neutrally charged, branched polymeric particle. These nanoparticles are of optimal molecular weight and size to drain into the lymphatics and accumulate in the dLNs, as opposed to smaller particles that are rapidly filtered through floor lymphatic endothelial cells and into systemic circulation via high endothelial venules, or to larger microparticles that are preferentially captured by migratory APCs at the site of injection for subsequent trafficking to the dLNs (*26*, *27*).

T cell interaction kinetics with APCs bearing peptide MHC (pMHC) antigen in the LN have been extensively studied. In a non-inflammatory scenario, where the unique priming signal is the TCR-pMHC interaction, immune synapses are incomplete, making APC-T cell interactions very transient (*28*). Thus, it is of utmost importance to ensure higher availability of antigen in the LN to generate robust antigen-specific priming of T cells from short but numerous APC-T cell interactions even if a tolerogenic consequence is desired. Strategies such as non-bolus injection modes, sustained-release hydrogels or albumin fusion have been explored to improve LN retention of antigen (*52*, *74*, *75*). The significantly higher accumulation of antigen-p(GluNAc) means that the threshold for naïve T cell activation can be lowered in the dLNs.

Canonical Foxp3$^+$CD25$^+$ Tregs play a crucial role in ensuring the maintenance of tolerance and, more recently, antigen-specific Tregs induced in the periphery are being increasingly recognized as important regulators (*76*–*78*). We have also shown the dependence of LN-targeted suppression on long-lived CD8$^+$ regulatory T cell subsets (**Fig. 3I-M**). These constitute an important arm in the natural control of autoimmunity (*79*) but can also be induced under different treatment conditions that have mostly been investigated in immune-privileged sites (*80*) and in the context of transplantation and peptide immunotherapy in lupus (*81*, *82*). The ability of antigen-p(GluNAc) to result in broad antigen-specific regulatory and suppressor subsets of T cells would be a highly desirable property.

There were noticeable differences in the response of antigen-specific CD4$^+$ and CD8$^+$ T cells to blockade of the distinct co-inhibitory pathways (Lag-3, PD-1 and CTLA-4). CD8$^+$ T cell tolerance was significantly more ablated when these signaling pathways were disrupted, indicating a higher dependence on these signaling pathways for tolerance induction (**Fig. 4**). All three pathways were found to be important to some extent for CD4$^+$ and CD8$^+$ T cell tolerance, a result that did not surprise us given that many of these co-inhibitory molecules form part of an immunosuppressive module co-regulated by overlapping signaling such as IL-27 (*48*). Lag-3 was found to be an essential suppressive pathway responsible for inducing deletional tolerance in CD8$^+$ T cells in both the dLNs and spleen and in CD4$^+$ T cells in the spleen (*115*). This also suggested to us that other signaling axes exist to ensure CD4$^+$ T cell peripheral tolerance is maintained. One example is considering how Lag-3 expressed on CD4$^+$ T cells interacts

with its ligands in the LN microenvironment. We have shown that OVA-p(GluNAc)-educated OTII cells express higher Lag-3 levels (**Fig. 2N**). Lag-3 binds to MHCII on various APCs, an interaction that contributes to $CD4^+$ T cell activation and is not blocked by the αLag-3 (C9B7W) antibody that we used in our experiments (*85*). Lag-3 on T cells has also been reported to interact with LSECtin that is highly expressed on LN-LECs (**Fig. 2**) (*57*). Another recently-identified ligand for Lag-3 is Fibrinogen-like protein 1, but is not expressed in LNs although it is dominantly expressed in the liver (*86*).

This is the first report of local LN macrophage depletion using a subcutaneous injection of CSF-1R depleting antibody, but s.c. administration is a recently validated strategy for the locoregional enrichment of blocking antibodies such as checkpoint antibodies in the sentinel LNs for tumor control (*87*). Francis et al. demonstrate that s.c. administration of αPD-1 or αCTLA-4 antibodies ipsilateral to the primary tumor results in accumulation in the local dLNs and anti-tumor efficacy but also a systemic abscopal effect. While we observed a robust decrease in macrophage subsets in the dLNs, we did not suppress macrophages in the spleen, indicating that antibodies rapidly drain to and are retained in the dLNs where they exert a local effect, leading to a systemic immunological response (*88*). While our data showed a dispensable role for macrophages in glycoconjugate-medicated antigen priming, it is possible that macrophages relay the acquired antigen to DCs for further processing and presentation onto MHC, as has been reported (*89*, *90*). This coordinated effort and transfer of antigen between different APC subsets through vesicular routes has been evidenced under steady-state (*91*) and,

more recently, elegantly demonstrated in the context of sentinel LN priming in cancer (*92*).

Dendritic cells have unique and varied intrinsic pathways of antigen presentation but can also be highly cooperative depending on context (*93*). For example, mannose receptor-directed antigen is channeled to early endosomes and the cross-presentation pathway (*94*). Even though the current paradigm is that DC1s (LN-resident $CD8^+$ or migratory $CD103^+$) are specialized in cross-presenting antigen to $CD8^+$ T cells, while DC2s (LN-resident or migratory $CD11b^+$) are better equipped to present to $CD4^+$ T cells, all DCs are capable of presenting to both $CD4^+$ and $CD8^+$ T cells given the right circumstances dictated by location (both anatomically and within the LN), antigen dose and administration route, and inflammatory stimulus (*30*, *95–102*). Consistent with this, we found that *ex vivo* priming with OVA-p(GluNAc) by DC1s and DC2s resulted in both OTI and OTII expansion and activation but primarily a $CD8^+$ T cell response with at least a two-fold difference in OTI proliferation, compared with OTII (**Fig. 5D-F**).

The divergence in $CD4^+$ and $CD8^+$ T cell proliferation is not surprising given that they have very different activation requirements (*103*). For instance, $CD4^+$ T cell proliferation is more dependent on prolonged antigen exposure compared to $CD8^+$ T cells (*104*). The APC antigen uptake and distribution landscape is also instrumental to regulating differential priming (*105*, *106*). Furthermore, while $CD4^+$ T cells are required for optimal $CD8^+$ T cell activation during a primary activation or memory recall response and for

survival (*107*, *108*), $CD8^+$ T cell memory formation has been shown to be intrinsic and $CD4^+$ T cell independent (*109*). In the context of peripheral tolerance, $CD4^+$ T cell help is usually an instigator of autoreactive $CD8^+$ T cell effector function in several autoimmune conditions ranging from type 1 diabetes to vitiligo and is undesirable in transplant tolerance (*110–114*). Since the antigen-specific $CD4^+$ and $CD8^+$ T cells were both in contact with the sorted DCs at the same time in our ex vivo sorting and priming experiment, the $CD4^+$ T cell help provided by OTII cells could be an additional factor that contributed to the OTI proliferation (**Fig. 5D, E**). The OTI and OTII proliferation was elicited by both sorted DC1 and DC2 populations, especially LN-resident subsets, which is what we expected given that OVA-p(GluNAc) drains rapidly to the LN and is not retained at the s.c. site of injection 72 h post-injection, which is the timeframe for when migratory DCs make their way to dLNs with captured antigen (**Fig. S1A**).

In conclusion, in this work, we present a novel approach of inducing antigen-specific tolerance using synthetically glycosylated antigen via peripheral s.c. routes of targeting. We leverage the biophysical, biochemical and immunological environment of the LN and its cellular players to induce robust and lasting tolerance to exogenous antigen. We believe this approach will be particularly beneficial in therapies where the orchestration of immune tolerance via a peripheral route is desired, such as in allergen subcutaneous immunotherapy.

Materials and Methods

Study Design

The objective of this study was to target synthetically glycosylated antigen to LN APCs to induce antigen-specific immunological tolerance, and investigate the molecular mechanisms of tolerance. We delivered p(GluNAc)-conjugated antigen to dLNs via s.c. administration, and characterized the antigen distribution, retention and uptake landscape, as well as downstream effects on the antigen-specific T cell response. We furthermore elucidated the contribution of specific APC subsets, T cell regulatory populations, and co-stimulatory signaling axes to the maintenance of tolerance. Flow cytometry and fluorescence microscopy were the primary analytical techniques used, and the OTI and OTII TCR-transgenic system was the main model studied. The number of experimental replicated are indicated in figure legends.

Mice

Mice were maintained in a pathogen-free facility at the University of Chicago. All experiments and procedures in this study were performed with the approval of the Institutional Animal Care and Use Committee at the University of Chicago. Female C57BL/6 mice, aged 7-12 weeks, were purchased from Charles Rivers (strain code: 027). OTI (JAX code: 003831) and OTII (JAX code: 004194) were crossed to CD45.1^{+} mice (JAX code: 002014) to yield congenically labeled OTI and OTII mice. Batf3$^{-/-}$ mice were originally a donation from Justin P. Kline's laboratory at the University of Chicago, and subsequently, bred in house.

OVA-p(GluNAc) synthesis and characterization

Detailed synthesis and characterization methods can be found in (*24*). Briefly, p(GluNAc) was synthesized using a reversible addition-fragmentation chain transfer (RAFT) polymerization using an azide-modified RAFT agent, a biologically inert comonomer (N-(2-hydroxypropyl) methacrylamide, HPMA) and the glycosylated methacrylamide N-acetyl glucosamine monomer. We use a copper-free click-based reaction in aqueous solvent at room temperature to conjugate the polymers to antigens to preserve the antigen's tertiary structure and function. To this end, the antigen is modified at terminal amines with an amine-reactive heterobifunctional bicyclononyne-decorated linker. Upon conjugation, this linker forms a reduction-sensitive chemical bond that is stable in serum but is cleaved when the conjugate encounters the reductive environment of the endosome inside the antigen presenting cell. The polymer ranges in size from 30-60 kDa, and can be visualized on a non-reducing SDS-page gel after conjugation to antigen. Conjugated OVA-p(GluNAc) was separated from unconjugated OVA by size exclusion in PBS buffer and the concentration of conjugated OVA was quantified by boiling the conjugate in reducing Laemmli buffer and running it on a reducing SDS-page gel alongside unmodified OVA samples of known concentrations. Finally, OVA-p(GluNAc) was tested for the presence of endotoxin before being used in tolerance experiments. For the synthesis of the fluorescent OVA_{647}-p(GluNAc) conjugate, Alexa Fluor™ 647 NHS ester was first conjugated to OVA before the click linker step.

S.c. tolerization

Unless otherwise specified, mice were injected s.c. in all four hocks at a dose of 5 μg of OVA antigen and volume of 20 μL per hock, under isoflurane anesthesia.

Whole-organ fluorescence imaging of LNs

15 h after s.c. hock injections, whole cardiac perfusion was performed with PBS (pH= 7.4) under isoflurane inhalation anesthesia, after which the liver and draining axillary and popliteal LNs were isolated. The organs were cleaned by removing extra fatty tissue and washed in PBS to remove blood that could contribute to auto-fluorescence. They were imaged on the In Vivo Imaging System (IVIS, PerkinElmer) using an excitation wavelength of 630 nm and an emission wavelength of 650 nm. For the time-dependent antigen retention study, mice were sacrificed without perfusion at timepoints of 1 h, 6 h, 15 h, 24 h, 48 h and 72 h post-injection and draining popliteal LNs were isolated and imaged using the same procedure described above.

LN APC biodistribution

24 h after s.c. hock injection, mice were sacrificed and draining LNs were isolated. The LN capsule was gently poked with 25 G needles. They were digested at 37 ^{0}C, first with 1 mg/mL Collagenase IV and 40 µg/mL DNAse1 for 30 min, followed by 3.3 mg/mL Collagenase D and 40 µg/mL DNAse1 in 300 µL of DMEM (Gibco 11966025) supplemented with 1.2 mM $CaCl_2$ for 15 min with magnetic stirring. The LNs were gently pipetted 100 times using an electronic pipette. An equal volume of ice-cold 10 mM EDTA in PBS supplemented with 1% FBS was added to the digestion mixes to quench the enzymatic reaction for a final concentration of 5 mM EDTA, followed by pipetting for another 100 times. The cell suspensions were filtered through a 70 µM filter to generate a single cell suspension which was stained for flow cytometry. Antibodies against the following markers were used: CD45, CD31, GP38, CD21/35, B220, CD3, CD11c, CD11b, CD8, CD103, CD169, Mertk, CX3CR1, F4/80 and MHCII.

Whole mount confocal imaging of LN

Popliteal lymph nodes were fixed in Zinc (pH= 6.5) at 4 ^{0}C for 24 h. The LNs were washed with TBS and permeabilized with filtered TBS 1% Triton X-100 5% DMSO (pH= 7.4) for 12 h at RT to degrade intracellular fat that could interfere with the staining. The LNs were washed and gently digested with a mixture of Collagenase IV (1 mg/mL), DNAse1 (40 µg/ml) and Collagenase D (3.3 mg/mL) enzymes in 0.5 % casein in TBS supplemented with 5 mM $CaCl_2$ for 45 min at room temperature. LNs were incubated with unlabeled or biotinylated primary antibodies at 1 µg/mL in 0.5 % casein in TBS overnight at 4 ^{0}C. 10 µg of DNAse1 was added to the primary antibody mix as an added precaution. After thoroughly washing with 0.1% Tween TBS, followed by TBS, the LNs were gently dried and stained with secondary labeled or streptavidin conjugated $F(ab)_2$ at 3.75 µg/mL in 0.5 % casein in TBS overnight at 4 ^{0}C. The LNs were thoroughly washed, dried, and dehydrated by sequentially washing in 70%, 95% and finally 100% ethanol. LNs were gently compressed on a microscopy slide, mounted with 25 mg/mL of propylgalate in a 2:1 solution of benzyl benzoate in benzyl alcohol (BABB). The cover slip was placed on the LN and edges were sealed using silicone glue. The mounted LNs were imaged using an Olympus confocal microscope equipped with CellSense software. Images were acquired using four lasers (488 nm, 594 nm, 647 nm and 750 nm excitation wavelengths) and a confocal stack, and analyzed using Imaris 9.1.2 software.

Adoptive transfer of OTI $CD8^+$ and OTII $CD4^+$ T cells

$CD8^+$ T cells were isolated from the spleen and s.c. LNs (axillary, brachial, inguinal, popliteal, cervical) of OTI mice using the EasySep $CD8^+$ isolation kit (Stemcell 19853).

Similarly, $CD4^+$ T cells were isolated from the spleen and s.c. LNs of OTII mice using the EasySep $CD4^+$ isolation kit (Stemcell 19852). Spleens were first mashed into a single cell suspension and lysed with ACK lysis buffer (Gibco A1049201). LNs were digested with 1 mg/mL Ca^{2+} supplemented Collagenase D (Roche 11088866001) for 45 min at 37 ^{0}C and gently mashed into a single cell suspension. Suspensions from the LNs and spleen were pooled and subjected to magnetic cell isolation using the kits. The OTI and OTII cells were labeled with 1 μM CFSE for 6 min at RT, washed with sterile PBS buffer, quantified and resuspended in saline buffer for injection. $5x10^5$ - $1x10^6$ cells of each OTI and OTII cells were injected into mice via i.v. tail vein injection.

Challenge following adoptive transfer and tolerization

Mice received an inflammatory s.c. challenge of 20 ug EndoFit OVA (InvivoGen vac-pova) and 50 ng LPS (Sigma) total in all four hocks under isoflurane anesthesia. Mice were sacrificed under CO_2 inhalation 5 days following challenge.

Preparation of cell suspensions for flow cytometry analysis

Draining s.c. LNs (axillary and popliteal) and the spleen were isolated from mice. Spleens were first mashed into a single cell suspension with plain DMEM media (Gibco 11966025), filtered through 70 μM cell strainers, and lysed with ACK lysis buffer (Gibco A1049201). LNs were digested with 1 mg/mL Ca^{2+} supplemented Collagenase D (Roche 11088866001) for 45 min at 37 ^{0}C and gently mashed into a single cell suspension, also with DMEM and through 70 μM cell strainers. The cells were resuspended in IMDM media (Gibco 12440053), supplemented with 10% FBS and 1% Penicillin-Streptomycin (Gibco 15140122), and counted using a LUNA automated

fluorescent cell counter (Logos biosystems). Cells were seeded at a count of $1x10^6$ - $3x10^6$ per well in 96-well round-bottom plates for subsequent antibody staining for flow cytometry.

Ex vivo antigen-specific restimulation

LN and spleen single-cell suspensions were seeded at a count of $1x10^6$ - $3x10^6$ per well in non-tissue culture treated round-bottom 96-well plates (Celltreat 229590), and stimulated ex vivo at 37 ^{0}C for 2 h with either $OVA_{257-264}$ peptide (Genscript) at a final concentration of 1 µg/mL, or $OVA_{323-339}$ peptide (Genscript) at 2 µg/mL, followed by Brefeldin A at a final concentration of 5 µg/mL for another 4 h. The cells were then washed with PBS before proceeding with cytokine antibody staining for flow cytometry. For long-term restimulations, grade V OVA (Sigma A5503) was added to cells at a final concentration of 100 µg/mL for 4 days. The culture supernatant was collected and frozen for subsequent cytokine ELISA and LegendPlex™ assays.

In vivo blockade of co-stimulatory molecules

Mice were administered via i.p. injection 250 µg of either αLag-3 (BioXCell BE0174, clone C9B7W), αPD-1 (BioXCell BE0146, clone RMP1-14) or αCTLA-4 (BioXCell BE0164, clone 9D9) on days 1, 3, 5, 7, 9 and 11 for a total of 6 injections.

In vivo macrophage depletion

For the depletion study in Fig. S5A, mice were treated s.c. in all four hocks with 250 µg of αCSF1R or an isotype IgG2a control once only on day 0 and sacrificed on day 7 to evaluate macrophage depletion. For the experiment described in Fig. 5A, mice were

treated s.c. in all four hocks with 250 µg of αCSF1R (BioXCell BE0213, clone AFS98) or an isotype IgG2a control (BioXCell BE0089, clone 2A3) on days 0, 3, 6 and 9.

Ex vivo DC sorting and priming

Pooled s.c. LNs (axillary, brachial, inguinal, popliteal, cervical) were isolated from wild-type mice, and digested into a single-cell suspension as described in the "LN APC biodistribution" section above. All reagents were kept sterile and all procedures were handled in a biosafety hood when possible. The cell suspension was washed with MACS buffer and the following biotinylated antibodies were added at a final concentration of 2 µg/mL to deplete specific cell populations: αCD3 (T cells), αCD19 (B cells), αB220 (B cells), αGr-1 (neutrophils), and αNK1.1 (NK cells). The cells were washed with MACS buffer, resuspended with Dynabeads Biotin Binder (Invitrogen 11047), and placed in a magnet. The depleted LN suspension was carefully pipetted out of the tube and washed with MACS buffer before proceeding with antibody staining for FACS. The following antibodies were added at these specified dilutions in FACS buffer: Streptavidin – APC-Cy7 (1:400), CD64 – PE-Cy7 (1:100), F4/80 – PE-Cy7 (1:100), CD11c – APC (1:200), MHCII – PacBlue (1:800), CD8α – PerCP-Cy5.5 (1:200), CD103 – PE (1:100), and CD11b – BV510 (1:400). The cells were washed before staining with near-IR Live-Dead dye in PBS, and resuspended in MACS buffer for sorting. The cells were then sorted into four populations: $CD8^+$ resident ($CD11c^+MHCII^{int}CD8^+CD11b^-$, denoted as $CD8^+$ rDC1), $CD103^+$ migratory ($CD11c^+MHCII^{high}CD103^+CD11b^-$, denoted as $CD103^+$ mDC1), $CD11b^+$ resident ($CD11c^+$ $MHCII^{int}CD8^-CD11b^+$, denoted as $CD11b^+$ rDC2) and $CD11b^+$ migratory ($CD11c^+MHCII^{high}CD103^-CD11b^+$, denoted as $CD11b^+$ mDC2) (see Fig. S5D for the gating strategy). The sorted cells were collected in

sterile RPMI media supplemented with 10% FBS, 1% Penicillin-Streptomycin, 0.1% Gentamicin and 50 μM β-mercaptoethanol. The DC populations were counted and plated at a number of 2.7×10^4 per well in triplicates in a 96-well round bottom plate. Each population was then stimulated in a 1:1 ratio with CFSE-labeled OTI and OTII cells in the presence of 2 μM of unmodified OVA or OVA-p(GluNAc) at 37 ^{0}C. Three days later, the cells were harvested, and the OTI and OTII cells were analyzed for proliferation and activation ($CD44^+$).

Statistical Analysis

Statistically significant differences between experimental groups were determined using Prism software (version 6.07, GraphPad). All n values and statistical analyses are stated specifically in the figure legends for all experiments. For most experiments, a one-way or two-way ANOVA, followed by Tukey's or Dunnett's post-hoc test was used. Comparisons were significant if $p < 0.05$.

Chapter 2

Synthetically glycosylated antigen promotes archiving in lymphatic endothelial cells and the generation of central memory CD8$^+$ T cells, that contribute to the maintenance of peripheral tolerance.

Abstract

This chapter of the thesis is devoted to understanding the interaction of unadjuvanted glyco-conjugated antigen with antigen presenting cells (APCs) of the lymph node (LN), especially lymphatic endothelial cells (LECs) and dendritic cells (DCs) and its retention (archiving) in these cells in the long term at steady-state, and the impact on adaptive T cell immunity and implications in vaccination or tolerogenic platforms.

Keywords: archiving, antigen, unadjuvanted, steady-state, lymphatic endothelial cells, dendritic cells, CD8$^+$ T cells, vaccination, tolerance, immunization.

Introduction

Vaccines are a revolutionary healthcare and immunological achievement of the 20th century. They confer protection to future infections through the induction of robust and lasting immunological memory that is specific to a protein of the pathogen (antigen). While most protective memory to viral or bacterial infections is humoral (antibody) based, there is a lack in eliciting and measuring long-term effective cellular (T cell-mediated) immunological tolerance which is crucial in the direct elimination of infected cells (*115*)(*116*)(*117*).

The classical route of activation of a vaccine or any immune reaction to a pathogen starts with an inflammatory phase characterized by a massive expansion of antigen-specific effector T cells, followed by a substantial contraction phase to generate a small pool of memory T cells poised to rapidly proliferate into effectors upon re-encounter of the pathogen. A combination of signals at the transcriptional, epigenetic and metabolic level regulate this effector to memory transition (*118*)(*119*)(*120*). For example, Tbet and Eomes are two lineage mapping markers where gradual decrease in T-bet accompanied by a higher Eomes expression favors memory precursor generation (*121*)(*122*)(*123*). Similarly, loss of KLRG-1 and up-regulation of IL7Rα in effectors is a requirement for differentiation into memory lineages (*124*)(*125*).

Local interaction networks and quorum sensing are also factors that determine the effector to memory balance (*126*). At the epigenetic level, memory cells have been shown to be derived from fate-permissible effectors and naïve T cell-related programs are expressed later in their differentiation (*127*)(*128*).There is emerging evidence suggesting non-classical routes of generating memory cells from naïve T cells through asymmetric division upon activation, resulting in the simultaneous existence of effector and memory fates (*129*)(*130*)(*131*). Memory T cells share functional and transcriptional similarities with naïve T cells in their quiescent and pluripotent phenotype and stem-cell like potential, for instance through expression of TCF1 transcription factor (*132*)(*133*). Furthermore, there are differences (e.g. metabolic demands) in the generation of memory T cells from infection or vaccination that we need to be mindful of when designing vaccines (*134*).

Memory T cells are a heterogeneous population of cells with plastic fates and diverse effector and survival potential (*135*)(*136*). Central memory T cells are more naïve-like and circulate between blood and secondary lymphoid organs scanning for their cognate antigen while effector memory T cells patrol tissues and secondary lymphoid organs. Resident memory T cells are specialized tissue-specific sentinels that share programs with terminal effectors and can provide rapid defense to local invaders (*137*)(*138*)(*139*)(*140*). Resident memory T cells can also act as bystander defenders, acting in an antigen-independent manner, making antigen spreading an important protective mechanism (*141*)(*142*). Recent evidence shows incredible plasticity among all memory subsets; for instance, resident memory T cells can also circulate systemically (*143*). Thus, a greater understanding of the origin of memory is useful for designing translational vaccination strategies that can result in their generation and maintenance (*144*)(*145*)(*146*).

Maintenance of long-term and durable memory responses is an essential component of immunity. For example, IL-7 and IL-15 cytokines have an important role in maintaining memory T cell survival and homeostasis (*147*)(*148*). Additionally, TCR signal strength can also dictate memory fate (*149*)(*150*). Duration of antigen availability controls optimal vaccination responses and memory differentiation (*151*)(*152*). For example, $CD4^+$ T cells require longer antigen presence to proliferate (*153*)(*104*).

The lymphatics constitute an extensive network of lymphatic vessels connecting the lymphoid organs and peripheral tissues to the systemic blood circulation and have important scavenging roles in draining lymph away from tissues and maintaining healthy interstitial fluid pressure. They also act as the structural foundation and gatekeepers to the LN where immune responses are orchestrated in the context of immunity or tolerance. In addition to drainage, chemo-attraction and barrier function in the LN, the lymphatics and lymphatic endothelium have been shown to have essential immune modulatory functions (*154*)(*155*)(*156*) in different contexts, whether in steady-state or under inflammatory conditions in disease and cancer (*157*)(*158*)(*159*)(*160*).

Lymphatic endothelial cells (LECs) that line the lymphatics have an essential role in the maintenance of peripheral tolerance to peripheral tissue-transcribed antigens as an additional mechanism to compensate for potentially autoreactive T cells that escape central tolerance through deletion of autoreactive cells or generation of autoantigen-specific $CD4^+$ regulatory T cells (Tregs) (*161*)(*162*)(*53*)(*163*). Due to their strategic localization along lymphatic vessels and at the entry of LNs, LECs are poised to be excellent uptakers of antigen draining from peripheral sites (*164*)(*165*). They can not only take up antigen but also retain or archive antigen for weeks after exposure following viral infection or immunization (*166*). Tamburini et al showed that this was possible only if antigen was taken up in the presence of an inflammatory stimulus such as a strong adjuvant. They furthermore showed that this LEC-archived antigen was transferred to migratory cross-presenting DCs for subsequent presentation to naïve $CD8^+$ T cells, resulting in their proliferation proportional to the archived antigen load

(*167*). However, the Swartz lab has showed that LECs induce tolerance to exogenous antigens draining from peripheral sites of immunization, inflammation and tumors, through direct antigen presentation to naïve CD8+ T cells (*164*)(*165*). This tolerogenic antigen presentation is accompanied by the up-regulation of co-inhibitory molecules with peptide-loaded MHC molecules, alongside soluble mediators such as IDO and iNOS that can directly suppress $CD8^+$ T cells or other APCs from maturing and presenting antigen to produce effectors (*154*)(*168*). While LECs can express MHCII and present antigen to $CD4^+$ T cells (*169*), they can also acquire peptide-MHCII complexes from other professional APCs such as dendritic cells (DCs) to then interact with $CD4^+$ T cells (*91*).

Recent strides in literature shedding light on immune modulatory functions of LECs have led to the generation of a wealth of single cell transcriptomic studies that reveal an immense heterogeneity among LECs that specialize in scavenging, antigen presentation and interactions with macrophages, T or B cells and location-function relationships within the LN referred to as niche-specific effects (*170*)(*32*)(*171*)(*172*)(*173*). These all show the dynamic nature of the stromal components of the LN that can quickly adapt to inflammatory changes to accommodate antigen drainage, lymphangiogenesis and lymphocyte traffic (*174*).

Recent work in our lab demonstrates that $CD8^+$ T cells that resist deletion after their interaction with LECs differentiate into a central memory, stem-cell like quiescent

memory state that can be reactivated upon challenge to protect the host (*175*). This opens up a novel role for LECs responding to exogenous antigen outside an inflammatory context to aid in the generation of a memory pool capable of protecting the host from antigenic challenges. We can imagine the ability to generate memory T cells without going through an effector phase would be an attractive and useful way to vaccinate immune-compromised people or patients suffering from autoimmune conditions, where inflammation is undesirable. LECs also produce survival and homeostatic factors important for naïve and memory T cell survival such as IL-7, IL-15 and S1P (*176*)(*177*)(*178*).

Another aspect of the location-function relationships of LECs are with respect to the uptake and filtering of different antigens from lymph. Upon entry into the subcapsular sinus (SCS) space of the LN, soluble antigens and nanoparticles (10-100 nm range ideal for lymphatic absorption) are taken up and sequestered by APCs lining and within the SCS, including LECs, $CD169^+$ SCS macrophages and some $CD11b^+$ DCs while the remaining fraction leave the SCS (*73*)(*179*)(*30*). Lower molecular weight antigens (<70 kDa) and nanoparticles are channeled to conduits surrounded by fibroblastic reticular cells (FRCs) and filtered on floor LECs entering the B cell follicles for direct B cell contact or sampling by follicular dendritic cells (FDCs), or alternatively into intranodal conduits of the LN for direct uptake by more deeply-located medullary DCs for presentation while unsampled antigen is directed into the systemic circulation through high endothelial venules (HEV) (*180*)(*181*). Heavier antigens (>70 kDa) and larger nanoparticles and microparticles are typically captured by immunization site-resident

APCs that traffic to the LN following chemokine gradients and can be further shuttled across the SCS by SCS macrophages. This migration process can take upwards of a few hours but Karahi et al showed that antibodies (~150 kDa) can be transcytosed from the sinusoidal to the cortical space within minutes of a subcutaneous injection, indicating that more rapid routes of dissemination along lymphatics for bulkier soluble particles exist (*88*).

The central ***hypothesis*** of this chapter is that targeting antigen to LECs at steady-state promotes archiving and the generation of central memory that can be protective against an infectious challenge.

Results

LECs take up differentially glycopolymerized antigen in a receptor-mediated fashion but preferentially take up antigen terminated in NAc-Glucosamine residues

Like many other phagocytic cells and APCs, LECs express a variety of scavenger receptors or C type lectin receptors that can be used as antigen targets. These receptors have been reported to be present on LECs and involved in antigen internalization for further downstream processing (*180*). Many of these receptors have transmembrane carbohydrate binding domains that recognize and bind to sugar

residues; while each receptor binds to different sugar motifs with different

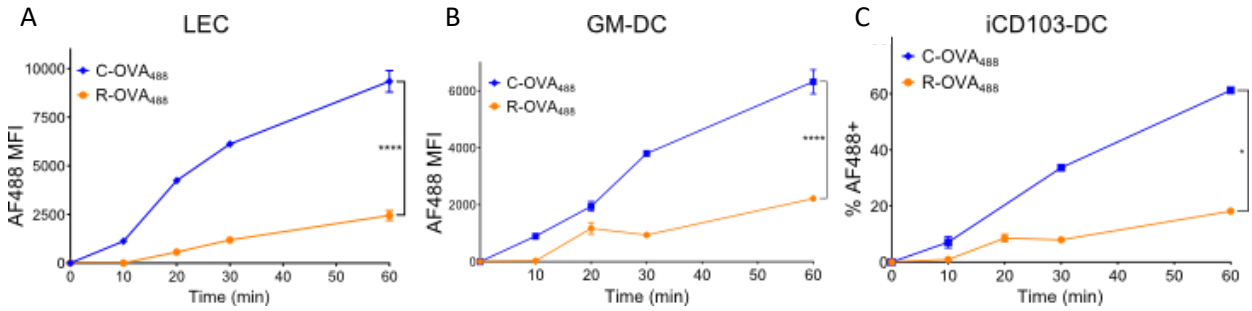

Fig 7. Recombinantly produced OVA (R-OVA) is taken up to a lower extent compared with naturally occurring chicken OVA (C-OVA) by different cell types in vitro. AF488-labeled R-OVA and C-OVA were added to cells in culture at 10 µg/mL, and the uptake was measured over time at the following timepoints following stimulation: 10 min, 20 min, 30 min and 1 h. (A) AF488 MFI (uptake) in primary mouse LECs. (B) AF488 MFI (uptake) in BMDCs. (C) % in vitro induced $CD103^+$ dendritic cells (*182*) that were $AF488^+$. Statistical differences were determined by the Mann Whitney t test at the 60 min timepoint (*p ≤ 0.05, **p ≤ 0.01, ***p ≤ 0.005).

affinities, the exact ligands for the receptors are difficult to pinpoint. Our lab has observed in the past that LECs are effective at taking up antigen because of the inherent glycosylation of the protein. For instance, chicken-derived ovalbumin (OVA) is naturally mannosylated, and is readily taken up for that reason. To accurately measure the difference in uptake of OVA compared with OVA decorated with synthetic glycosylations, we produced OVA recombinantly in e coli, which was devoid of glycosylation. *In vitro* characterization revealed that recombinant OVA was taken up less efficiently than regular chicken OVA both by LECs and bone marrow-derived dendritic cells (BMDCs) (**Fig. 7**). All experiments reported in this paper were carried out with recombinant OVA.

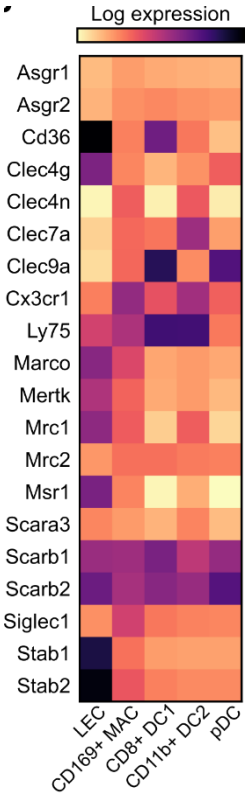

Fig 8. LECs, like other LN APCs, express various antigen uptake receptors. Heatmap showing the comparative expression of different classes of carbohydrate-binding and scavenger receptors on LECs, CD169$^+$ macrophages, CD8$^+$ DC1s, CD11b$^+$ DC2s and plasmacytoid DCs in the s.c. LNs of wild-type male C57BL/6 mice. Data analyzed from the immgen database (http://www.immgen.org/).

Uptake of synthetically glycosylated antigen by APCs is mediated through the carbohydrate binding domain of various C type lectin and scavenger receptors and can be inhibited by the addition of free sugars in media (*24*). We analyzed the immgen database (http://www.immgen.org/) for the expression of several scavenger and lectin receptors involved in the uptake of carbohydrates, including GluNAc-terminated residues, among APCs targeted by OVA-p(GluNAc) (**Fig. 8**). We found that they were broadly expressed, but to different extents on these cell types, including LECs, CD169$^+$ macrophages and three DC subsets (CD8$^+$ DC1, CD11b$^+$ DC2, plasmacytoid DC). We identified Asgr1 and 2 to be only minor players in LN APCs compared to hepatic APCs (*38*). Clec4g (LSECtin) was found to be highly expressed exclusively on LECs, justifying their high uptake of OVA-p(GluNAc) and their similarity in scavenging profile to liver sinusoidal endothelial cells (*23*, *39*). Other receptors found highly expressed by the hematopoietic APCs were DEC-205 (Ly75), commonly used as an antigen target for the induction of tolerance (*14*, *40*) and Clec9a, primarily used as apoptotic scavenger receptor by cross-presenting DCs (*41*). LECs and macrophages share MARCO expression that has been used for antigen targeting in tolerance induction (*22*, *42*). The mannose receptor (Mrc1), which can promiscuously bind GluNAc-glycosylated antigen, was also highly expressed on LECs (*43*). This analysis also revealed shared receptors between LECs and macrophages, which reflects their synergy

in scavenging in the LN subcapsular sinus, similar to the parallels between sinusoidal endothelial cells and Kupffer cells in the liver (*44*). Thus, by virtue of size, retention, expression of C-type lectin and scavenger receptors, synthetically glycosylated antigen is ideally poised for uptake by LN APCs to orchestrate downstream immune responses.

We thus modified OVA with sugar residues that are known to bind to various scavenger receptors expressed by LECs (**Fig. 8**) (*180*). We developed glyco-polymers composed of random co-polymers of monomers bearing either β-linked NAc-Glucosamine (p(GluNAc)), or β-linked NAc-galactosamine (p(Gal)), or mannose (p(Man)) (**Fig. 9A**). These polymer backbones were conjugated to antigen using free amine chemistry with high yield. The antigen was tethered to the rest of the polymer via a reduction-sensitive self-immolative linkage that can be cleaved in the reductive environment of the endosome, releasing the intact antigen for archiving or further processing- we verified that that was the case by running gel electrophoresis on the antigen-polymer conjugates under reducing and non-reducing conditions. The purified conjugates can be detected at a molecular weight range of 70-150 kDa, which is decreased to the original molecular weight of OVA of 43 kDa following reduction (**Fig. 9B**). Since the glyco-polymers increase the overall size of the antigen complex by 30-90 kDa which is known to impact uptake, drainage and biodistribution kinetics *in vivo*, we also synthesized a non-receptor targeting antigen-polymer conjugate with PEG-20k, which does not undergo a size change after reduction due to the lack of the self-immolative linker (**Fig. 9B**). All constructs were tested for the absence of endotoxin via a colorimetric HEK-TLR4 assay before they were used in all studies. The OVA content in each polymer conjugate was

determined by reducing and boiling the conjugate and running it on an SDS-page gel alongside standard OVA samples of known concentration, and interpolating concentration from gel band intensity.

We first characterized the uptake behavior of our OVA-polymer conjugate *in vitro* using freshly isolated mouse lymph-node LECs that were expanded in culture for 4 days (using an established protocol in our lab). To mimic the competitive setting of the draining LN where there are antigen uptakers other than LECs, we set up LECs in co-culture with BMDCs for comparison and evaluated the uptake of fluorescently-labeled OVA (OVA-$_{647}$) alone or in conjugation with our polymers (OVA$_{647}$-p((GluNAc)), OVA$_{647}$-p(Gal), OVA$_{647}$-p(Man)) at a dose of 2.5 μg/mL at a short competitive timepoint of 2 h or longer homeostatic timepoint of 24 h following stimulation *in vitro*. Uptake was measured as the amount of cell-associated OVA$_{647}$ by flow cytometry and reported as mean fluorescence intensity (MFI) of OVA$_{647}$ in LECs or BMDCs. The ratio of the corrected MFI (measured MFI- unstimulated control MFI) in LECs to BMDCs was calculated to determine the selectivity of each polymer conjugate for uptake by LECs over BMDCs. We found that while LECs were effective at taking up all forms of antigen, they were most effective at competitively capturing OVA$_{647}$-p((GluNAc)) conjugates over BMDCs after 2 h, suggesting that (GluNAc) terminated residues are better at targeting scavenger receptors expressed on LECs over DCs (**Fig. 9C, D**). There was no difference across groups, including unmodified OVA, after a longer stimulation of 24 h, suggesting equilibration in uptake had occurred, and was therefore too late of a timepoint to evaluate differences in uptake (**Fig. 9D**).

To make sure that the preferential uptake of OVA_{647}-p(GluNAc) by LECs at 2 h was receptor-mediated and not a result of passive uptake or reduced uptake by BMDCs in co-culture, we conducted competitive receptor-inhibition experiments *in vitro*. We incubated LECs or BMDCs with a high concentration (100 μM) of the free sugar monomers (GluNAc, GalNAc or mannose) or an irrelevant sugar (L-rhamnose) for 30 min before treating them with the fluorescent conjugates for another hour, and measured the amount of cell-associated OVA_{647}. The uptake of all three conjugates by LECs was abrogated when they were pre-treated with the free sugars, while the uptake of only OVA_{647}-p(Man) was inhibited for DCs, indicating that LECs expressed receptors to efficiently take up antigen terminated in all GluNAc, GalNAc or mannose residues while DCs were more equipped at taking up mannosylated antigen (**Fig. 9E**). On the contrary, L-rhamnose had no significant effect on the MFI of LECs treated with OVA_{647}-p(GluNAc) or OVA_{647}-p(Gal), showing that the uptake of these conjugates by LECs is receptor-mediated. Similarly, for DCs, L-rhamnose had no effect on the MFI when treated with OVA_{647}-p(Man), suggesting that the uptake of the mannosylated antigen occurs through specific recognition of the mannose residues by scavenger receptors on the DCs (**Fig. 9E**). Together, these suggested that the increase in OVA-p(GluNAc) uptake by LECs was most likely because LECs are more effective than DCs at taking up GluNAc-terminated antigen. These data suggested that OVA-p(GluNAc) could be used to selectively target LECs over DCs.

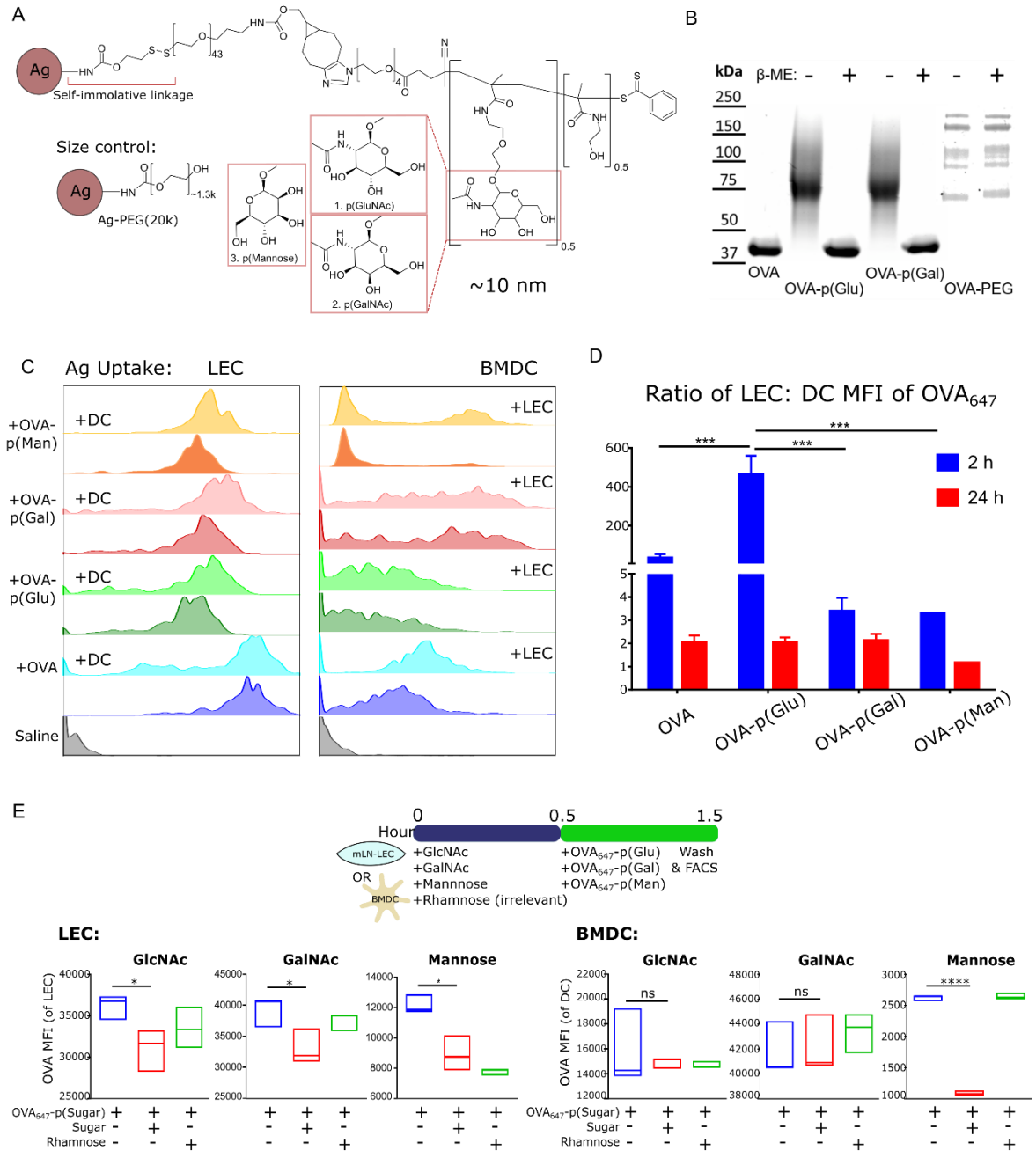

Fig 9. LECs preferentially take up p(GluNAC) conjugated antigen in vitro; uptake is receptor-mediated. (A) Structure of antigen chemically conjugated to three glycopolymers (p(GluNAc), p(Man), p(Gal)) via a reduction-sensitive reversible linkage, and of a size control consisting of antigen chemically and non-reversibly tethered to PEG (20k) polymer. (B) SDS-page gel showing OVA, non-reduced OVA-p(GluNAc), reduced OVA-p(GluNAc), non-reduced OVA-p(Gal), reduced OVA-p(Gal), non-reduced OVA-PEG and reduced OVA-PEG in that order. (C) LECs or BMDCs were stimulated in vitro with 2.5 µg/mL of AF647-labeled OVA, OVA-p(GluNAc), OVA-p(Gal) or OVA-p(Man) for 24 h, and histograms describing the MFI of the conjugated dye (uptake)

Fig 9. LECs preferentially take up p(GluNAC) conjugated antigen in vitro; uptake is receptor-mediated (continued) are shown for LECs (left) and BMDCs (right), acquired using flow cytometry. The cells were stimulated either on their own or in co-culture with each other, and the latter is indicated as +BMDC and +LEC on the histograms. (D) Calculated ratio of uptake in LECs to BMDCs at timepoints of 2 h and 24 h. (E) (Top) Experimental timeline of the in vitro receptor-blocking experiment. LECs or BMDCs were incubated with 100 μM of free sugars GluNAc, GalNAc or mannose) or an irrelevant sugar (L-rhamnose), followed by addition of the 647-abeled glycopolymerized antigen at 2.5 μg/mL for another hour. (Bottom) Uptake by LECs (left) and BMDCs (right), measured by flow cytometry, is shown. Statistical differences were determined by one-way ANOVA using Tukey's post hoc test (*p ≤ 0.05, **p ≤ 0.01, ***p ≤ 0.005).

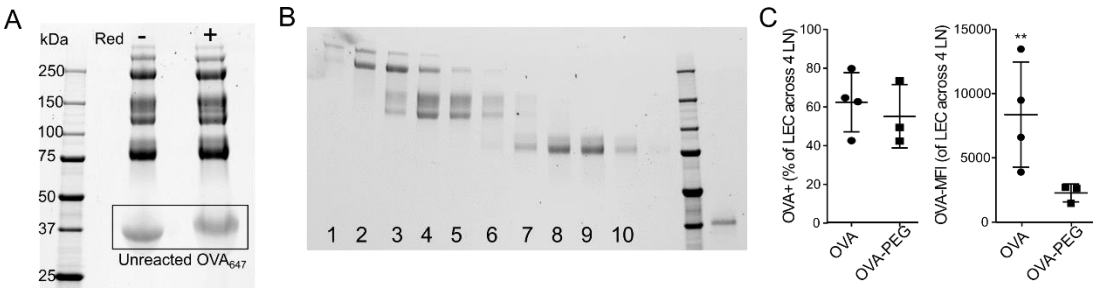

Fig 10. Characterization of synthesized OVA-PEG(20k) conjugates. (A) SDS-page gel showing synthesized OVA_{647}-PEG(20k) under non-reducing and reducing conditions. (B) OVA_{647}-PEG(20k) fractions 1-10 following size exclusion chromatography. (C) % OVA_{647}^{+} LECs (left) and MFI of OVA_{647}^{+} LECs (right) in LNs of mice 24 h following subcutaneous immunization with OVA_{647} or OVA_{647}-PEG. Statistical differences were determined by student t test (*p ≤ 0.05, **p ≤ 0.01).

Antigen-p(GluNAc) conjugate slightly promotes archiving in LECs in vivo at steady-state, comparable to archiving levels observed under inflammatory conditions

Next, we determined whether OVA-p(GluNAc) could target LECs *in vivo*. We have previously showed that LECs are effective at capturing OVA administered as soluble protein exogenously or expressed in the B16 melanoma tumor, but we have never measured the ability of LECs to archive the antigen over time delivered in its native form or across our different polymeric delivery platforms. Following s.c. injection in the hocks, we evaluated the uptake of antigen in LECs at a short-term timepoint of 24 h, and retention of antigen in LECs at a longer timepoint of 2 weeks, in the draining axillary and

popliteal LNs (**Fig. 11A**). We included all glycopolymerized antigen groups in this biodistribution experiment to provide non-LEC selective but receptor-mediated controls (p(Gal) and p(Man)). We immunized mice with OVA_{647}-PEG (size control), our polymer conjugates at steady-state (no adjuvant) or with the combined adjuvant of αCD40 and poly(I:C) as positive control shown previously to lead to antigen archiving in LECs (**Fig. 11A**). The choice of the LNs to analyze was educated by a previous experiment we did to compare antigen drainage and accumulation after hock injection. We found that OVA was detected to significantly higher levels in the direct draining LNs (pooled axillary and popliteal) compared with downstream LNs (pooled brachial and inguinal) (**Fig. 11B**). We compared LECs with the following APC subsets that can also take up antigen in the draining LN- blood endothelial cells (BEC; $CD31^+gp38^-$), fibroblast reticular cells (FRC; $CD31^-gp38^+CD21/35^-$), follicular dendritic cells (FDC; $CD31^-gp38^+CD21/35^+$), dendritic cells (DC; $CD11c^+$), and macrophages (MAC; $F4/80^+$). We visualized antigen uptakers and archivers in two ways, either as % OVA+, i.e., fraction of each APC subset that were OVA+, and OVA+ cell count, i.e., absolute number of cells that were OVA+ within each APC subset. 24 h post-immunization, LECs had the highest % OVA^+ but there was no difference across groups at steady-state or compared with the positive control- 30-60% LECs were OVA^+ across the five immunization groups (**Fig. 11C**). This high % uptaker fraction among LECs is what we usually observe since LECs are strategically located to take up antigen draining from peripheral sites. We however did not observe higher uptake of OVA-p(GluNAc) by LECs as we had seen *in vitro*. Zooming in on the other APC subsets, we noted no difference in uptake in FRCs and DCs, but FDCs and macrophages had taken up OVA-p(GluNAc) to significantly higher levels compared to

OVA-PEG (**Fig. 11D**). The higher uptake superiority of LECs is however minimized when absolute OVA^+ cell counts are considered- even at a low % OVA^+, OVA+ macrophages and DCs were more abundantly present in the antigen uptaker pool, with up to a 60-fold difference with the number of OVA^+ LECs, making the contribution of LEC antigen presentation to total presentation small (**Fig. 11C**). Two weeks post-immunization, LECs were still the major antigen archivers, i.e., there was a highest fraction of LECs that were OVA^+ and thus had retained antigen. There were upwards of 7-20% of LECs that were OVA^+ in the OVA-PEG and OVA-p(GluNAc) groups and within these two groups, LECs archived antigen at a significantly higher % compared with BECs, FRCs, DCs and MACs (**Fig. 11E**). Among the stromal cell populations, LECs retained most antigen at steady-state within the OVA-PEG and OVA-p(GluNAc) groups (**Fig. 11E**). The only other stromal cell type that retained a substantial amount of OVA (13%) was FDCs but only when immunized with an adjuvant which is consistent with what is reported in literature on the role of FDCs in retaining antigen complexes in the LN germinal center over weeks for gradual presentation to B cells for hyper affinity maturation (**Fig. 11E**). Less than 2% DCs and MACs were OVA^+ two weeks post-immunization, without exhibiting any differences across groups (**Fig. 11E**). However, when again considering OVA^+ counts, LECs fall behind as they compete with DCs as archivers (**Fig. 11E**). This is not consistent with what is reported in literature- LECs have been shown to be the major archiver both in terms of % positive and total positive counts, and this is not what we observe in our hands. LECs are easily outnumbered at a short or long timepoint and other APCs are also able to archive antigen, at a lower % positive but higher cell count comparable to LECs (**Fig. 11F**). Higher antigen retention in

LECs with OVA-p(GluNAc) was not observed when we plotted OVA^+ LECs as a % of LECs but only when we expressed the OVA^+ LECs as a % of a larger population such as the total live population which is an artefact when gating on generally smaller populations such as LECs (**Fig. 11G**). At steady-state, LECs only in OVA-p(GluNAc) immunized mice archived significantly more antigen compared to the non-targeting size control or the other receptor-targeting OVA-p(Man) or OVA-p(Gal) constructs; the number of OVA^+ LEC was comparable to the positive control (**Fig. 11F, G**). The scavenger receptors that bind to (GluNAc) residues must be responsible for archiving performance but they are not a direct explanation since we did not observe a difference in LEC uptake across groups 24 h after injection, indicating that the accumulation of p(GluNAc) shuttled antigen inside LEC endosomes only occurs and can be detected over time. This was in contrast to our *in vitro* uptake assays that showed higher LEC targeting with OVA-p(GluNAc) in the short-term (**Fig. 9**), demonstrating that lymphatic flow and filtering of the glycoconjugate nanoparticles in the LN are important factors to consider when targeting antigen to LECs *in vivo*. After these experiments, we can claim that OVA-p(GluNAc) slightly improves antigen archiving in LECs under non-inflammatory conditions but there is a LEC expansion effect (only detected when plotted as % live) that we still cannot account for. Also, this effect is most likely diluted by the presence of other antigen archivers at steady-state, shedding some doubt on the role of LECs in retaining total antigen inside the LN over time.

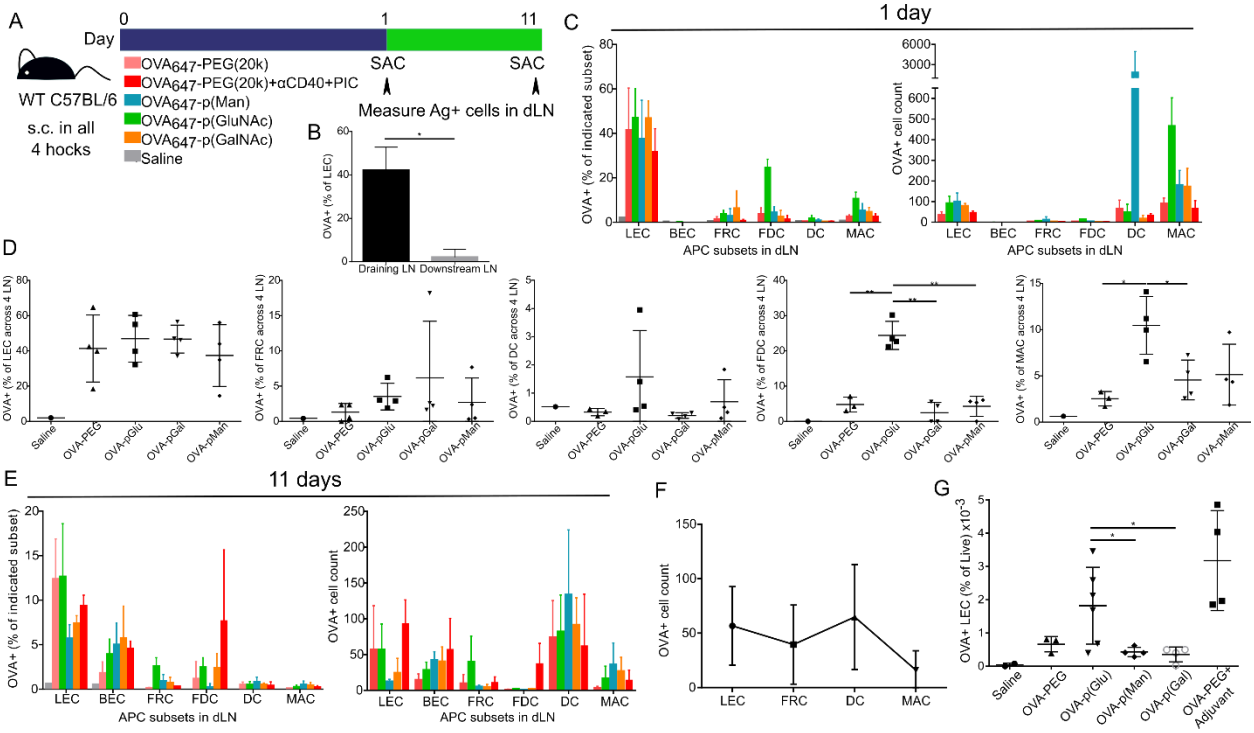

Fig 11. LECs archive antigen-p(GluNAc) to a slightly higher extent compared to other LN APCs at steady-state, comparable to the adjuvanted control. (A) Experimental timeline to evaluate antigen biodistribution in dLNs 1 or 11 days following immunization (6 groups) via flow cytometry. (B) % OVA$^+$ LECs in draining (axillary and popliteal) and downstream (brachial and inguinal) LNs 24 h post-immunization. (C) % OVA$^+$ LN APCs (left) and OVA$^+$ APC cell numbers (right) 24 h post-immunization. (D) Breakdown of % OVA$^+$ APC subsets 24 h post-immunization in LECs, FRCs, DCs, FDCs and macrophages in this order. (E) % OVA$^+$ LN APCs (left) and OVA$^+$ APC cell numbers (right) 11 days post-immunization (archivers). (F) OVA$^+$ numbers of indicated APC subsets in dLNs at 11 days. (G) % OVA$^+$ LECs of total live cells in dLNs. Statistical differences were determined by one-way ANOVA using Tukey's post hoc test (*p ≤ 0.05, **p ≤ 0.01, ***p ≤ 0.005).

The amount of antigen archived in LECs can be enhanced by boosting with antigen co-delivered with an adjuvant

While antigen archiving in LECs has been characterized in the context of a single bolus injection, it is unknow how an antigen boost (such as in the context of vaccination) can alter the archiving landscape in LECs. We immunized mice with AF647-labeled OVA, with or without the combined adjuvant, or saline in the hocks, and boosted them one

week later with AF488-labeled OVA with or without adjuvant or saline only and evaluated the archiving and proliferation response in LECs another week later (**Fig. 12A**). First, we confirmed that LECs remained the major antigen archiver in the dLNs from the highest percent of OVA_{647}^{+} cells compared to FRCs, DCs or macrophages (**Fig. 12B**). Interestingly, we found that the ability of LECs to retain the first injected (OVA_{647}) did not change in the presence or absence of an adjuvant, contrary to what is presented in literature (**Fig. 12B**). However, the response to the second wave of antigen was substantially different. We found that in this case, having an adjuvant co-delivered with the antigen boost significantly helped LECs take up and subsequently retain the second antigen (**Fig. 12C, D, E**). While the uptake of the boosted antigen was not as high as the first, which could be explained by LN inflammation dynamics that tend to favor a response to the antigen first encountered, having an adjuvant in the second immunization increased the uptake of the second antigen (**Fig. 12C, D, E**). This further antigen uptake can be partially explained by LECs being in a higher proliferative state and hence, present in larger numbers when an adjuvant is co-administered with antigen, especially when the mice are seeing adjuvant for the first time (**Fig. 12F**). Thus, we determined that an antigen boost can increase antigen archived by LECs, that can be made more responsive to further retention by co-delivering antigen with an adjuvant.

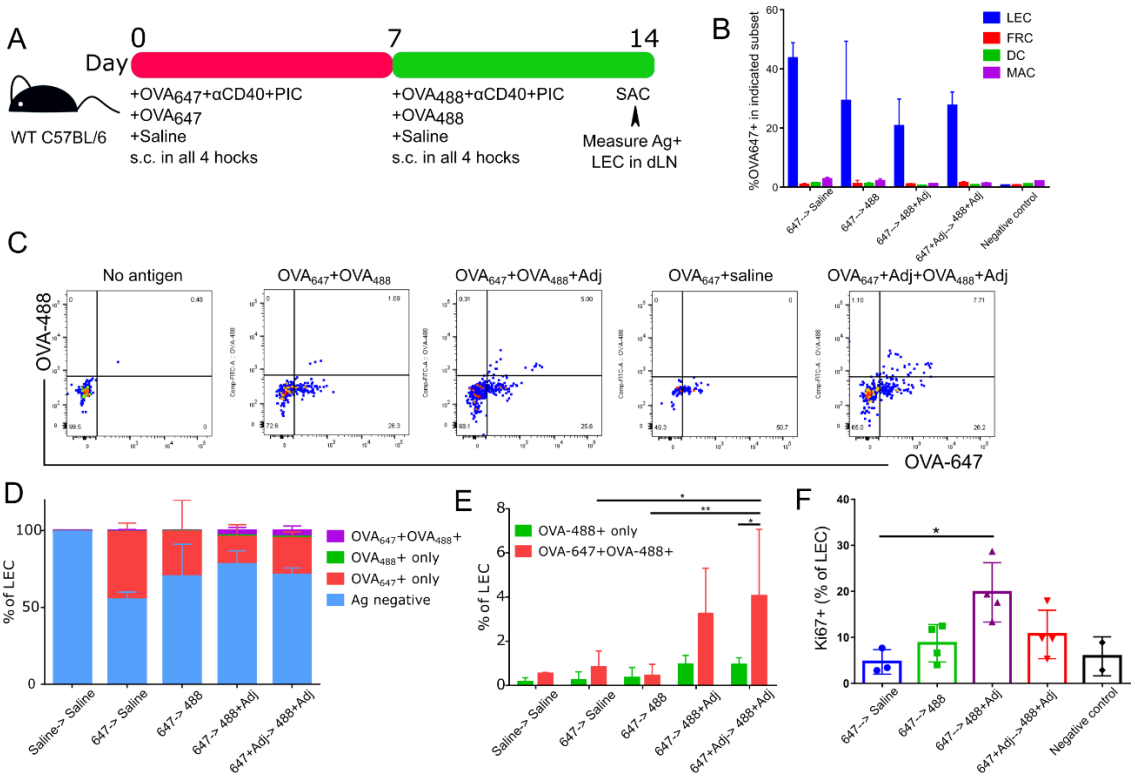

Fig 12. LECs archive more antigen when co-delivered with an adjuvant, in a prime-boost setting. (A) Experimental set-up, showing immunization with OVA_{647} at day 0, followed by a boost with OVA_{488} at day 7, either with or without adjuvant. (B) % OVA_{647}^{+} APC subset at day 14. (C) Representative flow cytometry plots showing uptake of OVA_{647} and OVA_{488} by LECs at day 14. (D) Distribution of LECs that are OVA^{-} and OVA^{+} in dLNs. (E) % LECs that are OVA_{488}^{+} only or double $OVA_{647}^{+}OVA_{488}^{+}$ at day 14. (F) % LECs that are $Ki67^{+}$ (proliferating) in dLNs. Statistical differences were determined by one-way ANOVA using Tukey's post hoc test (*p ≤ 0.05, **p ≤ 0.01, ***p ≤ 0.005).

Antigen is not retained at the site of subcutaneous injection but rapidly accumulates in the draining LNs

We and others showed that antigen is archived in LECs and other APCs in the LNs (*166*). A possibility that has, however, not been investigated is that antigen is retained at the site of injection and passively drains to the dLNs or is actively captured and transported by site-resident APCs that then migrate to the dLNs with the antigen. LECs in skin lymphatics also do not express scavenger receptors like LN-LECs that have

specialized immune modulatory roles (*39*). In order to prove that antigen archiving is a property unique to LN lymphatics and not of lymphatics at the site of s.c. injection in skin, we conducted an experiment where we utilized live intravital imaging of the ear dermis developed in our lab as a model and technique to monitor the amount of antigen draining from the site of injection into dLNs.

One to two days prior to injection, any hair present was removed from the ear of the WT C57BL/6 mice using depilatory cream and the mice were given time for any ear thereby caused inflammation to resolve. The mouse was anesthetized under inhalation isoflurane and a Hamiltonian syringe was used to inject saline or OVA_{647} in a small volume of 2 µL into the ear dermis and the ear was immobilized on a wooden block using tape and imaged through using the stereomicroscope **(Fig. 13A**). The ear was imaged on days 0, 9 and 13 near the site of the i.d. injection and we observed that the OVA_{647} fluorescence rapidly decayed within the first week until it was undetectable two weeks post-injection (**Fig. 13B**). We sacrificed the mouse at day 13 and evaluated antigen retention in APC subsets in the draining cervical LNs and in the skin at the site of injection using flow cytometry. We assessed the ability of APCs in the cervical LNs to retain antigen two weeks post-injection: we focused on conventional DCs ($CD11c^+$ $MHCII^{high}$ $CD11b^-$ and $CD11c^+$ $MHCII^{int}$ $CD11b^-$), migratory DCs ($CD11c^+CD11b^-$ $MHCII^{high}CD103^+$) and DC2s ($CD11c^+CD11b^+$) (**Fig. 13C**). Low % of DCs were OVA_{647}^+ in the LNs, with highest amount of OVA_{647} retained by ~2 % of DC2s, consistent with their role in the capture of soluble antigen (**Fig. 13D**). We also assessed the extent to which antigen was archived in APCs at the site of injection in the ear dermis by flow cytometry that provides a more sensitive measurement compared with the

stereomicroscope. We looked at archivers in skin stromal cells and DCs with high or low langerin (CD207) expression (**Fig. 13E**). No antigen could be detected in any of the DC subsets (**Fig. 13F**). However, we could detect upwards of ~10 % LECs that retained OVA_{647} in the LNs compared to the skin (**Fig. 13G**). This was in contrast with the other stromal cell type, FRCs, that failed to retain antigen in LNs but were rather associated with antigen at the site of injection in skin (**Fig. 13H**). Thus, we were able to show that antigen was only successfully archived in LN-LECs as a result of rapid drainage from the site of injection.

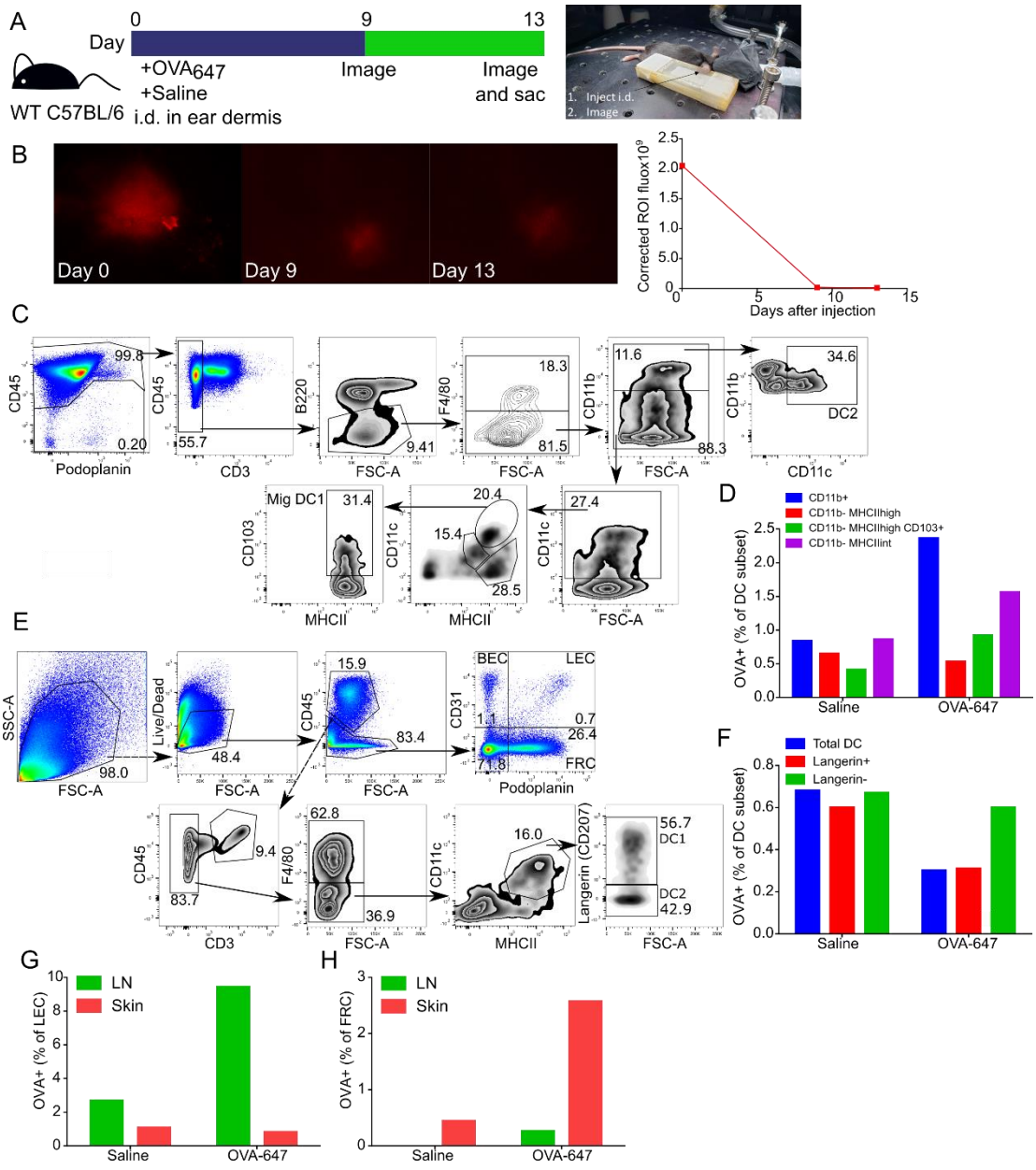

Fig 13. Antigen is not retained at the site of subcutaneous injection but rapidly drains to and accumulates in the draining LNs. (A) Experimental set-up and timeline for ear dermis injection and in vivo fluorescence imaging using the stereomicroscope. (B) (Left) Stereomicroscope images of the ear dermis around the site of injection taken at days 0, 9 and 13 post-injection, at the same red laser exposure, brightness and contrast settings. (Right) Quantification of the AF647 fluorescence taken of the ROI drawn around the site of injection at the different imaging timepoints. (C) Gating strategy of hematopoietic APCs in the draining cervical LNs. (D) % indicated APC subset that are OVA_{647}^{+} in the draining cervical dLNs. (E) Gating strategy of APCs at the site of immunization in the skin. (F) % indicated APC subset that are OVA_{647}^{+} in skin. (G) % LECs (left) and FRCs (right) that are OVA_{647}^{+} in draining cervical LNs or skin at the site of injection.

We repeated this above experiment where we assessed antigen archiving in the ear dermis but this time in Prox1-Tom mice that express the tdTomato gene under the control of the Prox1 promoter, restricting fluorescent expression in LECs (*183*). We injected these transgenic mice with OVA_{647}, OVA_{647}-p(GluNAc) or OVA_{647} with PIC using the technique described above, and monitored the ear fluorescence over the course of a few days. We observed that OVA was not retained in any of the groups from the drastic loss in fluorescence only three days following the i.d. injection, confirming that antigen is not archived at the site of injection in the skin irrespective of whether it is injected at steady state or with an inflammatory signal or when glyco-conjugated (**Fig. 14**).

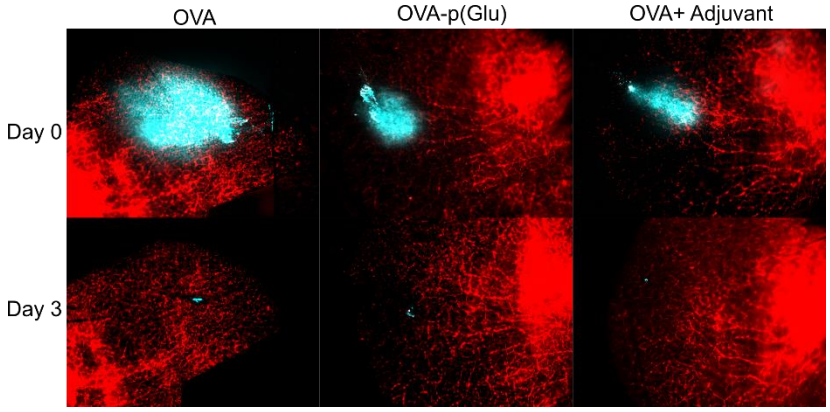

Fig 14. Antigen-p(GluNAc) is not retained at the site of subcutaneous injection. Prox1-Tom mice were injected in the ear dermis with OVA_{647}, OVA_{647}-p(GluNAc) or OVA_{647} with adjuvant and the ear dermis around the site of injection was imaged at days 0 and 3 post-injection using in vivo fluorescence microscopy. Lymphatics are shown in red, and antigen is shown in cyan.

Antigen-specific CD8+ T cells respond to archived antigen delivered via p(GluNAc) conjugation by down-regulating proliferation and type 1 cytokine production

We know that antigen-specific $CD8^+$ T cells adoptively transferred into mice in which antigen has been archived are able to proliferate, and the proliferation intensity is directly proportional to the amount of antigen archived in LECs. The amount of antigen archived has been enhanced in literature by delivering antigen using a combined adjuvant of PIC and agonistic CD40 antibody, but we describe a novel way of enhancing antigen archived in LECs at steady-state by delivering antigen glycopolymerized with p(GluNAc). Thus, we wanted to test the effect of archived antigen-p(GluNAc) on antigen-specific $CD8^+$ T cells. We set up an OVA transgenic model where we immunized mice with OVA as unmodified antigen control, OVA-p(GluNAc), OVA-p(Gal) as glycopolymerized antigen control that does not promote archiving, OVA with the combined adjuvant as positive control, and saline as the negative control, and adoptively transferred CFSE-labeled OTI and OTII cells two weeks post-immunization, and sacrificed the mice three days later. Because of the uncertainty of detecting any proliferation in the absence of an adjuvant, we also treated the mice with daily i.p. injections of FTY inhibitor starting on the day of adoptive transfer until sacrifice, to trap the T cells in the dLNs and increase the contact time of the T cells with archived antigen-bearing APCs (**Fig. 15A**). To our surprise, OTI cells massively proliferated in mice treated with unadjuvanted OVA, and the proliferation was not significantly different from the positive control with adjuvant (**Fig. 15B**). OTII cells barely proliferated under all conditions (**Fig. 15B, D**). OTI proliferated the least in mice treated

with OVA-p(GluNAc), suggesting an immune-suppressive effect (**Fig. 15B, C**). We did not think that the OTI proliferated less because OVA delivered with p(GluNAc) was less available for presentation or the antigen was diverted away from the MHCI loading pathway, because OVA-p(GluNAc)-treated LECs resulted in OTI proliferation in vitro. This decrease in proliferation observed with OVA-p(GluNAc) archiving was also detected in the downstream LNs of mice, though not to the same extent as in the draining LNs, educating our choice for only isolating the immediate dLNs for future immunological analysis (**Fig. 15E**). We noted a similar effect on the OTI with OVA-p(Gal) but the differences with respect to OVA or the positive control were not as striking (Fig. 9B-D). Very few OTI cells were harvested from the spleen because of dosing with the FTY inhibitor (**Fig. 15E**). We also evaluated cytokine production by OTI cells upon restimulation with H2kb cognate peptide $OVA_{257-264}$ and found that OTI cells educated by OVA-p(GluNAc) secreted significantly less IFNγ and IL-2 cytokines compared with the positive control (**Fig. 15F, G**). These results demonstrated that the ability of $CD8^+$ T cells to proliferate produce inflammatory cytokines was highly regulated by presentation of antigen conjugated to p(GluNAc).

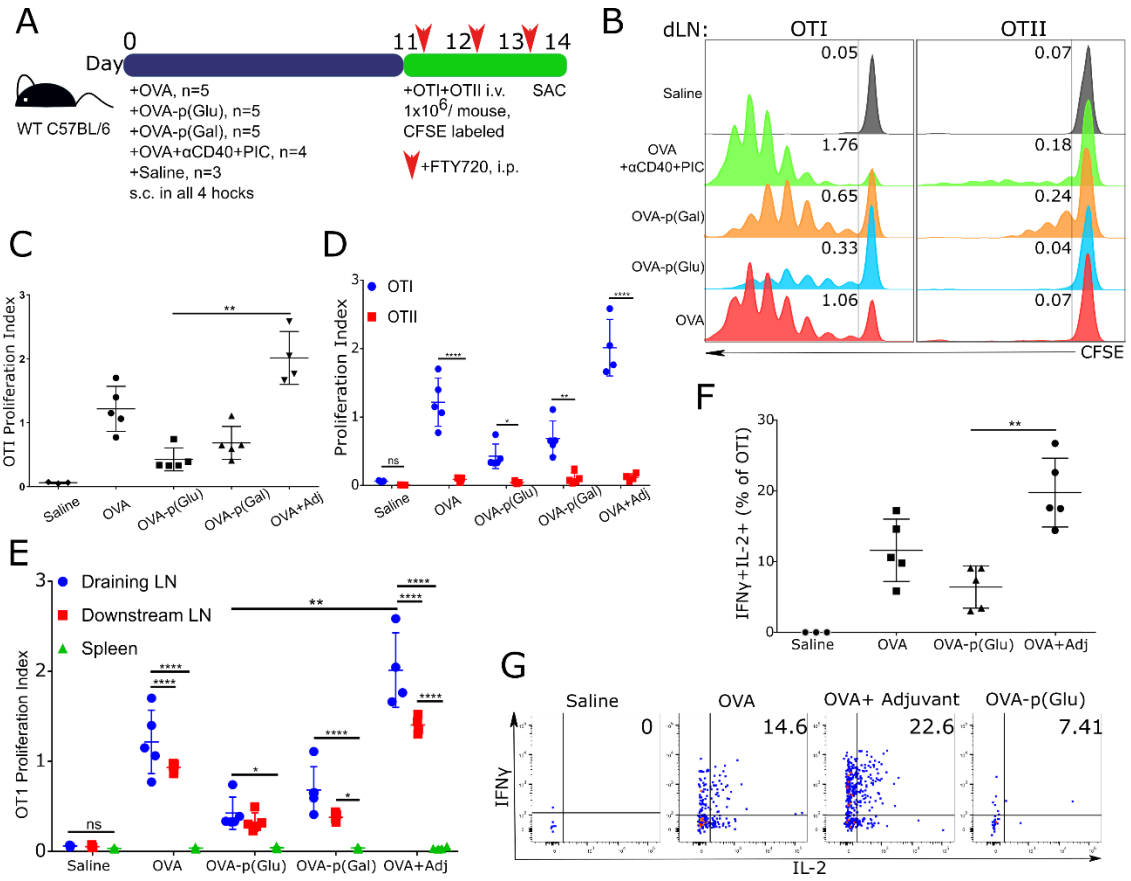

Fig 15. Antigen-specific CD8$^+$ T cells respond to archived antigen- p(GluNAc) by down-regulating proliferation and type 1 cytokine production. (A) Experimental timeline to assess the phenotype of CD45.1$^+$ OTI CD8$^+$ and OTII CD4$^+$ T cells adoptively transferred into mice that have archived antigen injected s.c. in all hocks under the indicated conditions. All mice received an equal dose of 20 μg OVA. αCD40 was used at 4 μg and poly(I:C) at 4 μg in the positive control. Mice were also treated with daily i.p. injections of FTY720 to block T cell egress from LNs from days 11-14. (B) CFSE-dilution proliferation trace of OTI and OTII cells from all groups at day 14; numbers represent the proliferation index in each group. (C) Proliferation index of OTI cells in dLNs. (D) Proliferation index of OTI and OTII cells in dLNs. (E) Proliferation index of OTI cells from draining LNs (axillary and popliteal), downstream LNs (brachial and inguinal) and the spleen. (F) LN OTI CD8$^+$ T cells that secreted IFNγ and IL-2 upon restimulation with $OVA_{257-264}$ peptide. (G) Representative flow cytometry plots showing cytokine secretion by OTI CD8$^+$ T cells. Statistical differences were determined by one-way ANOVA using Tukey's post hoc test (*p ≤ 0.05, **p ≤ 0.01, ***p ≤ 0.005).

Antigen-specific CD8+ T cells responding to archived antigen delivered via p(GluNAc) conjugation adopt a central memory phenotype but demonstrate a lower ability to differentiate into longer-lived memory

Glyco-conjugated antigen archived in mice impose a suppressive program on antigen specific $CD8^+$ T cells, but the effect on effector and memory markers was still unknown. These OTI $CD8^+$ T cells preferentially differentiated into central memory cells, characterized by a higher fraction of $CD44^+CD62L^+$ cells than effectors ($CD44^+CD62L^-$), compared with the positive adjuvanted control (**Fig. 16A-C**). It was important to note that while most OTI cells were antigen-experienced from their high CD44 expression, there was a substantial fraction of OTI cells that remained naïve in the OVA-p(GluNAc) group, indicating that there were regulatory mechanisms at play to inhibit initial TCR stimulation. The higher central memory phenotype generated was also visualized by the steady increase in this population over the generations, compared with OVA only or adjuvanted OVA where we saw the proportion of effectors increase with the divisions (**Fig. 16D**). This rise in central memory with p(GluNAc) archiving was further confirmed by assessing the expression of transcription factors known to regulate effector vs memory differentiation. Two such markers are T-bet (upregulated by effectors) and Eomes (upregulated by memory). OTI cells in mice treated with OVA-p(GluNAc) significantly upregulated Eomes compared to T-bet, indicating more memory (**Fig. 16E**). However, these OTI cells consisted of fewer long-lived memory precursor cells characterized by a failure to upregulate IL7Rα (CD127) relative to KLRG-1, and the ratio of these precursors to short-lived effector cells ($IL7R\alpha^-KLRG\text{-}1^+$) was significantly lower compared to the positive control (**Fig. 16F**). These data indicated that even if archived

antigen-p(GluNAc) gave a higher memory signature, that memory pool might not be long-lived or functionally active.

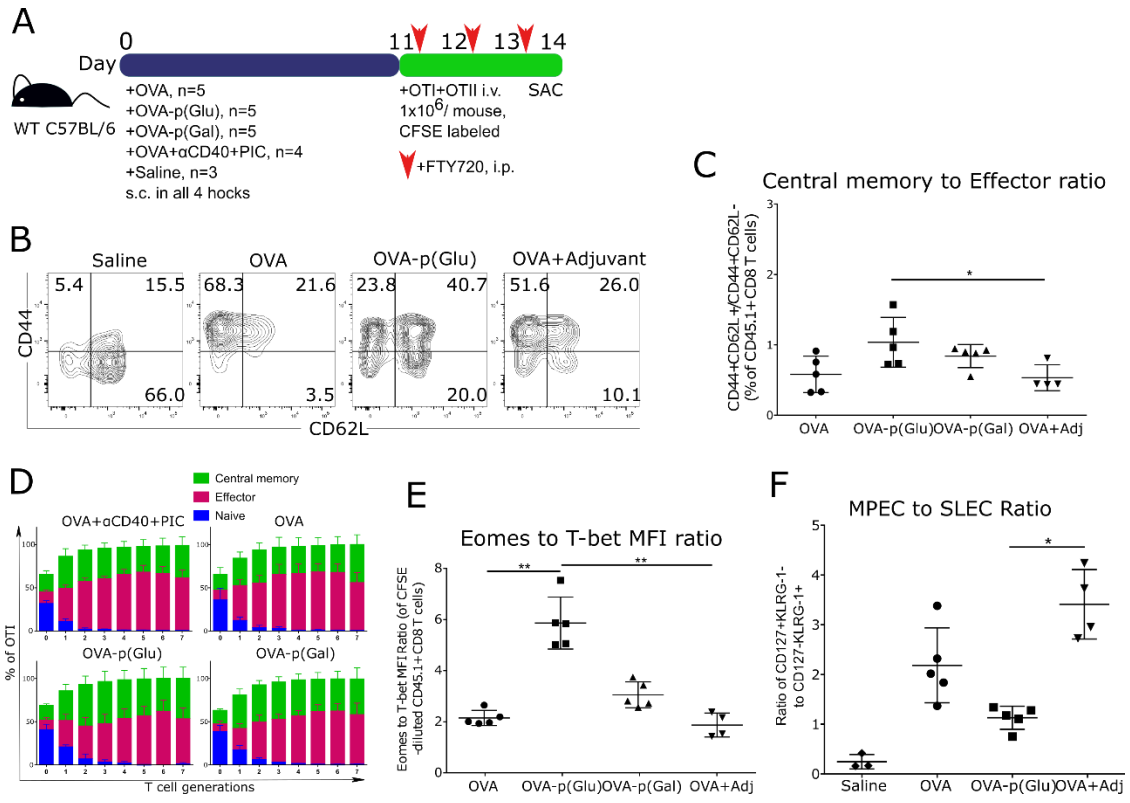

Fig 16. Antigen-specific CD8$^+$ T cells responding to archived antigen delivered via p(GluNAc) conjugation adopt a central memory phenotype but demonstrate a lower ability to differentiate into longer-lived memory. (A) Experimental timeline shown in the previous figure. (B) Representative flow cytometry plots showing CD44 and CD62L expression on OTI cells from all four groups. (C) Quantified ratio of central memory (CD44$^+$CD62L$^+$) to effector (CD44$^+$CD62L$^-$) OTI cells in dLNs. (D) Evolution of central memory, effector and naïve (CD44$^-$CD62L$^+$) OTI CD8$^+$ T cells over the generations, expressed as % of OTI in dLNs. (E) Ratio of MFI of Eomes to Tbet on OTI CD8$^+$ T cells that have proliferated (CFSE-diluted). (F) Ratio of OTI CD8$^+$ T cells that are memory precursors (CD127$^+$KLRG1$^-$) to short-lived effectors (CD127$^-$KLRG1$^+$), expressed as % OTI CD8$^+$ T cells in dLNs. Statistical differences were determined by one-way ANOVA using Tukey's post hoc test (*p ≤ 0.05, **p ≤ 0.01, ***p ≤ 0.005).

Archived glyco-conjugated antigen preferentially expands higher avidity CD8+ T cells in the LN, imprinting a suppressive program onto them

Naïve T cells respond differently to antigen bound MHC depending on the strength and avidity of the TCR-MHC interaction. Higher avidity interactions to exogenous antigen tend to result in an effector program whereas lower affinity interactions with self-antigen usually result in the maintenance of peripheral tolerance. In order to investigate whether the TCR avidity has an effect on how naïve $CD8^+$ T cells respond to archived antigen-p(GluNAc), we immunized mice with either unmodified OVA, OVA-p(GluNAc), OVA-p(Gal), OVA with the combined adjuvant or saline and adoptively transferred an equal number of OTI and OT3 cells 11 days post-immunization (**Fig. 17A**). OVA-transgenic OT3 cells recognize the same MHCI bound SIINFEKL epitope on OVA as OTI cells do, but with much lower avidity since they were isolated from the periphery of mice in a type 1 diabetes model with OVA expressed under the RIP promoter. Since both the OTI and OT3 were on the same $CD45.1^+$ congenic background, they were labeled with different fluorescent dyes to distinguish them from one another- OTI cells were VPD-labeled and OT3 cells were CFSE-labeled (**Fig. 17A**). While OTI were recovered in significantly less numbers in the OVA-p(GluNAc) and OVA-p(Gal) groups compared with OVA only or adjuvanted OVA, OT3 cells failed to proliferate in the dLNs, staying at constant low numbers (**Fig. 17B**). Overall fewer OVA-specific T cells were recovered from the spleen of mice, but while the trend with OTI was consistent with lowest numbers detected in the OVA-p(GluNAc) and OVA-p(Gal) groups, higher numbers of OT3 were detected in all conditions expect for the adjuvanted group (**Fig. 17C**). The OT3 cells thus detected were most likely not the product of proliferation but circulation at steady-state because

similar numbers were present across all conditions (**Fig. 17C**). Thus, the presence of an equal number of higher-avidity CD8$^+$ T cells in the secondary lymphoid organs inhibited the proliferation of the lower avidity cells most likely by forming longer synapses with SIINFEKL-bound MHCI presented by the same APC set. Interestingly though, OT3 had a higher residence time in the spleen compared to the LN under all conditions that involved immunizing without an adjuvant (**Fig. 17D, E**). Better insight into the phenotype of OT3 cells could be gained in a competition-free setting by adoptively transferring only OT3 cells. Consistent with prior results, OTI proliferation was lowest in the OVA-p(GluNAc) group (**Fig. 17F**) and was accompanied by lowest IFNγ secretion (**Fig. 17G**).

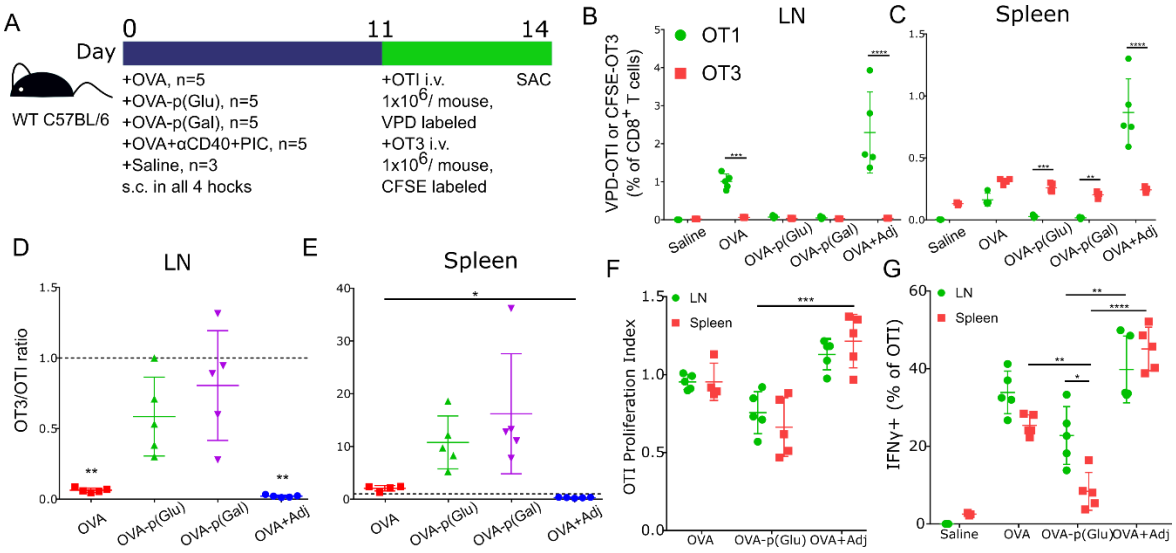

Fig 17. Archived glyco-conjugated antigen preferentially expands higher avidity CD8$^+$ T cells in the LN, imprinting a suppressive program onto them. (A) Experimental timeline for assessing the response of antigen-specific high avidity CD8$^+$ T cells (CD45.1$^+$ VPD-labeled OTI) or low avidity (CD45.1$^+$ CFSE-labeled OT3) to archived antigen. (B) OTI and OT3 recovered from the dLNs at day 14. (C) OTI and OT3 recovered from the spleen at day 14. (D) Ratio of numbers of OT3 to OTI in the dLNs at day 14. (E) Ratio of numbers of OT3 to OTI in the spleen at day 14. (F) Proliferation index of OTI in dLNs and spleen. (G) OTI that generated IFNγ in the dLNs and spleen upon restimulation with $OVA_{257-264}$. Statistical differences were determined by one-way ANOVA using Tukey's post hoc test (*p ≤ 0.05, **p ≤ 0.01, ***p ≤ 0.005).

Antigen-p(GluNAc) co-delivered and archived with an adjuvant enhances the proliferation of naïve CD8$^+$ T cells and differentiation into effectors and central memory, while retaining the skewed central memory signature

Next, we asked whether the reduction in activation and memory phenotype of antigen-specific CD8$^+$ T cells could be restored if the antigen was delivered and archiving was established with an adjuvant. We immunized mice with OVA-p(GluNAc), in the presence of absence of a poly(I:C) adjuvant (PIC). We picked PIC as our adjuvant, because of the extensive characterization done both in vitro and in vivo with this adjuvant in the context of a vaccine with antigen-p(GluNAc), and because PIC is an agonist of TLR3, which is highly expressed on LECs and other APCs in the dLNs. We adoptively transferred CFSE-labeled OTI and OTII T cells two weeks post-immunization and assessed differences in the phenotype of the T cells (**Fig. 18A**). First, we evaluated whether co-delivering OVA-p(GluNAc) with PIC had an impact on archiving in LECs- it did not and the percent of OVA$^+$ cells (**Fig. 18B**), absolute numbers of OVA+ cells (**Fig. 18C**) and MFI of OVA$^+$ cells (**Fig. 18D**) were unchanged. Co-delivery with PIC, however, significantly increased the total number of LN-resident cross-presenting CD8$^+$ DCs that retained antigen two weeks post-immunization compared to LECs (**Fig. 18E**). Addition of PIC also significantly increased the proliferation of OTI (**Fig. 18F**) and OTII (**Fig. 18G**) T cells. The improvement in proliferation was accompanied by an expansion of cells with an effector and central memory phenotype in both the OTI and the OTII compartment, though there was no improvement in the ratio of central memory to effectors (**Fig. 18H-L**). We also observed a significant increase in the number of T-bet$^+$ and Eomes$^+$ cells, but the ratio of Eomes$^+$ to T-Bet$^+$ cells stayed constant (**Fig. 18M-O**).

This consistency in the memory to effector ratio was also seen in the similar responses of mice to a Listeria challenge- no significant differences in bacteria burden were observed in the spleens of mice who archived antigen with OVA-p(GluNAc) delivered with or without PIC, and challenged with an attenuated strain of Lm-OVA (**Fig. 18P**). Thus, co-delivering antigen-p(GluNAc) with an adjuvant such as PIC improves the overall proliferation and activation without altering the preferential memory to effector phenotype observed with p(GluNAc) conjugation.

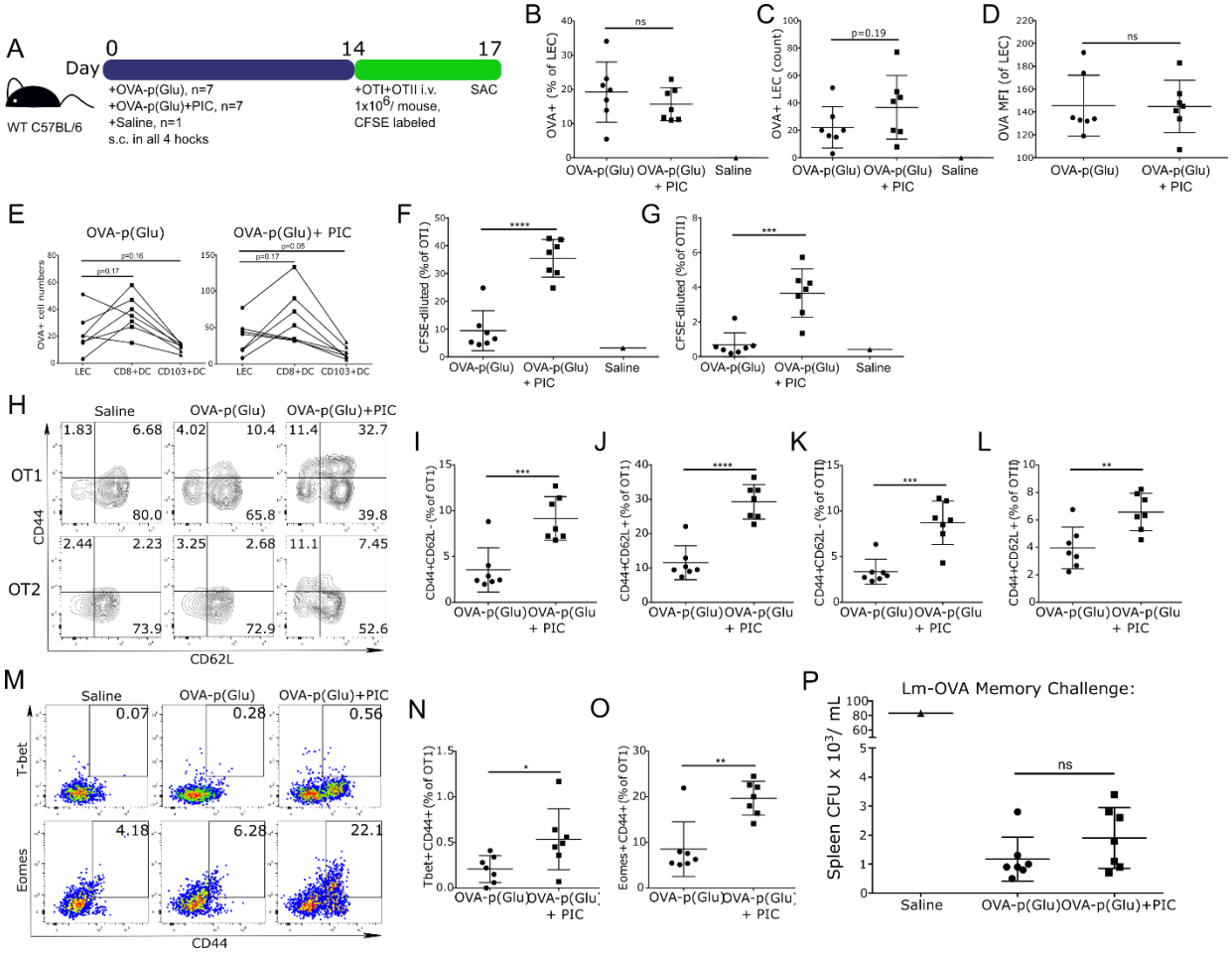

Fig 18. Antigen-p(GluNAc) co-delivered and archived with an adjuvant enhances the proliferation of naïve $CD8^+$ T cells and differentiation into effectors and central memory, while retaining the skewed central memory signature. (A) Experimental timeline to evaluate the effect of archiving glycopolymerized antigen with poly(I:C) adjuvant on archiving and the immune response at day 17. OVA dose was 25 ug and poly(I:C) dose was 10 ug per mouse. (B) OVA^+ LECs in dLNs. (C)

Fig 18. Antigen-p(GluNAc) co-delivered and archived with an adjuvant enhances the proliferation of naïve CD8$^+$ T cells and differentiation into effectors and central memory, while retaining the skewed central memory signature (continued) Number of OVA$^+$ LECs in dLNs. (D) MFI of OVA$^+$ LECs in dLNs. (E) Number of OVA$^+$ LECs, CD8$^+$ DCs and CD103$^+$ DCs in the OVA-p(GluNAc) group (left) and OVA-p(GluNAc) and poly(I:C) group (right). (F) OTI CD8$^+$ T cells that proliferated (diluted CFSE) in dLNs. (G) % OTII CD4$^+$ T cells that proliferated (diluted CFSE) in dLNs. (H) Representative flow cytometry plots showing CD44 and CD62L expression on OTI and OTII T cells in dLNs. (I) LN OTI CD8$^+$ T cells that are effectors (CD44$^+$CD62L$^-$). (J) LN OTI CD8$^+$ T cells that are central memory (CD44$^+$CD62L$^+$). (K) LN OTII CD4$^+$ T cells that are effectors (CD44$^+$CD62L$^-$). (L) LN OTII CD4$^+$ T cells that are central memory (CD44$^+$CD62L$^+$). (M) Representative flow cytometry plots showing Tbet and Eomes expression on activated (CD44$^+$) OTI in dLNs. (N) T-bet$^+$CD44$^+$ OTI CD8$^+$ T cells in dLNs. (O) Eomes$^+$CD44$^+$ OTI CD8$^+$ T cells in dLNs. (P) After the OTI CD8$^+$ T cell adoptive transfer on day 14, immunized mice were allowed to rest for a month before receiving a challenge of 10^8 CFUs of an attenuated strain of Lm-OVA via i.v. tail vein injection on day 39. CFUs present in the spleen post-challenge at day 42 were quantified. Statistical differences were determined by one-way ANOVA using Tukey's post hoc test (*$p \leq 0.05$, **$p \leq 0.01$, ***$p \leq 0.005$).

Antigen-p(GluNAc) antigen co-delivered and archived with an adjuvant imprints a suppressed phenotype on CD8$^+$ T cells, compared with unconjugated antigen

Given that co-administration of antigen-p(GluNAc) with an adjuvant such as PIC improved proliferation and activation, we asked the question whether that "restored" phenotype of antigen-p(GluNAc) alone was comparable to what would be obtained with unconjugated antigen delivered with the same adjuvant. Thus, we compared the response of OTI CD8$^+$ T cells to OVA archived with unmodified OVA and PIC with OVA-p(GluNAc) and PIC (**Fig. 19A**). The new higher OTI proliferation observed with OVA-p(GluNAc) and PIC failed to match the proliferation with OVA and PIC (**Fig. 19B**). This mismatch was also observed when comparing the effector and memory differentiation through markers such a CD44, CD62L and Eomes (**Fig. 19C-E**). Importantly, the skewed memory phenotype previously observed with p(GluNAc) conjugation was preserved and was significantly different from unmodified OVA and PIC (**Fig. 19F, G**). This memory signature was conserved in the dLNs but not in the spleen, showing that

the LN is an essential site for inducing this phenotype (**Fig. 19F, G**). Thus, archiving antigen-p(GluNAc) imprints the antigen-specific CD8$^+$ T cell response imprinted with regulatory properties that cannot be easily reversed by simply adding an adjuvant to the immunization, and apparent increases in the overall proliferation and effectors do not change a suppressed end result.

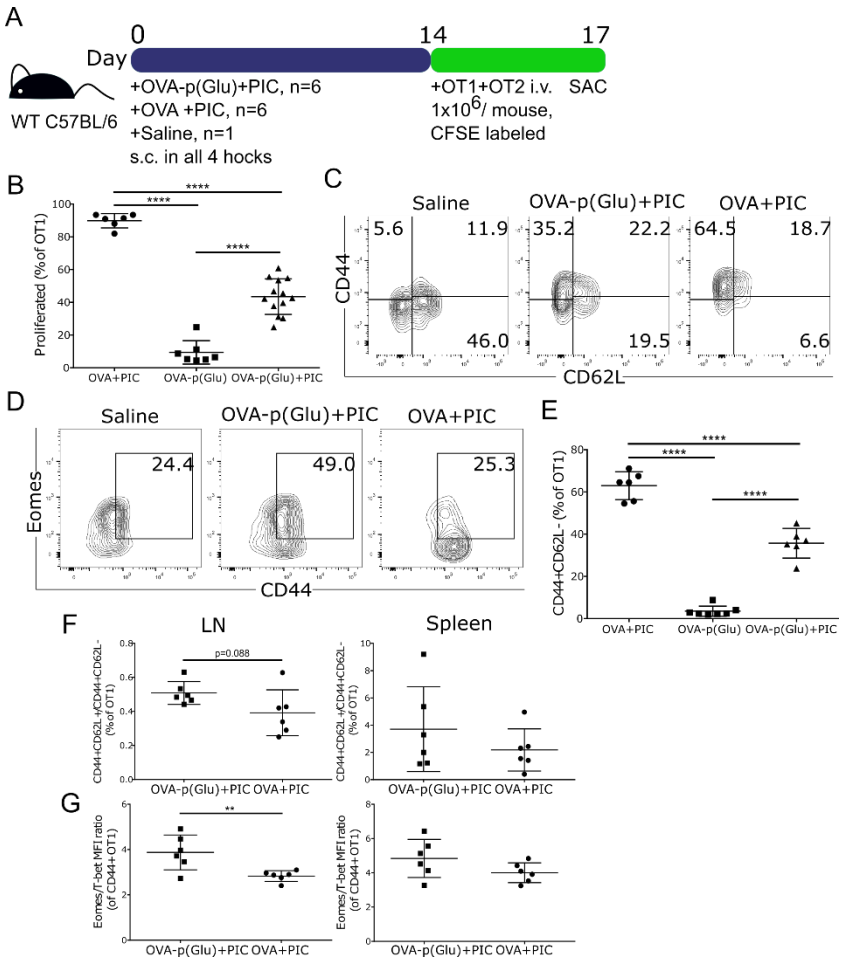

Fig 19. Antigen-p(GluNAc) antigen co-delivered and archived with an adjuvant imprints a suppressed phenotype on CD8$^+$ T cells, compared with unconjugated antigen. (A) Experimental timeline. (B) % OTI that proliferated in dLNs. (C) Representative flow cytometry plots showing CD44 and CD62L expression on OTI in all three groups. (D) Representative flow cytometry plots showing Eomes and T-bet expression on OTI cells in dLNs. (E) % effector (CD44$^+$CD62L$^-$) OTI cells in dLNs. (F) Ratio of central memory (CD44+CD62L+) to effector memory (CD44$^+$CD62L$^-$) OTI cells in LN (left) and spleen (right). (G) Ratio of Eomes to T-bet on activated (CD44$^+$) OTI cells in LN (left) and spleen (right). Statistical differences were determined by one-way ANOVA using Tukey's post hoc test (*p ≤ 0.05, **p ≤ 0.01, ***p ≤ 0.005).

T cell memory generated with archived antigen-p(GluNAc) does not protect mice against inflammatory challenges

The phenotype of OTI cells that responded to archived OVA-p(GluNAc) did not give a clear indication if the higher central memory generated could be protective. To determine the nature of the memory and role in future antigenic challenge, we challenged mice with B16-OVA melanoma two weeks following OTI adoptive transfer (**Fig. 20A**). The mice were immunized in the left hock and the tumor was implanted on the back of the mice ipsi (i.e., on the same side) of the draining left hock (**Fig. 20A**). This anti-tumor vaccination strategy of immunizing in one hock and using the opposite hock as unimmunized control has been explored in the Swartz lab before; anti-tumor efficacy can only be detected in the ipsi hock where T cells mount an immune response to local tumor-draining antigens. We found that tumor growth was significantly delayed only in the case when antigen was archived in mice in the presence of adjuvant (**Fig. 20B**). All other conditions where OVA was archived at steady-state, irrespective of the conjugation status, failed to protect the mice against tumor outgrowth; these mice behaved like their immune system has never seen OVA before as in the saline controls (**Fig. 20B**). Because melanoma is characterized by an immune suppressed microenvironment, and glycopolymerization had little bearing on modifying that tolerogenic state in the absence of an adjuvant, we decided to test the protective nature of archived antigen-p(GluNAc) in response to bacterial Listeria infection. A month after OTI adoptive transfer, mice were infected systemically with $1x10^8$ CFUs of Lm-OVA via i.v. injection and sacrificed three days later to analyze the bacterial load in the liver (**Fig.**

20C). Even though there was high variability in the saline untreated mice, we observed a significantly higher bacterial burden in the liver of the mice that had archived OVA-p(GluNAc) (**Fig. 20D, E**). These data confirmed that memory generated with OVA-antigen was suppressive and could not contribute to systemic protection against a bacterial infection.

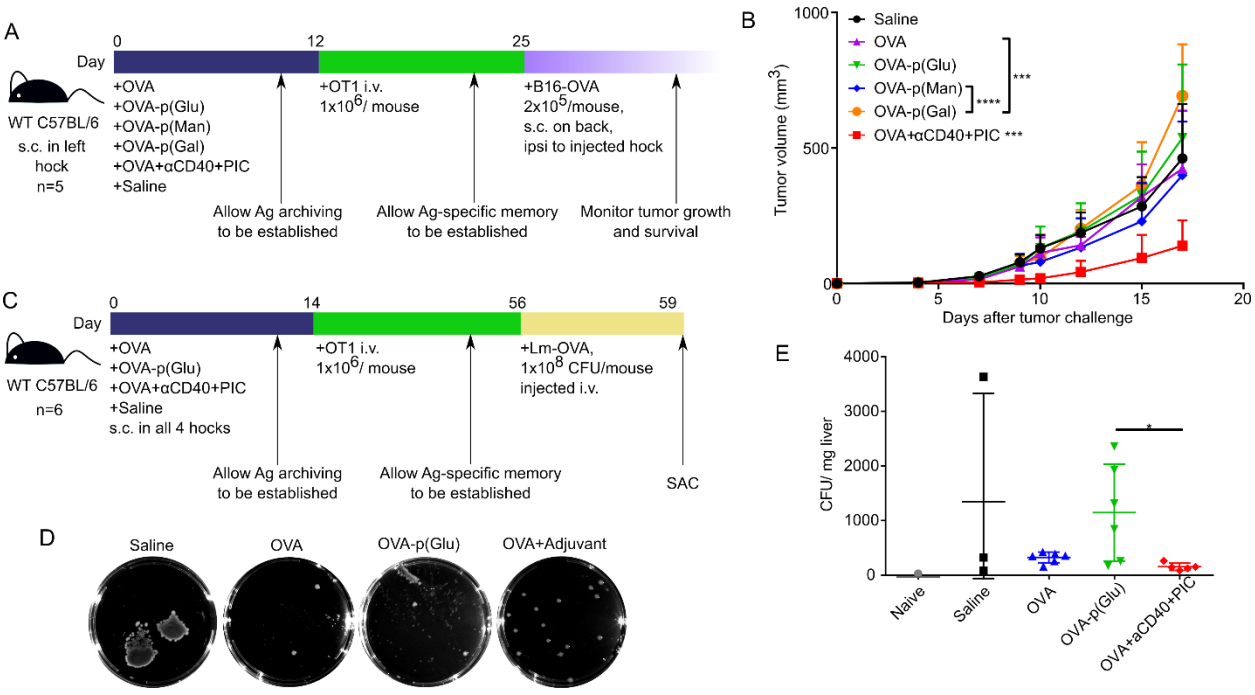

Fig 20. T cell memory generated with archived antigen-p(GluNAc) does not protect mice against inflammatory challenges, including an antigen-specific Listeria or melanoma challenge. (A) Mice were immunized with OVA in free or glycoconjugate form s.c. in the left hock and OTI cells were adoptively transferred via an i.v. injection on day 12. They received an intradermal challenge of B16-OVA melanoma cells on the back ipsi to the injected draining hock on day 25 and tumor size was monitored. (B) Tumor volume in mm^3 plotted over time, starting from day 25. (C) Mice were immunized with OVA in free or glycoconjugate form s.c. in the left hock and OTI cells were adoptively transferred via an i.v. injection on day 14. They received a systemic i.v. injection of 10^8 CFU of an attenuated Lm-OVA listeria strain on day 56, and the CFUs were quantified three days later in the liver. (D) Representative BHI (brain heart infusion medium) agar plates showing Lm-OVA colonies from processed livers. Single cell liver suspensions were plated and imaged 36 h later. (E) Bacterial CFUs per mg of weighed liver. Total counted CFUs per plate and dilution were normalized with the liver weight per mouse. Statistical differences were determined by one-way ANOVA using Tukey's post hoc test (comparisons were made at day 17 post tumor challenge for statistical analysis in B) (*$p \leq 0.05$, **$p \leq 0.01$, ***$p \leq 0.005$).

Further analysis of the OTI CD8$^+$ T cells in the spleen of the mice at day 59 yielded no insights into differences in response on challenge. OTI cells from all groups were recovered in similar numbers (**Fig. 21A**), proliferated to the same extent (**Fig. 21B**) and produced pro-inflammatory cytokines at similar levels upon restimulation with the cognate SIINFEKL peptide (**Fig. 21C**). This indicated to us that there were more regulatory mechanisms at play, possibly from the endogenous compartment, though we could not detect any differences there (data not shown). An ELISA of the restimulation culture supernatant revealed that IL-17 was produced in significantly larger quantities by splenocytes compared to IFNγ (**Fig. 21D**). Literature sources show that the source of the IL-17 could be conventional inflammatory Th17 αβ CD4$^+$ T cells or mucosal γδ T cells. Even though listeria was injected i.v., the bacteria could still have partially homed to the gut where it would have stimulated IL-17 production from these non-conventional T cells residing in the gut mucosal endothelium. Another potential source of IL-17 could be CD8$^+$ T cells but these have only been documented to be commensal-specific through non classical MHC, skin-resident and plastic and responsive to alarmins upon tissue damage (*184*).

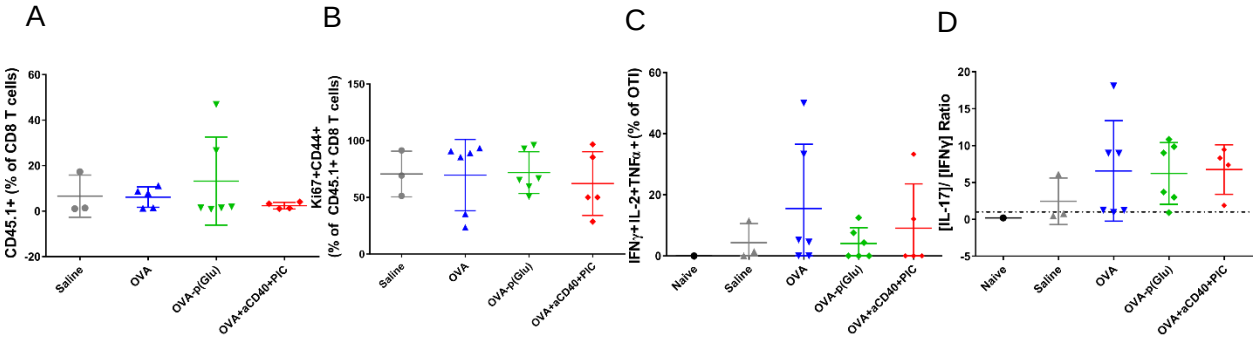

Fig 21. Immunological mechanisms behind the Listeria challenge to archived antigen-p(GluNAc) are not apparent at the conventional T cell level. (A) % CD45.1$^+$ CD8$^+$ T cells (OTI) in spleen at day 59. (B) % activated and proliferating (Ki67$^+$CD44$^+$) OTI cells in spleen at day 59. (C) % OTI that produced the pro-inflammatory cytokines (IFNγ, IL-2 and TNFα) upon 3 h restimulation in **Fig**

Fig 21. Immunological mechanisms behind the Listeria challenge to archived antigen-p(GluNAc) are not apparent at the conventional T cell level (continued) culture without exogenous peptides, measured by flow cytometry. (D) Ratio of IL-17 to IFNγ secreted into the culture supernatant and measured by ELISA. Statistical differences were determined by one-way ANOVA using Tukey's post hoc test (*p ≤ 0.05, **p ≤ 0.01, ***p ≤ 0.005).

In order to confirm our suspicions, we measured the production of IL-17 and IFNγ cytokines by γδ T cells and conventional $CD4^+$ T cells using flow cytometry, from the spleen of mice that we infected with Lm-OVA. This attenuated strain of Lm-OVA has the 2W1S peptide in its backbone, in addition to OVA peptides, conferring this strain the ability to stimulate endogenous 2W1s-specific $CD4^+$ T cells from the large precursor pool in addition to a strong $CD8^+$ cytotoxic response upon infection (**Fig. 22A**). Because the presence of the adjuvant made little difference to clearance of the infection seen from the similar bacterial burdens between mice that had archived OVA vs OVA and PIC adjuvant, we suspected that the ability of this Lm strain to get cleared easily could also be due to the strong elicited endogenous $CD4^+$ T cell response, beyond the fact that it is attenuated and cannot replicate inside infected cells (**Fig. 20E**). Thus, we isolated and digested splenocytes five days after the mice were infected with $1x10^7$ CFU of Lm(2W1s)-OVA, and restimulated the cells for 6 h in the presence of BFA, either without peptide, or with SIINFEKL, ISQ or 2W1S peptide. We isolated ~1 % γδ T cells from $CD4^-CD8^-$ gated $CD3^+$ T cells in the spleen (**Fig. 22B**). This low frequency is expected from non-mucosal tissues such as the spleen. These γδ T cells produced significantly more IL-17 than IFNγ in culture, expressed as a ratio of $IL\text{-}17^+$ to $IFN\gamma^+$ cells, compared with conventional $CD4^+$ αβ T cells (**Fig. 22C, D**). The response was similar across groups, showing that exogenously added peptide antigens do not enhance the response to restimulation when whole infected splenocytes from which

bacterial antigens can be easily derived are already present in the culture (**Fig. 22C, D**). Thus, IL-17 read-out could be important in interpreting future immunological experiments with this Lm strain. Importantly, we now knew that the blunted response with archived antigen-p(GluNAc) upon challenge was most likely due to a previous deletional response in the initial activation, generated a smaller reservoir of central memory cells that can respond to antigen re-encounter, but their potential to re-activate

A is B unchanged. C The game is D in the numbers.

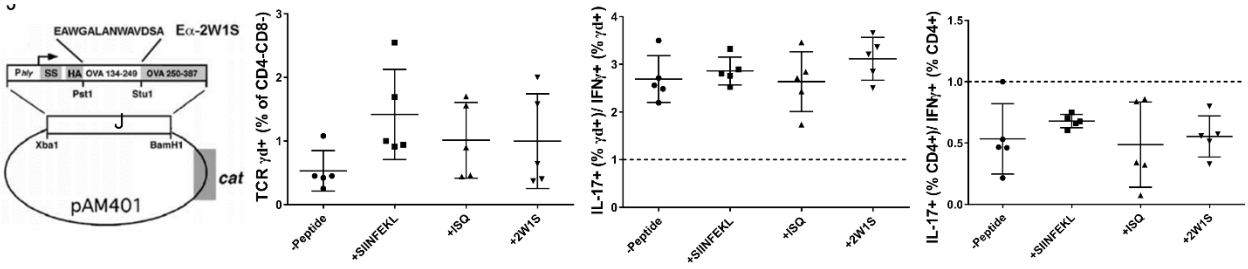

Fig 22. Listeria infection with the attenuated strain elicits an important IL-17 response, mediated by splenic TCR γδ$^+$ T cells. (J) Plasmid map of the attenuated act-A mutant strain of Listeria showing the immunodominant epitopes of OVA and of the 2W1S peptide in the backbone. (K) % TCR γδ$^+$ of CD4$^-$CD8$^-$ double-negative T cells in the spleen under all restimulation conditions. (L) Ratio of % IL-17$^+$ TCR γδ$^+$ to IFNγ$^+$ TCR γδ$^+$ cells upon restimulation with $OVA_{257-264}$ or $OVA_{323-339}$ or 2W1S peptides or plain media. (M) Ratio of % IL-17$^+$ conventional (TCR αβ$^+$) CD4$^+$ T cells to IFNγ$^+$ conventional (TCR αβ$^+$) CD4$^+$ T cells upon restimulation with $OVA_{257-264}$ or $OVA_{323-339}$ or 2W1S peptides or plain media. Statistical differences were determined by one-way ANOVA using Tukey's post hoc test (*p ≤ 0.05, **p ≤ 0.01, ***p ≤ 0.005).

Lymphatic endothelial cells cross-present archived p(GluNAc)-antigen but are not responsible for the enhanced central memory phenotype of CD8$^+$ T cells

We have shown that OVA-p(GluNAc) antigen is archived in LECs to a significantly higher extent at steady state compared with free OVA. Archived antigen-p(GluNAc) also results in a suppressed CD8$^+$ T cell response characterized by lower proliferation, most likely deletion and generation of non-protective central memory pool. Recent published

work in the Swartz lab shows that LECs are able to educate naïve $CD8^+$ T cells into a central memory phenotype at steady state and in short term, and these cells, when generated in vitro and adoptively transferred in vivo, have the ability to behave like normal central memory $CD8^+$ T cells and defend the host against a bacterial infection. Our result, though in a different model of archiving and in vivo, was in contrast to what the Swartz lab had previously observed with the protective potential of the central memory cells generated by LECs. However, we needed to determine the contribution of LECs to presentation of archived antigen before making any conclusions.

There are various challenges associated with evaluating antigen presentation and education of T cells by lymph node stromal cells (LNSC) including LECs in vivo (*180*). This is because completely knocking them out would destroy the LN architecture and draining lymphatics critical for the normal course of any immune reaction. Conditional knock-outs have been made possible using the Cre recombinase system with the gene of choice floxed. Specific genes have been conditionally knocked out in LECs this way using Prox1 or Lyve1 promoters. A caveat is that these genes are not specific to LECs only- Prox1 is expressed by hepatocytes and Lyve1 is expressed by macrophages- making results hard to interpret. MHCII has been knocked out in LECs conditionally using the Prox1-Cre system, generating a useful tool for studying the role of LECs in presenting exogenous antigen to $CD4^+$ T cells. This strategy cannot be used with MHCI because LECs play an essential role in the maintenance of peripheral tolerance and abrogating MHCI in LECs would compromise homeostatic immunity and would introduce confounding variables in the investigation of cross-presentation of exogenous

antigen to $CD8^+$ T cells. Moreover, recent single-cell transcriptomic analyses of LECs have revealed extraordinary heterogeneity of LECs in localized in various areas of the LN, in their expression of genes related to scavenging, antigen presentation and regulation, making selecting a gene or promoter difficult to generate a conditional knock-out (*32*, *172*). We can, however, take advantage of the fact that LECs are resistant to radiation and thus would remain intact if mice received sublethal whole body irradiation to deplete their hematopoietic compartment from the bone marrow. Thus, generating bone marrow chimeras where the mice are then reconstituted with hematopoietic cells that are unable to cross-present, would constitute a good model for studying the contribution of LECs when it is the only APC type that can cross-present.

First, we gamma irradiated WT C57BL/6 mice with either a sublethal bolus dose of 900 rad or in two rounds of 450 rad spaced 4 h apart, using a Caesium-137 radiation decay source (**Fig. 23A**). These doses have been found to effectively deplete circulating and bone marrow resident mature immune cells as well as immature progenitor hemopoietic cells that are the fastest replicating cells in the host. The 450x2 schedule has the reported advantage that it can minimize adverse effects associated with radiation but it was necessary to conduct our own radiation dose-response study. To prevent radiation-associated morbidity, mice were adoptively transferred with $1x10^7$ bone marrow cells each within an hour of the last radiation dose via a tail vein i.v. injection (**Fig. 23A**). Mice start recovering soon after the bone marrow reconstitution, and it typically takes them 4-6 weeks to allow the injected bone marrow precursor cells to fully implant into the recipient's bone marrow to give rise to a new hematopoietic compartment. Thus, it is

essential to leave the mice undisturbed in that window to allow full recovery and bleeding them to monitor reconstitution can remove a considerable fraction of the circulating bone marrow progenitor cells, causing morbidity (data not shown). Indeed, we detected significantly lower numbers of all circulating immune cells in the blood of mice at 1-2 weeks following radiation and bone marrow reconstitution. The bone marrow injected into the WT recipients were either from WT hosts (control) or $\beta 2m^{-/-}$ hosts that are MHCI-deficient such as to generate two sets of bone marrow chimeras where the WT→WT chimeras have a functional APC compartment and $\beta 2m^{-/-}$→WT chimeras have stromal radioresistant APCs such as LECs capable of antigen presentation but a hematopoietic APC compartment that is unable to present because of the lack of an essential molecule (β2m) in its MHCI machinery (**Fig. 23B**).

We first determined if we generated successful chimeras from irradiation and reconstitution by bleeding mice 6 weeks after when it was safe to do so, and staining for the numbers and MHCI expression of different circulating cells using flow cytometry (**Fig. 23C**). We quantified the numbers of T cells, B cells, granulocytes, dendritic cells (DCs) and monocytes and showed the gating strategy used (**Fig. 23C**). We also included naïve WT BL/6 mice as a benchmark comparison to make sure immune cells in the chimeras were regenerated to numbers normal in WT mice. Lymphocytes were present in normal quantities in all chimeras (**Fig. 23D, E**). A higher fraction of T and B cells were detected in the WT→ WT chimeras that had undergone the higher bolus 900 rad dose, possibly from homeostatic proliferation generated from higher inflammation in these mice, and these mice were excluded from further experiments to reduce variability

(**Fig. 23D, E**). We observed normal reconstitution of DCs (**Fig. 23F**), granulocytes (**Fig. 23G**), classical monocytes (**Fig. 23H**) and non-classical monocytes (**Fig. 23I**) in all chimeras, compared with the naïve WT mice. As observed before with lymphocytes, we also observed a significantly higher number of DCs (**Fig. 23F**) and non-classical monocytes (**Fig. 23I**) with the higher rad dose, further justifying why we excluded them in later experiments. Beyond reconstituted numbers, we also measured differences in H2-kb MHCI expression on these circulating cells. We found that as expected, while MHCI expression in cells in the WT→ WT chimeras was intact and comparable to levels in naïve WT mice, it was significantly decreased in the $\beta 2m^{-/-}$→WT chimeras (**Fig. 23J-N**). This was the case for all relevant APC subsets that we checked, including all hematopoietic $CD45^{+}$ cells (**Fig. 23J**), B cells (**Fig. 23K**), DCs (**Fig. 23L**), classical monocytes (**Fig. 23M**) or non-classical monocytes (**Fig. 23N**). These confirmed that we had successfully generated and reconstituted bone marrow chimeras, where the control WT→ WT chimeras had normal MHCI expression and only the $\beta 2m^{-/-}$→WT chimeras had MHCI-deficient expression on circulating hematopoietic cells.

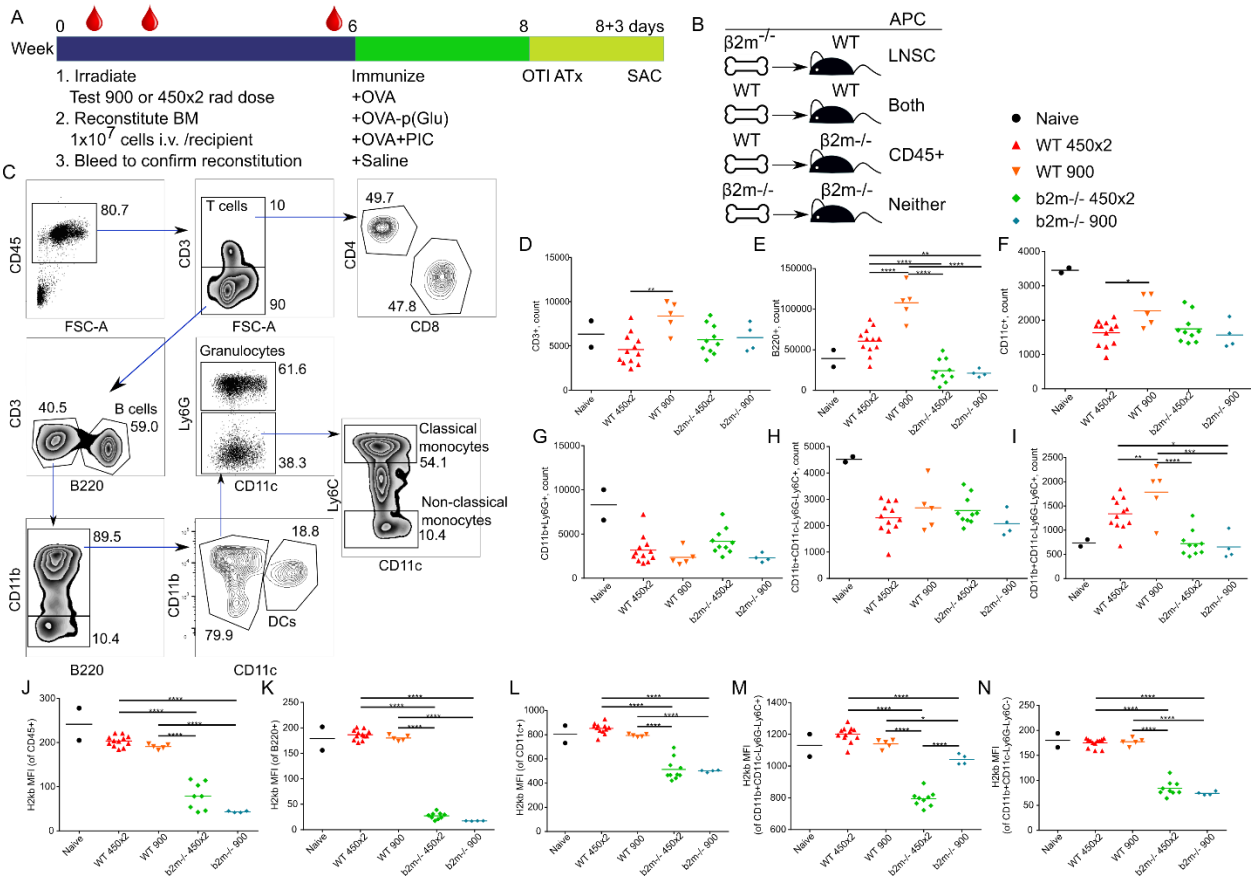

Fig 23. Characterization of APC reconstitution and phenotype in blood following bone marrow irradiation and chimera generation. (A) Experimental timeline describing the irradiation and generation of the bone marrow chimeras using two different radiation doses and reconstitution via i.v. injection of bone marrow cells from either WT or β2m$^{-/-}$ hosts. Mice were allowed to recover from the procedure for 6 weeks and the APCs in the blood were characterized for recovered numbers and MHC I expression. (B) Types of bone marrow reconstitutions and the outcome on the identity of the APC in each case. Only the top two bone marrow chimeras in this schematic were generated. (C) Flow cytometry gating strategy showing relevant CD45+ hematopoietic APCs and other cell populations in the blood at week 6 post-irradiation and bone marrow reconstitution. (D) Numbers of T cells in blood at week 6. (E) Number of B cells in blood at week 6. (F) Number of dendritic cells in blood at week 6. (G) Number of granulocytes in blood at week 6. (H) Number of classical monocytes in blood at week 6. (I) Number of non-classical monocytes in blood at week 6. (J) MFI of MHC I on CD45+ hematopoietic cells. (K) MFI of MHC I on B cells. (L) MFI of MHCI on dendritic cells. (M) MFI of MHC I on classical monocytes. (N) MFI of MHC I on non-classical monocytes. Statistical differences were determined by one-way ANOVA using Tukey's post hoc test (*p ≤ 0.05, **p ≤ 0.01, ***p ≤ 0.005).

We divided up these chimeras into four groups that we immunized s.c. with free OVA,

OVA-p(GluNAc) or saline as negative control or OVA and adjuvant as positive control,

adoptively transferred OTI cells two weeks post-immunization, and sacrificed the chimeras 3 days following adoptive transfer (**Fig. 24A**). We first evaluated the MHCI expression on all APC subsets of interest that we were able to isolate from LNs, spleen and the site of injection (skin) at the time of sac. We analyzed MHCI expression of APCs from the dLNs (**Fig. 24A**). LECs retained MHCI expression in the $\beta2m^{-/-}$→WT chimeras, which was expected from their radioresistant property (**Fig. 24B**). The MHCI expression of another stromal cell type FRCs, however, was significantly affected (**Fig. 24C**). MHCI expression on $CD45^+$ APCs was significantly reduced in the $\beta2m^{-/-}$→WT chimeras, including in macrophages (**Fig. 24D**), LN-resident cross-presenting $CD8^+$ DCs (**Fig. 24E**), migratory $CD103^+$ DCs (**Fig. 24F**) and plasmacytoid DCs (**Fig. 24G**). While the MHCI expression, measured by flow cytometry, was reduced to FMO control levels (= zero) in many subsets, it was still measurable (above zero) in the FRCs (**Fig. 24C**) or $CD8^+$ DCs (**Fig. 24E**) that suggested that they could also potentially contribute to antigen presentation in these $\beta2m^{-/}$→WT chimeras. We could nonetheless confidently conclude that LECs were the major antigen presenter in the dLNs of $\beta2m^{-/-}$→WT, which are a good tool for studying the contribution of LEC to cross presentation of archived antigen.

Because antigen immunized s.c. can be partially taken up by skin-resident APCs for further migration and trafficking to the dLNs, it was important to verify MHCI expression on these skin APCs at the time of sac. We confirmed that MHCI expression was abrogated to zero levels in the $\beta2m^{-/-}$→WT chimeras on skin LECs (**Fig. 24H**), FRCs (**Fig. 24I**), BECs (**Fig. 24J**), $CD207^+$ Langerin DCs (**Fig. 24K**), $CD11b^+$ DCs (**Fig. 24L**)

and skin DC monocytes (**Fig. 24M**), showing that they would have no contribution to antigen presentation in these chimeras.

MHCI expression on APCs in the spleen was also completely abrogated in the β2m$^{-/-}$→WT chimeras, including on macrophages (**Fig. 24N**), total conventional DCs (**Fig. 24O**), cross-presenting CD8^{+} DCs (**Fig. 24P**), CD11b^{+} DCs (**Fig. 24Q**) and plasmacytoid DCs (**Fig. 24R**). Thus, we were confident that we could attribute most of the antigen presentation contribution to LN-LECs only in our generated β2m$^{-/-}$→WT chimeras.

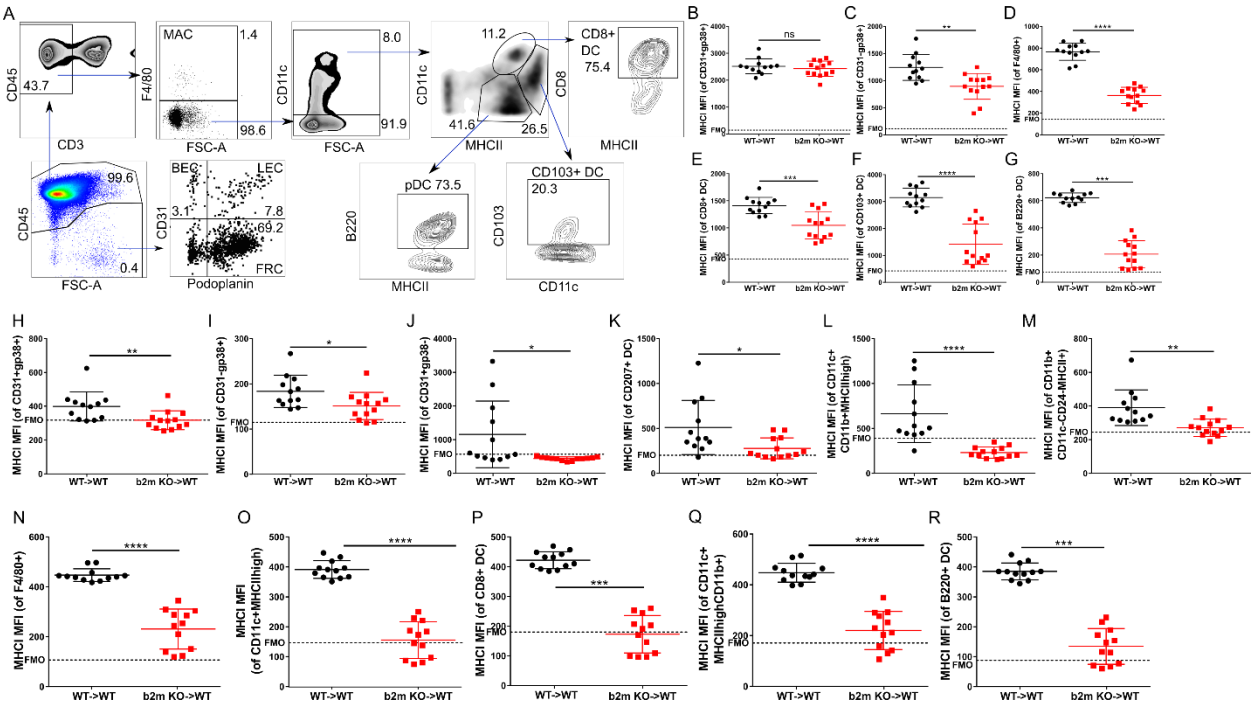

Fig 24. Characterization of APC phenotype in dLNs of chimeras at time of sacrifice following treatment with antigen-p(GluNAc) and adoptive transfer. Following the timeline proposed in the previous fig, bone marrow chimeras were immunized and OTI cells were adoptively transferred two weeks later to assess their phenotype. (A) Gating strategy of CD45^{+} hematopoietic and CD45^{-} stromal APCs in the dLNs of the chimeras at week 8. (B) MFI of MHC I on LECs. (C) MFI of MHC I on FRCs. (D) MFI of MHC I on BECs. (E) MFI of MHC I on CD8^{+} resident DCs. (F) MFI of MHC

Fig 24. Characterization of APC phenotype in dLNs of chimeras at time of sacrifice following treatment with antigen-p(GluNAc) and adoptive transfer (continued) I on $CD103^+$ migratory DCs. (G) MFI of MHC I on plasmacytoid DCs. (H-M) MFI of MHC I on skin-resident APCs at week 8. (H) MFI of MHC I on LECs. (I) MFI of MHC I on FRCs. (J) MFI of MHC I on BECs. (K) MFI of MHC I on $Langerin^+$ DCs. (L) MFI of MHC I on $CD11b^+$ DCs. (M) MFI of MHC I on skin monocytes. (N-O) MFI of MHC I on splenic APCs. (N) MFI of MHC I on macrophages. (O) MFI of MHC I on $CD8^+$ DCs. (P) MFI of MHC I on conventional DCs. (R) MFI of MHC I on plasmacytoid DCs. Statistical differences were determined by the Mann Whitney t test (C) (*$p \leq 0.05$, **$p \leq 0.01$, ***$p \leq 0.005$).

Next, we analyzed the phenotype of OTI cells that responded to archived antigen in the control and $\beta2m^{-/-}$→WT chimeras. We found that the OTI cells proliferated to a similar extent in the $\beta2m^{-/-}$→WT chimeras than they did in the WT→ WT chimeras, demonstrating that LECs are sufficient to cross-present antigen in circumstances where other professional $CD45^+$ APCs cannot (**Fig. 25A**). Moreover, we noted no difference in the production of inflammatory cytokines such as IFNγ, IL-2 or TNFα between the two types of chimeras (**Fig. 25B**). We could detect slightly higher levels of cytokines in the adjuvanted condition, which is probably due to higher homeostatic inflammation present in the chimeras. However, the ability of OTI to differentiate into central memory cells, measured from the surface expression of CD44 and CD62L and the ratio of central memory ($CD44^+CD62L^+$) to effector memory ($CD44^+CD62L^-$) was significantly decreased in the $\beta2m^{-/-}$→WT chimeras compared to the WT chimeras (**Fig. 25C, D**), showing that LECs are not responsible for the enhanced central memory phenotype seen with archived antigen-p(GluNAc) and that the archived antigen is probably transferred to another CD45+ APC for subsequent presentation.

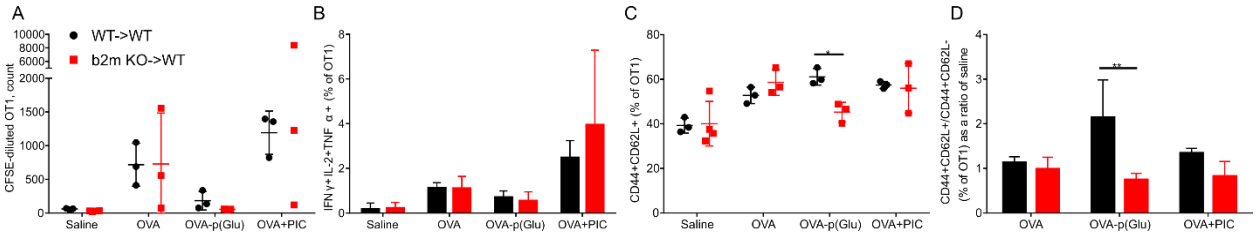

Fig 25. Antigen-specific CD8+ T cells proliferate to the same extent but lose their central memory phenotype in chimeras where only LECs are able to cross-present archived antigen. (A) Counts of proliferative (that had diluted CFSE) OTI from dLNs of chimeras at week 8. (B) % OTI that produced the pro-inflammatory cytokines (IFNγ, IL-2, TNFα) upon restimulation with $OVA_{257-264}$. (C) % OTI that were of a central memory ($CD44^+CD62L^+$) phenotype. (D) Ratio of central memory ($CD44^+CD62L^+$) to effector memory ($CD44^+CD62L^-$) OTI in dLNs, normalized to the ratio in saline controls. Statistical differences were determined by the Mann Whitney t test (C) (*p ≤ 0.05, **p ≤ 0.01, ***p ≤ 0.005).

Batf3-dependent dendritic cells are not responsible for the enhanced central memory phenotype of CD8+ T cells observed with archived antigen-p(GluNAc)

In order to investigate what APC type contributed to the enhanced central memory phenotype observed with antigen-p(GluNAc), we turned to a genetic knock-out model where Batf3-dependent cross-presenting DCs were absent. LN-resident cross-presenting DCs were one of the cell types to take up and retain antigen delivered with p(GluNAc). These DCs are also particularly efficient at cross-presentation and were found to present archived antigen transferred from apoptotic LECs following resolution of inflammation in the LNs. The $Batf3^{-/-}$ mice were originally developed on the 129S background where complete depletion of $CD8^+$ DCs was reported in the spleen. Depletion of these DCs in the LN was however not shown. The $Batf3^{-/-}$ mice used in this study were a generous donation of Justin Kline's lab where they bred the original 129S mice to WT C57BL/6 mice to generate hybrid mice that would not reject certain tumors. These mice unfortunately have a substantial number of residual DCs due to compensation from the Batf1 developmental gene. This compensation is shown in both

the spleen and LNs, where the number of $CD8^+$ or $CD103^+$ DCs is reduced in the KO mice but still present, and should be considered in interpretation of our results (**Fig. 26A**). We first wanted to check whether the partial absence of these DCs can result in a change in the phenotype of T cells that responded to antigen archived with or without adjuvant. We conducted a similar experiment where we immunized WT or $Batf3^{-/-}$ mice with 20 μg of OVA or 20 μg of OVA in combination with PIC (4 μg) or αCD40 (4 μg), waited two weeks to adoptively transfer OTI cells and assessed their phenotype 3 days post adoptive transfer. We found that Batf3 DCs played an essential role in the priming of archived antigen only when delivered with an adjuvant signal since OTI proliferated and were recovered in significantly fewer numbers in KO mice in the adjuvanted group, whereas OTI proliferation and recovery were unaffected in the WT mice treated with OVA only (**Fig. 26B, C**). OTI cells responding to adjuvanted OVA also expressed significantly lower levels of Tbet and Eomes transcription factors in the KO mice, demonstrating lower activation potential (**Fig. 26D**). The ability of these OTI to produce inflammatory cytokines, especially IFNγ, was severely decreased in the KO mice that archived adjuvanted OVA, showing the importance of Batf3 DCs in sensing antigen in the context of TLR activation.

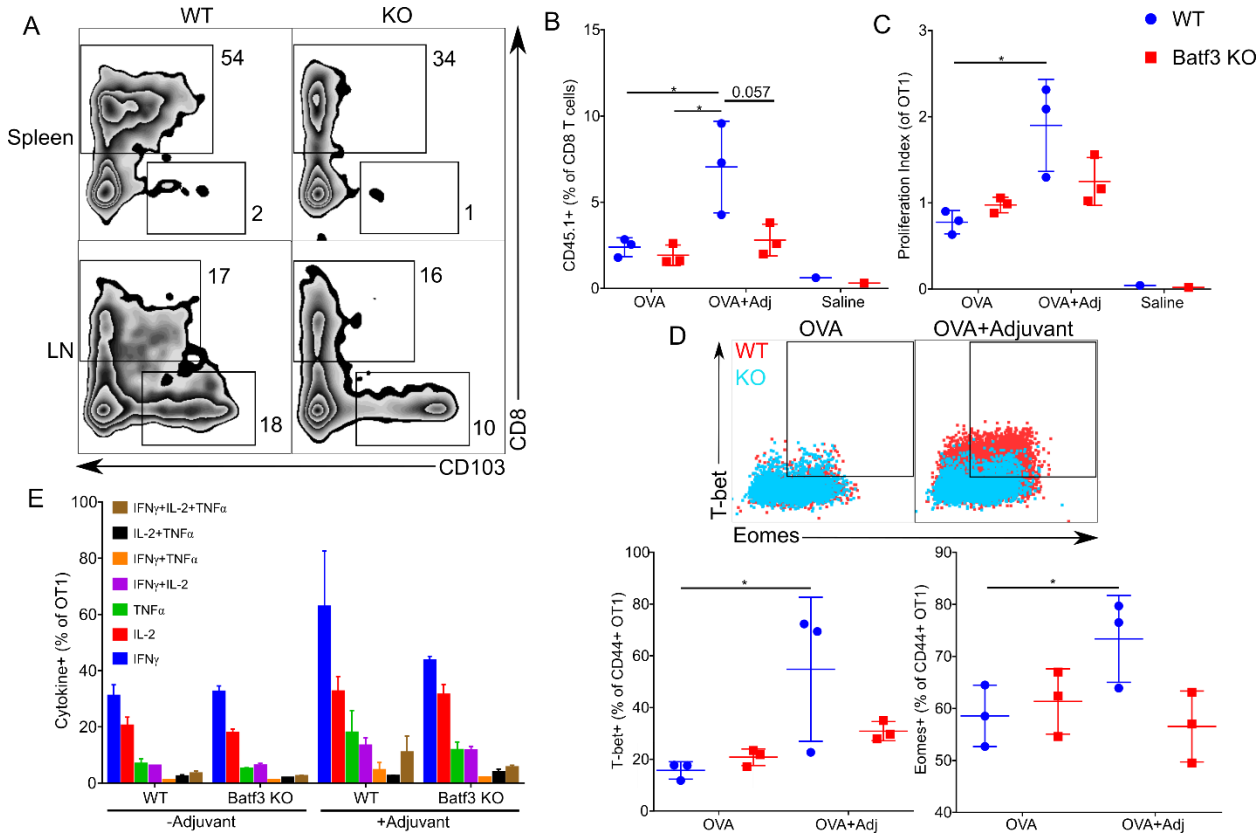

Fig 26. Validating the Batf3$^{-/-}$ mouse model; Batf3 DCs are dispensable to antigen priming in the absence of an adjuvant. (A) Representative flow cytometry plots showing frequencies of CD8^{+} and CD103^{+} DCs in the pooled axillary and popliteal LNs and spleen of WT C57BL/6 and Batf3$^{-/-}$ (KO) mice. (B-E) Mice of each genotype were immunized with 20 µg OVA without or with adjuvant (10 µg poly(I:C) and αCD40 antibody) and received an adoptive transfer of CD45.1^{+} CD8^{+} OTI T cells 11 days later, and the phenotype was assessed in a further three days. (B) % OTI recovered from the dLNs of WT or KO mice. (C) Proliferation of OTI cells in dLNs of WT or KO mice. (D) (Top) Representative flow cytometry plots of LN OTI showing T-bet and Eomes expression. (Bottom) Quantification of % activated (CD44^{+}) OTI that are T-bet^{+} (left) and Eomes^{+} (right). (E) % OTI cells that are cytokine producers upon restimulation with OVA$_{257-264}$. Single, double and triple positive OTI cells are shown. Statistical differences were determined by one-way ANOVA using Tukey's post hoc test (*p ≤ 0.05, **p ≤ 0.01, ***p ≤ 0.005).

Having validated the model, we set out to test the role of these Batf3 DCs in presentation of archived antigen-p(GluNAc) to antigen-specific CD8^{+} T cells, and whether the response was dependent on TCR strength. Based on our previous studies with OTI and OT3 cells, we knew that OT3 cells, that exhibit lower TCR avidity to the same OVA epitope, were unable to proliferate in a competitive environment. We thus

adoptively transferred OT3 cells at a 3:1 ratio with OTI cells into either WT or Batf3$^{-/-}$ mice two weeks after immunizing them with either unmodified OVA or OVA-p(GluNAc), and assessed the phenotype of the T cells three days post-adoptive transfer (**Fig. 27A**). In order to distinguish the OTI from the OT3 cells and avoid the variability of using different fluorescent cell proliferation markers, we used OTI from a different congenic strain that expresses CD90.1 in addition with CD45.1, such that we identified OTI cells as CD90.1^{+}CD45.1^{+} and the OT3 cells as CD90.1^{-} after applying the CD45.1^{+} gate (**Fig. 27B**). We observed the ratio of OT3: OTI cells in the mice increased to >1 and to a significantly higher extent in WT mice immunized with OVA compared with OVA-p(GluNAc) (**Fig. 27C**). However, in Batf3$^{-/-}$ mice, this ratio was significantly lower in the OVA-treated mice but not in the p(GluNAc) group (**Fig. 27C**). Analyzing the OTI and OT3 cells individually, it was apparent that OTI behaved the way we expected in WT mice, exhibiting lower recovery in OVA-p(GluNAc) treated mice (**Fig. 27D**). The higher recovery seen with OVA was abrogated in the Batf3$^{-/-}$ mice, showing that these DCs are more instrumental in presenting unmodified archived antigen compared with antigen-p(GluNAc) (**Fig. 27D**). OT3 cell numbers recovered barely changed in response to archived antigen in all groups, confirming that CD8^{+} T cells below a certain avidity threshold are not activated in response to archived antigen (**Fig. 27E**). We previously showed that in the absence of an adjuvant, the absence of the Batf3 DCs does not make a difference to OTI proliferation, and this is consistent with what we observe here. OTI in mice with archived OVA-p(GluNAc) proliferate less than with OVA, and to the same extent in Batf3$^{-/-}$ mice (**Fig. 27F**). OT3 cells do not proliferate at all (**Fig. 27G**). Importantly, we were able to show that the higher central memory to effector ratio seen

with archived OVA-p(GluNAc) education was not affected in the Batf3$^{-/-}$ mice, indicating that these cross-presenting DCs are dispensable in the differentiation of these cells into a memory phenotype (**Fig. 27H**). Moreover, the ratio of Eomes to T-bet transcription factors was also unchanged in the KO mice (**Fig. 27I**). Interestingly, even though the OT3 cells showed no indication of activation through recovery numbers or proliferation, they had a higher number of memory precursor cells (CD127^{+}KLRG-1^{-}) in Batf3$^{-/-}$ mice with archived antigen-p(GluNAc), suggesting that these DCs might have a role in activating lower avidity CD8^{+} T cells from a less cytotoxic to a more memory fate (**Fig. 27J**). This might also be an indication that antigen archiving cross-presenting DCs retain the antigen for long enough to engage lower avidity CD8^{+} T cells in an antigen-competitive environment. Overall, these data demonstrated that Batf3 DCs are dispensable to presenting antigen archived with p(GluNAc) and skewing them to a central memory phenotype.

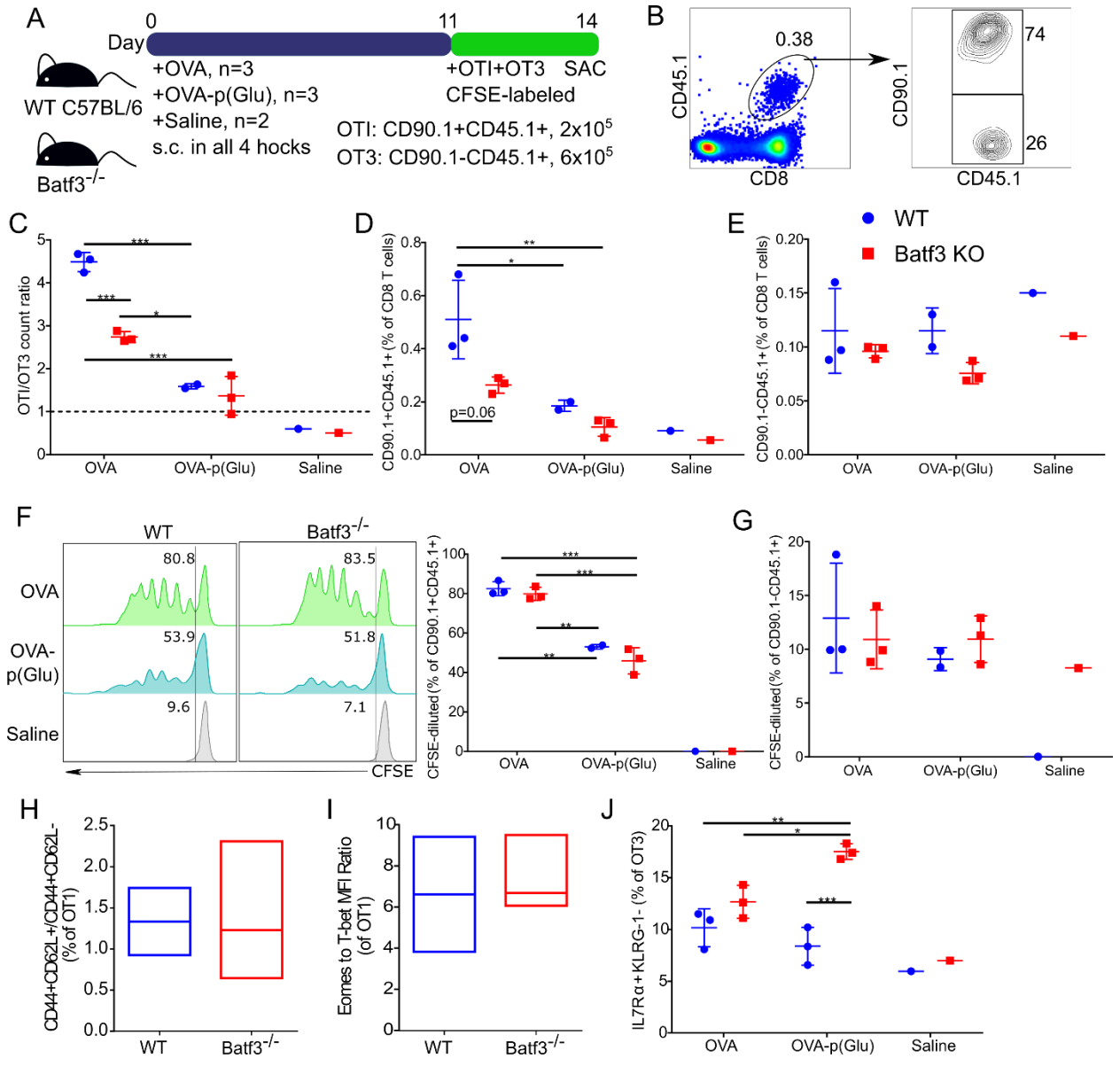

Fig 27. Batf3-dependent dendritic cells are not responsible for the enhanced central memory phenotype of CD8+ T cells observed with archived antigen-p(GluNAc). (A) Experimental set-up: WT or KO mice were immunized s.c. in all hocks, followed by an adoptive transfer of $CD45.1^+CD90.1^+$ OTI and $CD45.1^+CD90.1^-$ OT3 mice, after which the T cell phenotype was analyzed at day 14. (B) Gating strategy showing 74% OTI and 26% OT3 from the dLNs of WT mice. (C) Ratio of numbers of OTI to OT3 cells in the dLNs of WT and KO mice. (D) % OTI cells in the dLNs of WT and KO mice at day 14. (E) % OT3 cells in the dLNs of WT and KO mice at day 14. (F) Histograms showing CFSE dilution traces of OTI cells in the dLNs of WT and KO mice (left) and a quantification of % CFSE-diluted (proliferated) OTI. (G) % CFSE-diluted (proliferated) OT3 cells in dLNs of WT and KO mice. (H) Ratio of central memory ($CD44^+CD62L^+$) to effector memory ($CD44^+CD62L^-$) OTI cells in dLNs of WT and KO mice. (I) Ratio of Eomes to T-bet on LN OTI. (J) % OT3 cells that are memory precursors ($CD127^+KLRG\text{-}1^-$) in dLNs of WT and KO mice. Statistical differences were determined by one-way ANOVA using Tukey's post hoc test and the Mann-Whitney t test (for H and I) (*p ≤ 0.05, **p ≤ 0.01, ***p ≤ 0.005).

The response to archived antigen at steady state is independent of antigen glycosylation

We knew from literature that Batf3 DCs have an important contribution to presentation of archived antigen, especially antigen delivered with an inflammatory stimulus including a CD40 agonist. In this model, OTI $CD8^+$ T cell proliferation is abrogated to significant levels in the absence of these DCs. In my work, we have shown that OTI proliferation, while decreased in the Batf3 KO DCs, are still in a highly proliferative state (>90% CFSE-diluted) when antigen is archived with the same adjuvant. This difference could be due to three reasons: (1) we used a lower antigen dose in our immunizations (5 ug per hock compared with 10-20 ug per site), (2) the $Batf3^{-/-}$ mice we used are on a C57BL/6 background, and (3) we used recombinant OVA protein in our experiments. We did not think dose was important because the OTI proliferation was very high in the dLNs that we isolated, indicating that ample antigen was available for cross-presentation to the T cells. We showed earlier that the mice we used have a significant number of residual $CD8^+$ and $CD103^+$ DCs in their LNs, which can cross-present archived antigen, leading to a smaller reduction in proliferation in our hands. Lastly, we wanted to rule out that antigen glycosylation was not a factor. Recombinant OVA produced in e coli (R-OVA) lacks glycosylation while native chicken OVA (C-OVA) is mannosylated at two residues.

We conducted the archiving education experiment where we immunized mice with R-OVA or C-OVA with the combined adjuvant at an equal dose of 20 ug per mouse, adoptively transferred CFSE-labeled OTI cells 11 days later, and evaluated the OTI

phenotype 3 days following transfer (**Fig. 28A**). As highlighted before, these mice have substantial residual cross-presenting $CD8^+$ and $CD103^+$ DCs in their LNs (**Fig. 28B, C**). To our surprise, these KO mice also had a significantly lower number of LECs (**Fig. 28D**) and FRCs (**Fig. 28E**) in their LNs, something that no one else had ever looked at before. This was a crucial finding as it suggested to us that our observations using these mice could have been confounded by a lower number of LECs in addition to a reduced number of these Batf3-dependent DCs. BEC numbers were unchanged (**Fig. 28F**). The spleens of the KO mice also had a significantly lower number of the $CD8^+$ cross-presenting DCs (**Fig. 28G**).

Next, we verified whether antigen archiving in the KO mice was affected. Among the LECs present in the mice, the fraction of cells that had archived antigen was constant across the mouse strain but also across the OVA type (**Fig. 28H**). The same observation as made with OVA archived in the cross-presenting $CD8^+$ DCs (**Fig. 28I**).

We were able to recapitulate the decrease in OTI recovery in the $Batf3^{-/-}$ mice, which was consistent across OVA type both in the LNs and spleen (**Fig. 28J**). While there was a significant difference in recovery, we did not observe any differences in OTI proliferation across groups and in the LNs and spleen of these mice (**Fig. 28K**). A slight increase in the central memory to effector ratio was observed in the R-OVA treated mice in the LNs of the $Batf3^{-/-}$ mice, suggesting that the absence of these DCs might hurt the effector phenotype of the OTI cells but it is unclear why it would not happen in the C-OVA group or in the spleen (**Fig. 28L**). Finally, the Eomes to T-bet ratio, another measure of a skewed central memory phenotype, is slightly decreased in the LNs only

of the Batf3$^{-/-}$ mice and consistent across groups (**Fig. 28M**). These data allowed us to conclude that the glycosylation status of OVA does not make a difference in the extent it is archived, and the response of CD8^{+} T cells, and the Batf3$^{-/-}$ mice are not a reliable tool for studying a LEC-centric phenomenon because of the lower LEC numbers in these mice.

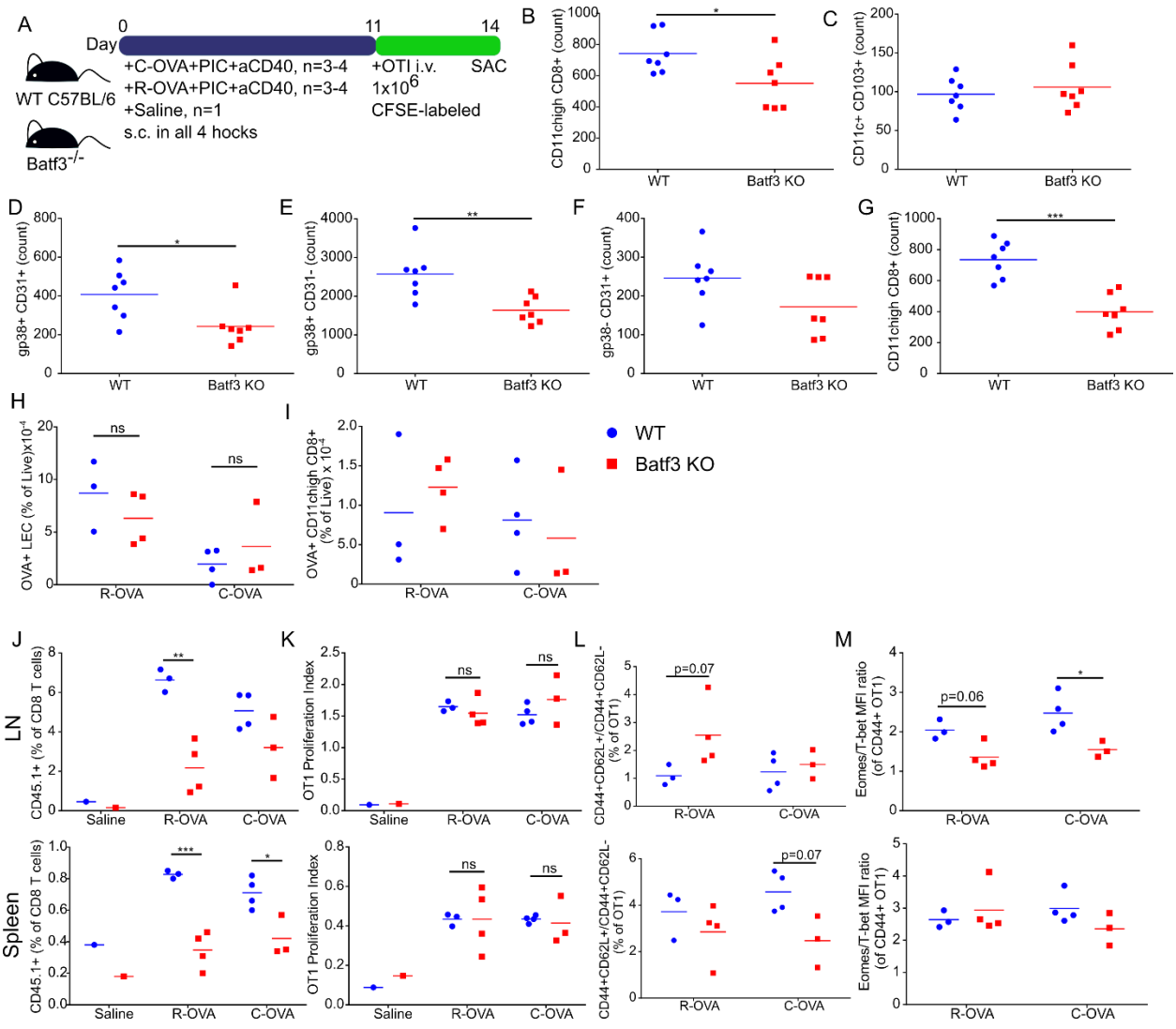

Fig 28. Batf3$^{-/-}$ mice have lower overall LEC numbers; the response to archived antigen at steady state is independent of antigen glycosylation. (A) Experimental set-up comparing the response of OTI cells to archived OVA- naturally glycosylated (chicken) or completely non-glycosylated (recombinantly produced in e coli). (B-I) Characterization of the number of APCs and degree of archiving in these APCs in the dLNs and spleen of WT and KO mice. (B) Number of CD8+ DCs

Fig 28. Batf3$^{-/-}$ mice have lower overall LEC numbers; the response to archived antigen at steady state is independent of antigen glycosylation (continued) in dLNs. (C) Number of CD103^{+} DCs in dLNs. (D) Number of LECs in dLNs. (E) Number of FRCs in dLNs. (F) Number of BECs in dLNs. (G) Number of CD8^{+} DCs in the spleen. (H) % OVA^{+} LECs as a frequency of total live cells in dLNs. (I) % OVA^{+} CD8+ DCs as a frequency of total live cells in dLNs. (J-M) OTI cell phenotype at day 14 in the dLNs (top) and spleen (bottom). (J) % OTI recovered. (K) OTI proliferation index. (L) Ratio of central memory (CD44^{+}CD62L^{+}) to effector memory (CD44^{+}CD62L^{-}) OTI. Statistical differences were determined by one-way ANOVA using Tukey's post hoc test (*p ≤ 0.05, **p ≤ 0.01, ***p ≤ 0.005).

Discussion

Compared to the liver or oral mucosa, where immune responses are skewed toward tolerance because of the abundance of oral antigen insults that need to be interpreted in an innocuous manner, immune responses to exogenous antigens in the peripheral lymphatics usually aim to generate an inflammatory response in the context of an infection. However, LNs under homeostasis do continually drain self-antigen from the local tissue, and this constant antigen exposure may be important in maintaining peripheral tolerance. For example, in mice lacking skin-draining lymphatics, skin-specific autoimmunity was observed to develop (*185*). Furthermore, LECs have an essential role in the maintenance of tolerance to peripheral tissue-transcribed antigens via the deletion of autoreactive cells or the generation of autoantigen-specific CD4^{+} Tregs, thereby acting as an additional mechanism to compensate for potentially autoreactive T cells that escape central tolerance (*53*, *161*, *163*). LECs can also induce tolerance to exogenous antigens draining from peripheral sites of immunization, inflammation and tumors, through direct antigen presentation to both naïve CD8^{+} and CD4^{+} T cells (*164*, *169*, *186*). This tolerogenic antigen presentation is accompanied by the up-regulation of co-inhibitory molecules, as well as soluble mediators such as IDO

that can directly suppress T cells and prevent APCs from maturing and presenting antigen to produce effectors (*154*).

However, it is possible to reverse the default program imprinted by LECs onto T cells from suppressive to potentially immune-activating. For example, LNSCs stimulation with TLR3 ligand PolyI:C can shift the patterns of tissue restricted antigen expression, thereby reducing the capacity to induce $CD8^+$ T cell tolerance to a transgenically expressed self-antigen (*187*). Moreover, the Swartz lab has demonstrated that $CD8^+$ T cells that survive the first deletion wave, following education by antigen-bearing LECs, differentiate into central memory cells that are able to contribute to functional memory and protection against inflammatory challenges (*175*). Nevertheless, the significance of this occurrence *in vivo* is debatable, mainly because of LECs are outnumbered by other antigen uptakers and presenting cells in a LN under either steady-state or inflammatory conditions. Thus, it is difficult to imagine a scenario where this central-memory skewing property of LECs could be leveraged in a normal immune-sufficient organism in the context of a vaccine. Further studies exploring the epigenetic factors controlling this $CD8^+$ T cell lineage differentiation pathway would be useful in understanding the conditions under which this phenotype could be tuned for potentially translational applications.

The work presented in this chapter contradicts previous work done in our lab (*175*) to characterize the relationship between LECs and the quality of the $CD8^+$ T cell central

memory induced. Here, we demonstrate that memory induced with archived antigen-p(GluNAc) promotes a tolerogenic phenotype, suppressing the immune response to future inflammatory antigenic challenges. Memory has been found to contribute beneficially or harmfully to the maintenance of tolerance in a context-dependent manner. Liver-generated memory T cells under non-inflammatory conditions can contribute to protective immunity in infection (*188*). Furthermore, the absence of alloreactive T cell memory correlates with graft acceptance (*189*). In particular, central memory cells but not effector memory T cells have been shown to worsen graft-versus-host disease (*190*). On the other hand, in type 1 diabetes, lower avidity auto-reactive clones adopt a central memory phenotype that serves to regulate antigen presentation and activation of destructive high-avidity autoreactive clones in the pancreatic dLNs (*191*). Memory $CD8^+$ T cells have also been shown to promote tolerance to graft through nitric oxide production (*55*). The reservoir of memory $CD8^+$ T cells thus generated through archived glyco-modified antigen further establishes a lasting mechanism of tolerance, especially given the literature that shows that long-term memory $CD8^+$ T cells are more resistant to apoptosis compared to their $CD4^+$ T cell counterparts (*192*). In future mechanistic studies, it will be of interest to evaluate the contribution of $TCF1^+$ stem-cell like memory to the central memory compartment and tolerogenic state induced by s.c. antigen-p(GluNAc) administration (*132*).

The type of antigenic challenge can be crucial in dictating the fate of the memory $CD8^+$ T cells generated by LECs under steady-state. It is known that LECs are very sensitive to environmental stimuli. For example, lymphatic expansion (lymphangiogenesis) and

contraction during the course of an inflammatory reaction is regulated by expression of external type 1 IFN and LEC-expressed PD-L1, resulting in LEC apoptosis to return the LNs back to homeostatic levels (*167*). Kedl et al. showed that type 1 IFN inhibits LEC proliferation and promotes the upregulation of PD-L1 during expansion. Post-inflammation, during LN contraction, PD-L1^{+} LECs are protected against apoptosis, and loss of expression leads to apoptosis, such that PD-L1^{+} LECs remain in place to maintain peripheral tolerance. We used two distinct types of challenges to evaluate the quality of memory generated by archived antigen-bearing LECs, delivered via glyco-conjugation. One was B16-OVA, immune-suppressed melanoma refractory to checkpoint blockade, and the other was attenuated Lm-OVA, type 1 inflammatory infectious challenge. Even though both these environments were contextually very different, the observed immunological outcome to challenge was the same: tolerance. This suggests that the regulatory tolerogenic factors are T cell-intrinsic and independent of external environmental cues coming from either a local suppressed tumor microenvironment or a systemic inflammatory environment.

It, however, still remains to be determined what cell type is responsible for presenting archived antigen to naïve CD8^{+} T cells. We know that LECs are a strong candidate, resulting in equal levels of T cell proliferation seen in the β2m$^{-/-}$ → WT chimeras as in the WT → WT chimeras. We have shown that Batf3-dependent DCs are likely not responsible. While LECs might cross-present archived antigen, their presentation does not result in the enhanced central memory phenotype on antigen-specific CD8^{+} T cells, according to our results. Further studies shedding light on the mechanistic details

underlying antigen transfer from LECs to other LN APCs will be crucial in helping us understand the dynamics of central memory education, helping us design better tuned inverse vaccines for the induction of lasting antigen-specific tolerance.

Materials and Methods

More comprehensive methods can be found at the end of chapter 1. Methods unique to chapter 2 that have not been presented in chapter 1 are described here.

Recombinant OVA production and purification

A starter culture was prepared by spotting a colony of OVA-Bl21 (obtained from streaking LB-carbenicillin agar plates with the OVA-Bl21 glycerol stock 24 h earlier) in 5 mL of LB (21 g/L) with 120 µg/mL carbenicillin in 15 mL bacterial tubes, and cultured overnight at 37 ^{0}C with shaking. The morning of protein expression, the culture was diluted 300-fold with more LB supplemented with carbenicillin and was shaken at 37 ^{0}C for a further 2.5- 3 h until an O.D. of 0.6- 0.8 was reached. The culture was induced with 330 µM of IPTG (78.64 mg per L of culture) and incubated at 37 ^{0}C for a further 3 h with shaking. 500 mL bacterial flasks were weighed out and used to harvest the culture. They were spun down at 4000 xg for 20 min and the wet weight of the pellets was measured and calculated. Protease inhibitor (CAT# P8849-5ML) was added to the pellets at 1 mL per 20 g of wet weight, followed by triton X-100 at 500 µL/L and lysozyme at 50 mg/L, and mixed in 50 mL of 1x PBS per L of culture, using a serological pipet. The mixture was sonicated on ice for a total of 2 min involving 10 s pulses and 15 s rests. Benzonase was added at 20 µL/L and 1 M $MgCl_2$ at 1 mL/L to the mixture, further mixed and left to lyse overnight at 4 ^{0}C with stirring. The next day, the lysate was

spun down at 12000 xg for 30 min. The supernatant was collected and after adjusting the pH to 7.5, was filtered under vacuum using a 0.22 μM filter. This was purified first using His affinity chromatography (binding buffer: 20 mM phosphate, 0.5 M NaCl, pH 7.5; elution buffer: 20 mM phosphate, 0.5 M NaCl, 1 M imidazole, pH 8), then using anion exchange chromatography (binding buffer: 20 mM phosphate buffer, pH=6.3; elution buffer: 500 mM phosphate buffer, 0.5 M NaCl, pH=6.3) on an AKTA FPLC. The resultant peak fractions were pooled and dialyzed versus sterile 1x PBS, concentrated using a 50 mL 10K MWCO Amicon tube, and tested for the absence of LPS.

Synthesis of OVA_{647}-PEG conjugate (size control)

Recombinant OVA was first reacted with a 10 mg/mL DMSO stock of AF647 NHS ester at a 1:5 molar equivalency in PBS buffer at a pH of 7.4 for 1-2 h, with constant magnetic stirring at room temperature. The labeled mixture was purified with a Zeba spin desalting column (7K MWCO, thermo 89882) using PBS as wash buffer. Labeled OVA-AF647 was then reacted with powdered sterile PEG (MW= 20 kDa) at a 1:10 molar equivalency for 12 h with constant stirring at room temperature. When run on an SDS-page gel, the OVA647-PEG conjugate appears to have a molecular weight between 75 and 250 kDa and stays unchanged when reduced with β mercaptoethanol prior to loading, showing that we obtain a conjugate of comparable size to our glycopolymerized OVA but that does not contain a reduction-sensitive linker (**Fig. 4A**). The final reaction mixture was purified to remove unreacted OVA_{647} using size exclusion and fractions 1-10 containing the conjugate were pooled and concentrated using an Amicon filter (30K MWCO) and checked for the presence of endotoxin before in vivo use (**Fig. 4B**). Finally, the fluorescence intensity of the conjugate was measured relative to the other

glycoconjugates using a fluorescent plate reader at an excitation wavelength of 630 nm and an emission wavelength of 670 nm. All above reactions were handled under sterile conditions inside a biosafety hood to avoid contaminating reagents and products with endotoxin. The importance of using a size control is demonstrated where following s.c. injection in mice, plain OVA without the PEG conjugate, results in a similar uptake by LECs, measured by % OVA^+ LECs, but a significantly higher MFI inside the OVA^+ LECs, even though the fluorescence intensity of the two OVA species were matched before injection (**Fig. 4C**). Thus, we describe a method to control for size and uptake kinetics in instances when the antigen and antigen glyco-conjugates have very different sizes.

Live fluorescent intravital imaging of the mouse ear dermis

One to two days prior to injection, any hair present was removed from the ear of WT C57BL/6 or Prox1-Tom mice using depilatory cream and the mice were allowed to rest for 24 h. The mouse was anesthetized under inhalation isoflurane and a Hamiltonian syringe was used to carefully inject saline, OVA_{647} or OVA_{647} in 2 µL into the ear dermis and the ear was immobilized on a wooden block using tape and imaged through using a stereomicroscope. Antigen was detected in the Cy5 channel, and fluorescent lymphatics in Prox1-Tom mice were detected in the 594 channel. The ear was imaged on days 0, 3, 9 and 13 near the site of the i.d. injection.

Skin processing for flow cytometry

The ear dermis including the injection site was isolated and cut into small 1 mm^2 pieces using a blade. Cut skin pieces were transferred into 5 mL polystyrene tubes and were

digested, first using 1 mg/mL Collagenase IV and 10 µg/mL DNAse1 for 30 min in a 37 ^{0}C water bath with magnetic stirring, then using 3.3 mg/mL Collagenase D and 10 µg/mL DNAse1 for a further 15 min at 37 ^{0}C with magnetic stirring. All digestions were performed in DMEM media supplemented with 2% FBS, 1% P/S and 1.2 mM $CaCl_2$, at a volume of 750 µL per skin sample. The sin digests were gently pipetted 100 times using an electronic pipette. An equal volume of ice-cold 10 mM EDTA in PBS supplemented with 1% FBS was added to the digestion mixes to quench the enzymatic reaction for a final concentration of 5 mM EDTA, followed by pipetting for another 100 times. The cell suspensions were filtered through a 70 µM filter to generate a single cell suspension which was stained for flow cytometry. Antibodies against the following markers were used: CD45, CD31, GP38, B220, CD3, CD11c, CD11b, CD8, CD103, Langerin (CD207).

Adoptive transfer of OT3 CD8^{+} T cells

CD8^{+} T cells were isolated from the spleen and s.c. LNs (axillary, brachial, inguinal, popliteal, cervical) of OT3 mice using the EasySep CD8^{+} isolation kit (Stemcell 19853). Spleens were first mashed into a single cell suspension and lysed with ACK lysis buffer (Gibco A1049201). LNs were digested with 1 mg/mL Ca^{2+} supplemented Collagenase D (Roche 11088866001) for 45 min at 37 ^{0}C and gently mashed into a single cell suspension. Suspensions from the LNs and spleen were pooled and subjected to magnetic cell isolation using the kits. The OT3 CD8^{+} T cells were labeled with 1 µM CFSE for 6 min at RT, washed with sterile PBS buffer, quantified and resuspended in saline buffer for injection. 1x10^{6} cells were injected into mice via i.v. tail vein injection.

Melanoma challenge

Mice were administered intradermally with 0.25 million of B16-OVA melanoma cells (harvested from in vitro culture) on the back ipsi to the injected draining hock on day 25 and tumor size was measured every other day. Mice were euthanized when the tumor volume reached 1000 mm^3 and/ or they experienced reduced mobility around the cage.

Listeria challenge

An attenuated Listeria strain (ΔactA) encoding for OVA antigen (Lm-OVA) was used for all infectious challenges described in this work. The characterized generation time is about 40 min, where an OD of 0.1 corresponds to $1x10^8$ CFU/mL. The day before inoculation, Lm-OVA was put in culture in 5 mL of BHI broth (DIFCO cat 237500) with 10 µg/mL chloramphenicol antibiotic, at 37 ^{0}C with shaking. The morning of inoculation, the starter culture was diluted 20-fold in BHI broth and shaken at 37 ^{0}C for a further 3 h. The OD was measured at 600 nm and, using the growth curve, the total amount required to inoculate mice at 10^8 CFU in a volume of 100 µL for each mouse was calculated and measured out. Mice received an i.v. injection of 10^8 CFU of Lm-OVA, via the tail vein. The exact inoculation dose was confirmed by preparing serial dilutions of the injected dose in BHI broth, plating on BHI-chloramphenicol plates and counting the number of Lm-OVA colonies 36 h later.

Three days post-challenge, the mice were sacrificed and the livers, spleens and s.c. LNs (axillary and popliteal) were isolated in a BSL2 facility. Spleens and LNs were processed as previously described. Livers were weighed and mashed through 70 µM strainers into 50 mL conicals using PBS. They were spun down and resuspended in 5 mL PBS, 100 µL of which was mixed with 100 µL of 0.14% tergitol solution in PBS. 100 µL of this mixture was plated on BHI-chloramphenicol plates. Ten-fold further serial

dilutions (10^2-10^5) of the mixture were made in 0.14% tergitol solution and subsequently plated and incubated at 37 ^{0}C for 36 h. The plates were then imaged and the colonies counted and CFUs quantified using ImageJ software. Bacterial CFUs were calculated and normalized per mg of weighed liver for each mouse.

Generation of bone marrow chimeras

WT C57BL/6 mice were gamma irradiated with either a sublethal bolus dose of 900 rad or two rounds of 450 rad spaced 4 h apart, using a Caesium-137 radiation decay source. To prevent radiation-associated morbidity, $1x10^7$ bone marrow cells (that were isolated from $\beta2m^{-/-}$ mice) were injected into each irradiated mouse via a tail vein i.v. injection within an hour of the last radiation dose. The bone marrow recipients were bled one- and two-weeks following reconstitution, then six weeks after to confirm, using flow cytometry, chimerism and the expression of MHCI on APCs present in the control WT→WT and experimental $\beta2m^{-/-}$→WT chimeras.

Chapter 3

Synthetically glycosylated antigen induces a tolerogenic endogenous immune response, both at the cellular and humoral levels.

Abstract

This chapter of the thesis is devoted to understanding the impact of glyco-antigen immunization on the endogenous cellular and humoral immune response.

Keywords: endogenous, cellular, humoral, antibodies.

Introduction

Adoptive transfer of antigen-specific transgenic models are useful models for studying the antigen-specific response in a controlled and methodic fashion but are not representative of endogenous responses. This is because adoptive transfer introduces naïve cells present at an artificially higher frequency than normal and usually using clones of artificially high avidity to their cognate MHC-peptide complex. These introduce experimental artifacts that impede our understanding of the immune response to our antigen vector on the endogenous T and B cell repertoire that are ultimately the goal of vaccination for immunity or tolerance. Fortunately, in the OVA model antigen model, we have pentamer tools available to help us identify OVA-specific cells present in the endogenous repertoire of the mice that can respond to our constructs. The pentamer technology is, however, only restricted to $CD8^+$ T cells and there is no available MHC multimer available to detect OVA-specific $CD4^+$ T cells. In these series of experiments, we investigate the impact of immunizing with glycopolymerized antigen on education of endogenously present T and B cells.

Unadjuvanted immunization with antigen-p(GluNAc) suppresses endogenous antigen-specific cellular and humoral responses

We immunized WT BL/6 mice with a single dose of OVA or OVA-p(GluNAc) in all four hocks, followed by a challenge with OVA and LPS and evaluation of the T cell response 3 days following challenge (**Fig. 29A**). We detected significantly fewer pentamer positive (i.e., OVA-specific) $CD8^+$ T cells induced with OVA-p(GluNAc) immunization compared with OVA, showing that p(GluNAc) leads to a smaller expansion of effector OVA-specific $CD8^+$ T cells in the endogenous repertoire, predictive of a tolerogenic response (**Fig. 29B**). Endogenous $CD8^+$ T cells in the p(GluNAc) group also had a significantly reduced KLRG-1 expression compared to OVA or saline controls, indicating a lower propensity to differentiate into effectors in response to the challenge (**Fig. 29C**). Even though we were unable to detect OVA-specific $CD4^+$ T cells using multimers, we measured their ability to produce inflammatory cytokines upon restimulation with the cognate peptide $OVA_{323-339}$. The frequency of multi-functional $CD4^+$ T cells, i.e., those cells with the ability to produce more than one inflammatory type 1 cytokine, was slightly blunted, which could suggest suppressed behavior among endogenous $CD4^+$ T cells (**Fig. 29D**).

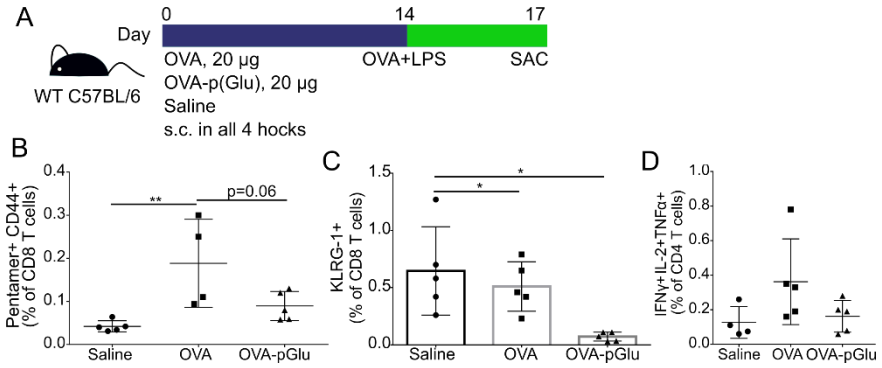

Fig 29. Unadjuvanted immunization with antigen-p(GluNAc) suppresses endogenous antigen-specific CD8+ and CD4+ T cell responses. (A) Experimental timeline for endogenous vaccination with OVA or OVA-p((GluNAc)) following a prime-boost schedule. (B) OVA-specific activated (Pentamer$^+$CD44$^+$) CD8$^+$ T cells in dLNs. (C) Short-lived effectors (KLRG-1$^+$) CD8$^+$ T cells in dLNs. (D) CD4$^+$ T cells that secreted all three cytokines IFNγ, IL-2, TNFα upon restimulation with $OVA_{323-339}$. Statistical differences were determined by one-way ANOVA using Tukey's post hoc test (*p ≤ 0.05, **p ≤ 0.01, ***p ≤ 0.005).

Next, we used a prime and boost strategy to immunize mice with two identical doses of OVA or OVA-p(GluNAc) or saline, four days apart, followed by an OVA and LPS challenge three weeks later. We picked these timepoints because prior observations in our lab pointed to this closely-spaced schedule as being most effective for tolerance induction (**Fig. 30A**). Also, we challenged mice at a later timepoint to allow us to better gauge the endogenous memory response and any effects on the humoral response which takes longer to form via germinal center reactions compared with T cell responses. Similar to the previous experiment with one-dose immunization, we observed a significant decrease in the frequency of pentamer positive CD8$^+$ T cells with an effector phenotype induced with OVA-p(GluNAc) compared with OVA, showing that p(GluNAc) is suppressive also in a prime-boost strategy (**Fig. 30B**). Endogenous CD8$^+$ T cells educated with OVA-p(GluNAc) and isolated from dLNs exhibited an anergic phenotype seen from a diminished ability to produce IL-2 upon restimulation with $OVA_{257-264}$ (**Fig. 30C**). Abrogated IL-2 secretion was also observed with endogenous

$CD4^+$ T cells (**Fig. 30D**), showing that p(GluNAc) can act to suppress both $CD4^+$ and $CD8^+$ T cells in the LNs. A similar response was observed in the spleen where endogenous $CD4^+$ T cells demonstrated a severely diminished ability to produce IFNγ (**Fig. 30E**), TNFα (**Fig. 30F**) and a combination of all three inflammatory cytokines including IFNγ, IL-2 and TNFα in the spleen upon restimulation with $OVA_{323-339}$ (**Fig. 30G**).

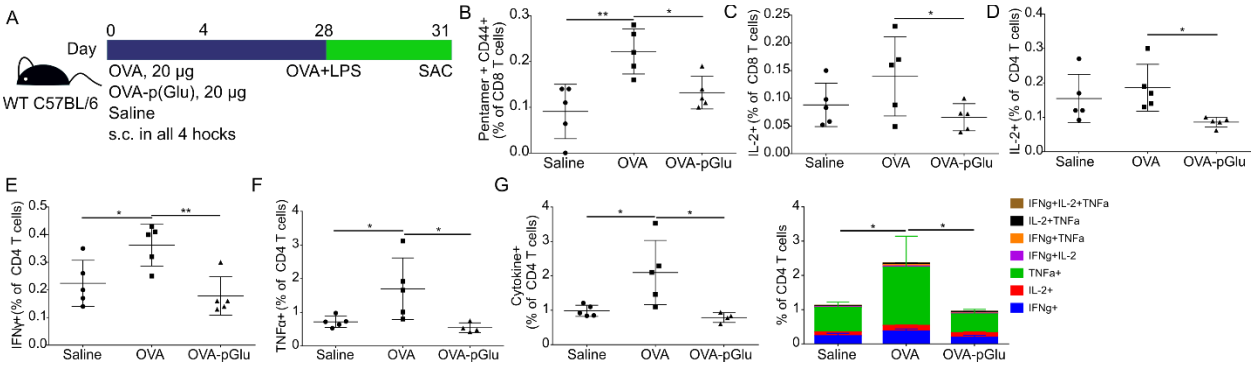

Fig 30. Unadjuvanted immunization with antigen-p(GluNAc) abrogates an endogenous polyfunctional T cell response upon an inflammatory antigenic challenge. (A) Experimental timeline for long-term endogenous vaccination prime-boost schedule with OVA or OVA-p(GluNAc), followed by a challenge with OVA and LPS, to evaluate the memory response at day 31. (B) OVA-specific activated (pentamer$^+$CD44$^+$) $CD8^+$ T cells in dLNs. (C) IL-2^+ $CD8^+$ T cells in LNs upon restimulation with $OVA_{257-264}$. (D) IL-2^+ $CD4^+$ T cells in LNs upon restimulation with $OVA_{323-339.}$ (E) IFNγ$^+$ $CD4^+$ T cells in spleen upon restimulation (F) TNFα$^+$ $CD4^+$ T cells in spleen upon restimulation. (G) $CD4^+$ T cells that secreted all three cytokines IFNγ, IL-2 and TNFα upon restimulation in spleen. Statistical differences were determined by one-way ANOVA using Tukey's post hoc test (*p ≤ 0.05, **p ≤ 0.01, ***p ≤ 0.005).

Following this same experimental timeline, we asked whether OVA-p(GluNAc) immunization had an impact on the humoral immune response, measured by OVA-specific antibody production in the serum of these mice at days 4, 10 and 30 using ELISA (**Fig. 31A**). No substantial titers were measured at day 4 because it was too early for any detectable germinal center reaction to take place such that all titers reported in this section are from days 10 and 30 of the experiment (**Fig. 31B**). An

interesting observation was the difference in kinetics where OVA-specific total IgG decreased by one whole log-fold in the OVA group but had the opposite effect of increasing in the OVA-p(GluNAc) group (**Fig. 31B**). This differential kinetics can be broken down into the individual analysis of kinetics for IgG1 and IgG2b where OVA-p(GluNAc) saw modest increases in titer (**Fig. 31C, D**) and also in IgG2c where OVA induced titers saw a decrease (**Fig. 31E**). Nevertheless, all OVA-specific antibody titers were significantly suppressed in the p(GluNAc) group, compared with OVA, indicating strong humoral tolerance (**Fig. 31F-I**). This strong suppression in OVA-specific antibody production was seen as early as day 10 and as late into the response at day 30 in total IgG (**Fig. 31F**), IgG1 (**Fig. 31G**), IgG2b (**Fig. 31H**), IgG2c (**Fig. 31I**), indicating suppression at the level of several antibody subtypes and the maintenance of suppressive memory.

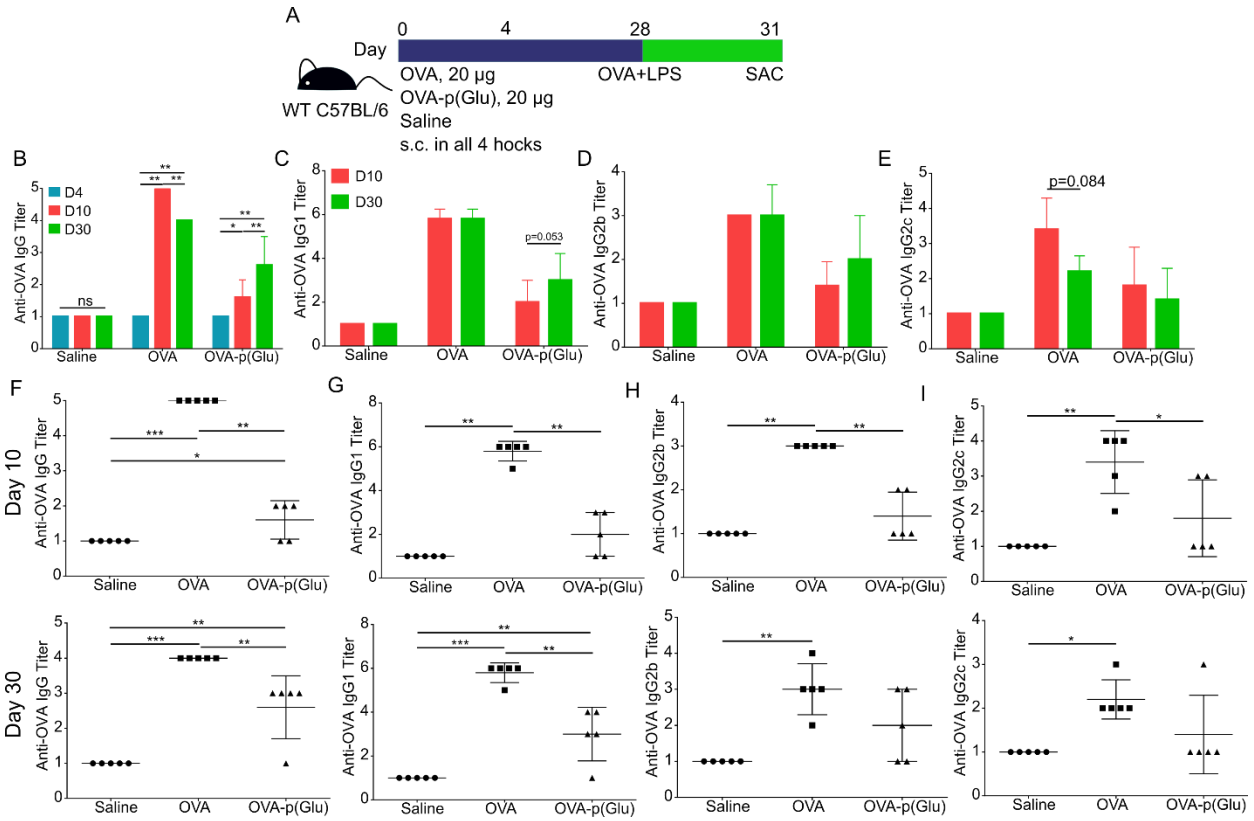

Fig 31. Unadjuvanted immunization with antigen-p(GluNAc) severely suppresses the endogenous B cell response. (A) Experimental timeline showing long-term memory evaluation of endogenous vaccination response, with a focus on the humoral response. (B) Titers of anti-OVA IgG antibody measured in the serum of mice by ELISA at days 4, 10 and 30. (C) Titers of anti-OVA IgG1 antibody measured in the serum of mice by ELISA at days 10 and 30. (D) Titers of anti-OVA IgG2b antibody measured in the serum of mice by ELISA at days 10 and 30. (E) Titers of anti-OVA IgG2c antibody measured in the serum of mice by ELISA at days 10 and 30. (F) Detailed comparison of the anti-OVA IgG titers between groups at day3 10 (top) and 30 (bottom). (G) Detailed comparison of the anti-OVA IgG1 titers between groups at days 10 (top) and 30 (bottom). (H) Detailed comparison of the anti-OVA IgG2b titers between groups at days 10 (top) and 30 (bottom). (I) Detailed comparison of the anti-OVA IgG2c titers between groups at days 10 (top) and 30 (bottom). Statistical differences were determined by one-way ANOVA using Tukey's post hoc test (*p ≤ 0.05, **p ≤ 0.01, ***p ≤ 0.005).

Glyco-conjugated antigen immunized with poly(I:C) adjuvant leads to more effective vaccination responses in vitro and in vivo

Our earlier vaccination experiments aiming to provoke a more effective immunization and memory recall response with the glycopolymerized antigen led us to select a potent

adjuvant. Ideally, we would have antigen-p(GluNAc) or p(Gal) polymerized in the same backbone as the polymeric adjuvant as was done with pMan-TLR7 (*193*) but that material was not available. Moreover, human LECs do not express TLR7/8, which made translation for a LEC targeting platform difficult (*194*). Instead, we picked poly(I:C) (PIC), a TLR3 agonist, which is highly expressed on both LECs and DCs, rationalizing the glycopolymer as the unique modulatory method in the presence of the same adjuvant. Additionally, high molecular weight PIC is a better TLR3 agonist than low molecular weight PIC, informing our choice for the use of the high molecular weight version (*195*).

We first validated the use of PIC, acquired from two vendors (Invitrogen or Adipogen) on the stimulation of BMDCs or primary mouse LECs through an in vitro dose response study. We stimulated these two cell types separately with increasing doses of PIC, back-calculated at the doses they would have been used in vivo, i.e., 2, 5, 10, 20 and 30 µg per mouse, for a total of 6 h with BMDCs or 18 h with LECs based on previous in vitro culture optimization studies, and added naïve CFSE-labeled OTI $CD8^+$ T cells at a 1:3 ratio to the stimulated cells. The OTI $CD8^+$ T cell phenotype was evaluated three days later. OTI $CD8^+$ T cells proliferated under all conditions with stimulated BMDCs and no significant differences were noted between vendor-specific PIC versions; the proliferation was highest at the 5 and 10 µg doses (**Fig. 32A**). The culture supernatant was collected after the 3-day culture to measure the level of lFNγ produced using ELISA, and highest production was obtained with 10 µg of PIC (**Fig. 32B**). There was no difference in OTI proliferation caused by stimulated LECs but the higher central memory differentiation compared with effector cells was conserved at all doses (**Fig.**

32C). However, at the 10 μg dose, the proportion of OTI CD8$^+$ T cells that were apoptotic, measured by positive Annexin V expression, was significantly lower such that increasing the dose had not further effect on the apoptotic phenotype of the cells (**Fig. 32D**). Thus, the 10 μg dose represented a good compromise for *in vivo* use at the level of proliferation, effector differentiation and survival.

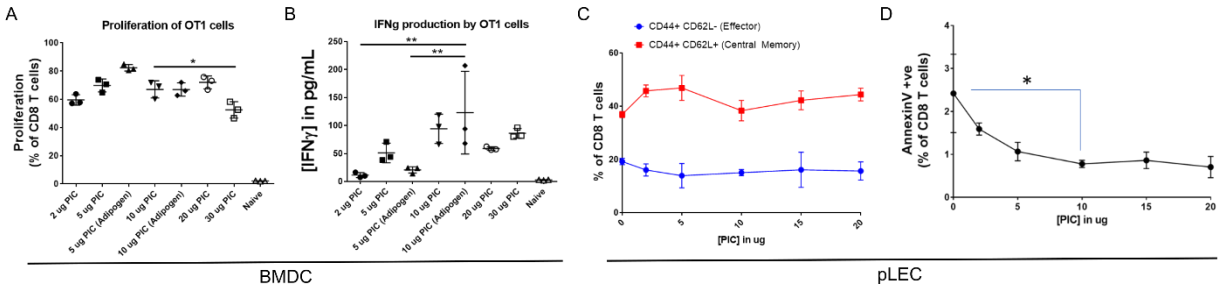

Fig 32. Optimal proliferation, effector differentiation, and survival of antigen-specific CD8+ T cells occurs at a PIC dose of 10 μg *in vitro*. (A) PIC dose-dependent BMDC-educated OTI CD8$^+$ T cell proliferation. (B) PIC dose-dependent IFNγ secretion by BMDC-educated OTI CD8$^+$ T cells. (C) PIC dose-dependent LEC-educated differentiation of OTI CD8$^+$ T cells into effector or central memory. (D) PIC dose-dependent Annexin V expression by LEC-educated OTI CD8$^+$ T cells.

We conducted an *in vivo* endogenous vaccination experiment where we immunized mice and boosted two weeks later with either saline, OVA, OVA-p(GluNAc) or OVA-p(Gal), and sacrificed mice five days post-boost to assess the endogenous immune response to the immunization. All OVA groups included a 20 μg dose of the OVA antigen with the optimized 10 μg dose of the high molecular weight PIC (**Fig. 33A**). We also bled mice on days 13 and 19 to measure the antibody response to our vaccination regimen. At day 13, all OVA groups had induced upwards of titers of 6-7 of anti-OVA IgG antibodies in the serum of mice, but with small differences across groups; OVA-p(GluNAc) was better than OVA-p(Gal) at inducing a humoral response (**Fig. 33B**). The titers slightly evolved over the course of another week, abolishing the difference

between OVA-p(GluNAc) and OVA-p(Gal) at day 19 (**Fig. 33C**). All OVA groups resulted in a similar induction of OVA-specific pentamer$^+$ CD8$^+$ T cells, as well as pentamer+ cells that were in an effector state in the LN (**Fig. 33D, E**). However, in the spleen, OVA-p(GluNAc) was more effective at inducing a systemic OVA-specific CD8$^+$ T cell response from a higher fraction of pentamer$^+$ cells and effector pentamer$^+$ cells produced (**Fig. 33F, G**). Overall, OVA-p(GluNAc) generated a more activated (CD44$^+$CD62L$^-$) endogenous CD8$^+$ T cell reservoir in response to the immunization boost in the LN (**Fig. 33H**). This trend was mirrored in the spleen where the OVA-p(GluNAc) was almost significantly higher than with OVA alone (**Fig. 33I**). There was no difference in cytokines produced by endogenous CD8$^+$ T cells (not shown) but in the endogenous CD4$^+$ T cell compartment, highest cytokine production (IFNγ, IL-2, TNFα) was observed with OVA-p(Gal)in the LN (**Fig. 33J**) and spleen (**Fig. 33K**). These data showed that when paired with an adjuvant such as PIC, glycopolymerized antigen can be used to expand a pool of antigen-specific endogenous CD8$^+$ T cells and boost functional effector cells and antibody titers, especially in the spleen.

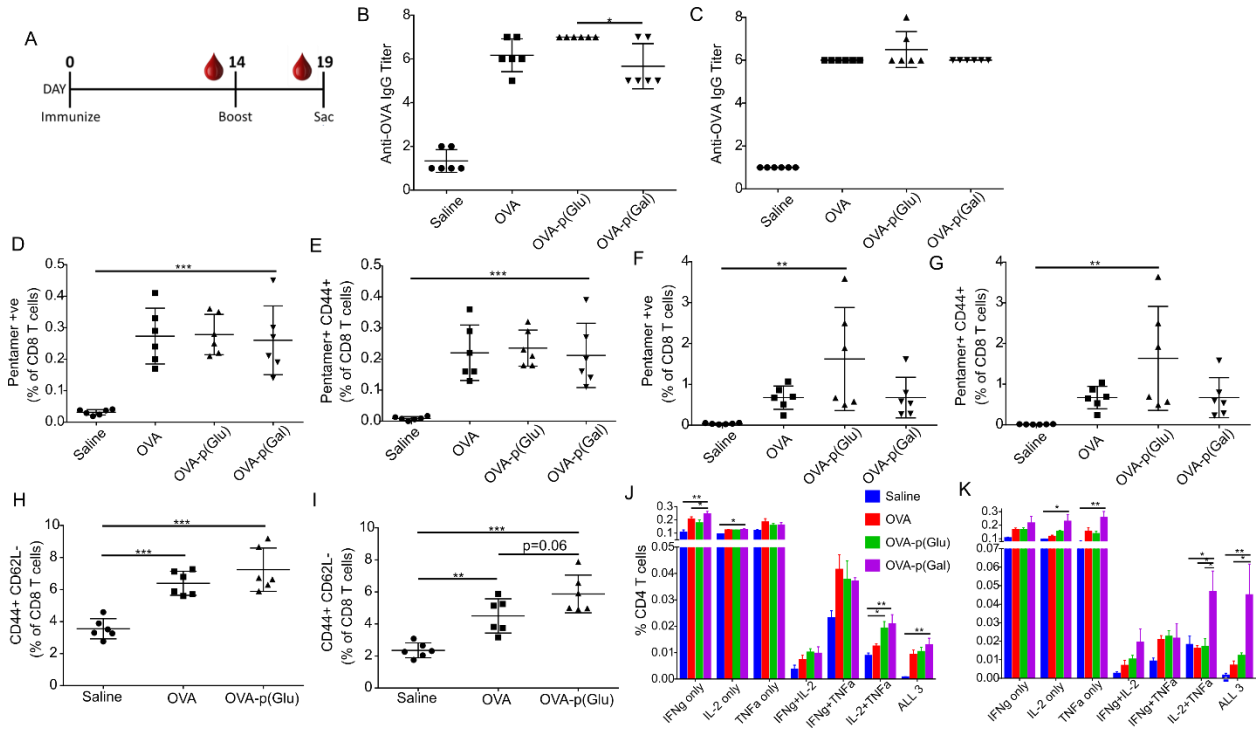

Fig 33. Glyco-conjugated antigen immunized s.c. with poly(I:C) adjuvant leads to more effective endogenous vaccination responses in vivo. (A) Experimental timeline. (B) Anti-OVA IgG titer at day 13. (C) Anti-OVA IgG titer at day 19. (D) LN OVA-specific pentamer$^+$ CD8$^+$ T cells at time of sac on day 19. (E) LN OVA-specific pentamer$^+$ effector CD8$^+$ T cells at day 19. (F) Splenic OVA-specific pentamer$^+$ CD8$^+$ T cells time at day 19. (G) Splenic OVA-specific pentamer$^+$ effector CD8$^+$ T cells at day 19. (H) LN effector CD8$^+$ T cells. (I) Splenic effector CD8$^+$ T cells. (J) Polyfunctional CD4$^+$ T cell response upon restimulation with $OVA_{323-339}$ peptide in the dLNs. (K) Polyfunctional CD4$^+$ T cell response upon restimulation with $OVA_{323-339}$ peptide in the spleen.

Glycopolymerized antigen injected subcutaneously with poly(I:C) adjuvant leads to rapid clearance from the draining lymphatics into systemic circulation

To gain a better understanding of the mechanisms underlying enhanced vaccination responses observed with glycopolymerized immunization with PIC adjuvant, we conducted a biodistribution study where we injected mice s.c. in all hocks with 10 μg each fluorescently labeled (AF647$^+$) OVA construct, unmodified or conjugated, with 10 μg PIC, and evaluated the distribution in various organs 12 h post-immunization. This PIC dose was found to be most effective after the dose optimization studies presented

earlier. The antigen dose was, however, lower than what we injected for in our vaccination studies due to material limitations. OVA delivered in all forms was detected in the LNs at that timepoint, but to a higher extent in the axillary and popliteal LNs that were determined to be the direct draining LNs (dLNs) for future immunization studies (**Fig. 34A**). Substantial fluorescent signal was also detected in the livers injected with the various OVA constructs, and was highest for OVA-p(GluNAc) and lowest for OVA-p(Gal) at the same injected dose (**Fig. 34B**). The OVA constructs had not escaped to other systemic organs such as the heart (**Fig. 34C**), lungs (**Fig. 34D**), spleen (**Fig. 34E**) and kidneys (**Fig. 34F**). Notably, there was no significant difference in LN fluorescence detected across groups but the liver fluorescence was significantly higher for OVA-p(GluNAc) (**Fig. 34G**). This was also the group that had the highest difference in the amount accumulated in the LNs vs that escaped systemically into the liver (**Fig. 34G**). It made sense that OVA-p(GluNAc) would accumulate in the liver after escaping because the glycosylations make it prone to being taken up efficiently by hepatic APCs (*24*). OVA-p(GluNAc) was also detected to significantly high levels in the blood of mice, showing that it had leaked from the skin-draining peripheral lymphatics into the blood before getting preferentially taken up by the liver (**Fig. 34H**). These data also suggest that the addition of the adjuvant can impact the clearance kinetics of the conjugate to promote escape from the lymphatics into the periphery, something that can be leveraged in vaccination (*196*).

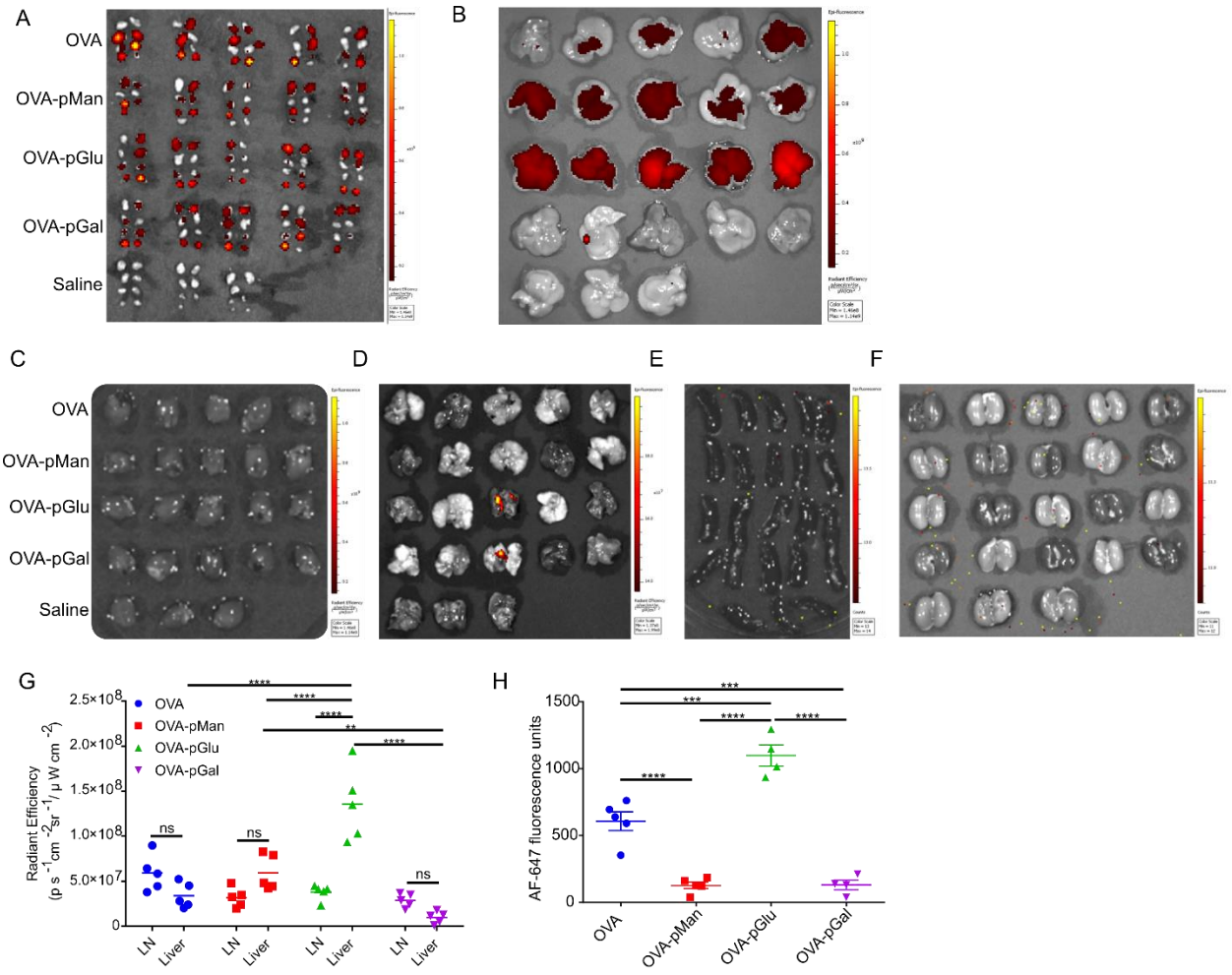

Fig 34. Glyco-conjugated antigen injected s.c. with poly(I:C) adjuvant leads to rapid clearance from the draining lymphatics into systemic circulation. Mice were injected with either 10 µg OVA_{647}, OVA_{647}-p(Man), OVA_{647}-p(GluNAc) or OVA_{647}-p(Gal)with 10 µg PIC, or saline controls, and were sacrificed 12 h later to assess organ biodistribution via IVIS imaging. (A) Average radiant efficiency of dLNs. (B) Average radiant efficiency of livers. (C) Average radiant efficiency of hearts. (D) Average radiant efficiency of lungs. (E) Average radiant efficiency of spleens. (F) Average radiant efficiency of kidneys. (G) Average radiant efficiency quantified across LNs and livers. (H) AF647 fluorescence of blood samples, measured using a plate reader with an excitation wavelength of 630 nm and emission wavelength of 670 nm. Statistical differences were determined by one-way ANOVA using Tukey's post hoc test (*p ≤ 0.05, **p ≤ 0.01, ***p ≤ 0.005).

Discussion

These studies performed in immune-sufficient mice demonstrate that inverse vaccination with glyco-conjugated antigen is capable of inducing a tolerogenic response in the endogenous immune compartment. This effect was seen at both the T cell level

from a suppression in antigen-specific cells and inflammatory cytokine secretion upon restimulation, and at the B cell level from a severe abrogation in antibody production. Antigen-specific antibodies were broadly suppressed in both IgG1 and IgG2 subtypes, indicating that this strategy can be effective in promoting tolerance to both infectious and allergic challenges. It would be of interest to evaluate the impact on antigen-specific IgE antibodies in future studies. The humoral response was increasingly down-regulated over time post-immunization, suggesting that memory B cells were likely affected. Further changes in B cell populations will help answer this question. The induced tolerogenic response was reversed by immunizing with an adjuvant, showing that glyco-conjugated antigen can also be used as an improved antigen delivery method in a vaccination context.

REFERENCES CITED

1. X. Feng, W. Xu, Z. Li, W. Song, J. Ding, X. Chen, Immunomodulatory Nanosystems. *Adv. Sci.* **6** (2019), p. 1900101.

2. A. Y. Peleg, S. Husain, E. J. Kwak, F. P. Silveira, M. Ndirangu, J. Tran, K. A. Shutt, R. Shapiro, N. Thai, K. Abu-Elmagd, K. R. McCurry, A. Marcos, D. L. Paterson, Opportunistic Infections in 547 Organ Transplant Recipients Receiving Alemtuzumab, a Humanized Monoclonal CD-52 Antibody. *Clin. Infect. Dis.* **44**, 204–212 (2007).

3. L. H. Calabrese, N. N. Zein, D. Vassilopoulos, Hepatitis B virus (HBV) reactivation with immunosuppressive therapy in rheumatic diseases: Assessment and preventive strategies. *Ann. Rheum. Dis.* **65** (2006), pp. 983–989.

4. S. D. Miller, D. M. Turley, J. R. Podojil, Antigen-specific tolerance strategies for the prevention and treatment of autoimmune disease. *Nat. Rev. Immunol.* **7** (2007), pp. 665–677.

5. P. Serra, P. Santamaria, Antigen-specific therapeutic approaches for autoimmunity. *Nat. Biotechnol.* **37** (2019), pp. 238–251.

6. E. Feuille, A. Nowak-Wegrzyn, Allergen-specific immunotherapies for food allergy. *Allergy, Asthma Immunol. Res.* **10** (2018), pp. 189–206.

7. X. Han, J. W. Krempski, K. Nadeau, Advances and novel developments in mechanisms of allergic inflammation. *Allergy*. **75**, 3100–3111 (2020).

8. J. M. Carballido, C. Regairaz, C. Rauld, L. Raad, D. Picard, M. Kammüller, The

Emerging Jamboree of Transformative Therapies for Autoimmune Diseases. *Front. Immunol.* **11**, 472 (2020).

9. G. Goel, T. Mayassi, S.-W. Qiao, C. Ciszewski, T. King, A. J. Daveson, J. M. Andrews, J. Krishnarajah, R. Krause, G. J. Brown, R. Fogel, C. F. Barish, R. Epstein, T. Kinney, P. B. Miner, J. A. Tye-Din, A. Girardin, K. Goldstein, J. L. Dzuris, L. J. Williams, R. Xavier, L. M. Sollid, B. Jabri, R. P. Anderson, Sa1396 A Single Intradermal (ID) Injection of Nexvax2®, a Peptide Composition With Dominant Epitopes for Gluten-Reactive CD4+ T Cells, Activates T Cells and Triggers Acute Gastrointestinal Symptoms in HLA-DQ2.5+ People With Celiac Disease (CeD). *Gastroenterology*. **150**, S304 (2016).

10. S. L. Thrower, L. James, W. Hall, K. M. Green, S. Arif, J. S. Allen, C. Van-Krinks, B. Lozanoska-Ochser, L. Marquesini, S. Brown, F. S. Wong, C. M. Dayan, M. Peakman, Proinsulin peptide immunotherapy in type 1 diabetes: Report of a first-in-man Phase I safety study. *Clin. Exp. Immunol.* **155**, 156–165 (2009).

11. H. B. Streeter, R. Rigden, K. F. Martin, N. J. Scolding, D. C. Wraith, Preclinical development and first-in-human study of ATX-MS-1467 for immunotherapy of MS. *Neurol. Neuroimmunol. NeuroInflammation*. **2** (2015), p. e93.

12. T. S. Hong, A. Hu, G. Fahim, E. R. Hermes-DeSantis, Emerging Therapies for Peanut Allergy. *J. Pharm. Pract.*, 089719002097076 (2020).

13. L. Ardouin, H. Luche, R. Chelbi, S. Carpentier, A. Shawket, F. Montanana Sanchis, C. Santa Maria, P. Grenot, Y. Alexandre, C. Grégoire, A. Fries, T. P. Vu Manh, S. Tamoutounour, K. Crozat, E. Tomasello, A. Jorquera, E. Fossum, B.

Bogen, H. Azukizawa, M. Bajenoff, S. Henri, M. Dalod, B. Malissen, Broad and Largely Concordant Molecular Changes Characterize Tolerogenic and Immunogenic Dendritic Cell Maturation in Thymus and Periphery. *Immunity*. **45**, 305–318 (2016).

14. J. S. Lewis, T. D. Zaveri, C. P. Crooks, B. G. Keselowsky, Microparticle surface modifications targeting dendritic cells for non-activating applications. *Biomaterials*. **33**, 7221–7232 (2012).

15. G. Cappellano, A. D. Woldetsadik, E. Orilieri, Y. Shivakumar, M. Rizzi, F. Carniato, C. L. Gigliotti, E. Boggio, N. Clemente, C. Comi, C. Dianzani, R. Boldorini, A. Chiocchetti, F. Renò, U. Dianzani, Subcutaneous inverse vaccination with PLGA particles loaded with a MOG peptide and IL-10 decreases the severity of experimental autoimmune encephalomyelitis. *Vaccine*. **32**, 5681–5689 (2014).

16. R. A. Maldonado, R. A. LaMothe, J. D. Ferrari, A. H. Zhang, R. J. Rossi, P. N. Kolte, A. P. Griset, C. O'Neil, D. H. Altreuter, E. Browning, L. Johnston, O. C. Farokhzad, R. Langer, D. W. Scott, U. H. Von Andrian, T. K. Kishimoto, Polymeric synthetic nanoparticles for the induction of antigen-specific immunological tolerance. *Proc. Natl. Acad. Sci. U. S. A.* **112**, E156–E165 (2015).

17. B. Lepenies, J. Yin, P. H. Seeberger, Applications of synthetic carbohydrates to chemical biology. *Curr. Opin. Chem. Biol.* **14** (2010), pp. 404–411.

18. C. Fasting, C. A. Schalley, M. Weber, O. Seitz, S. Hecht, B. Koksch, J. Dernedde, C. Graf, E. W. Knapp, R. Haag, Multivalency as a chemical organization and action principle. *Angew. Chemie - Int. Ed.* **51** (2012), pp. 10472–10498.

19. J. O. Sestak, B. P. Sullivan, S. Thati, L. Northrup, B. Hartwell, L. Antunez, M. L. Forrest, C. M. Vines, T. J. Siahaan, C. Berkland, Codelivery of antigen and an immune cell adhesion inhibitor is necessary for efficacy of soluble antigen arrays in experimental autoimmune encephalomyelitis. *Mol. Ther. - Methods Clin. Dev.* **1**, 14008 (2014).

20. R. Kikkeri, B. Lepenies, A. Adibekian, P. Laurino, P. H. Seeberger, In vitro imaging and in vivo liver targeting with carbohydrate capped quantum dots. *J. Am. Chem. Soc.* **131**, 2110–2112 (2009).

21. C. A. Aarnoudse, M. Bax, M. Sánchez-Hernández, J. J. García-Vallejo, Y. Van Kooyk, Glycan modification of the tumor antigen gp100 targets DC-SIGN to enhance dendritic cell induced antigen presentation to T cells. *Int. J. Cancer*. **122**, 839–846 (2008).

22. D. R. Getts, A. J. Martin, D. P. Mccarthy, R. L. Terry, Z. N. Hunter, W. T. Yap, M. T. Getts, M. Pleiss, X. Luo, N. J. King, L. D. Shea, S. D. Miller, Microparticles bearing encephalitogenic peptides induce T-cell tolerance and ameliorate experimental autoimmune encephalomyelitis. *Nat. Biotechnol.* **30**, 1217–1224 (2012).

23. L. Tang, J. Yang, W. Liu, X. Tang, J. Chen, D. Zhao, M. Wang, F. Xu, Y. Lu, B. Liu, Q. Sun, L. Zhang, F. He, Liver sinusoidal endothelial cell lectin, LSECtin, negatively regulates hepatic T-cell immune response. *Gastroenterology*. **137**, 1498-508.e1–5 (2009).

24. D. S. Wilson, M. Damo, S. Hirosue, M. M. Raczy, K. Brünggel, G. Diaceri, X.

Quaglia-Thermes, J. A. Hubbell, Synthetically glycosylated antigens induce antigen-specific tolerance and prevent the onset of diabetes. *Nat. Biomed. Eng.* **3**, 817–829 (2019).

25. M. Damo, D. S. Wilson, E. A. Watkins, J. A. Hubbell, Soluble N-Acetylgalactosamine-Modified Antigens Enhance Hepatocyte-Dependent Antigen Cross-Presentation and Result in Antigen-Specific CD8+ T Cell Tolerance Development. *Front. Immunol.* **12**, 1–15 (2021).

26. D. J. Irvine, M. A. Swartz, G. L. Szeto, Engineering synthetic vaccines using cues from natural immunity. *Nat. Mater.* **12**, 978–90 (2013).

27. N. A. Rohner, S. N. Thomas, Flexible Macromolecule versus Rigid Particle Retention in the Injected Skin and Accumulation in Draining Lymph Nodes Are Differentially Influenced by Hydrodynamic Size. *ACS Biomater. Sci. Eng.* **3**, 153–159 (2017).

28. S. Hugues, L. Fetler, L. Bonifaz, J. Helft, F. Amblard, S. Amigorena, Distinct T cell dynamics in lymph nodes during the induction of tolerance and immunity. *Nat. Immunol.* **5**, 1235–1242 (2004).

29. G. Shakhar, R. L. Lindquist, D. Skokos, D. Dudziak, J. H. Huang, M. C. Nussenzweig, M. L. Dustin, Stable T cell-dendritic cell interactions precede the development of both tolerance and immunity in vivo. *Nat. Immunol.* **6**, 707–714 (2005).

30. M. Y. Gerner, P. Torabi-Parizi, R. N. Germain, Strategically localized dendritic cells promote rapid T cell responses to lymph-borne particulate antigens.

Immunity. **42**, 172–85 (2015).

31. C. G. Figdor, Y. Van Kooyk, G. J. Adema, C-type lectin receptors on dendritic cells and langerhans cells. *Nat. Rev. Immunol.* **2** (2002), pp. 77–84.

32. L. B. Rodda, E. Lu, M. L. Bennett, C. L. Sokol, X. Wang, S. A. Luther, B. A. Barres, A. D. Luster, C. J. Ye, J. G. Cyster, Single-Cell RNA Sequencing of Lymph Node Stromal Cells Reveals Niche-Associated Heterogeneity. *Immunity*. **48** (2018), pp. 1014-1028.e6.

33. J. Grabowska, M. A. Lopez-Venegas, A. J. Affandi, J. M. M. den Haan, CD169+ Macrophages Capture and Dendritic Cells Instruct: The Interplay of the Gatekeeper and the General of the Immune System. *Front. Immunol.* **9**, 2472 (2018).

34. M. Baratin, L. Simon, A. Jorquera, C. Ghigo, D. Dembele, J. Nowak, R. Gentek, S. Wienert, F. Klauschen, B. Malissen, M. Dalod, M. Bajénoff, T Cell Zone Resident Macrophages Silently Dispose of Apoptotic Cells in the Lymph Node. *Immunity*. **47**, 349-362.e5 (2017).

35. E. E. Gray, J. G. Cyster, Lymph node macrophages. *J. Innate Immun.* **4** (2012), pp. 424–436.

36. R. S. Allan, J. Waithman, S. Bedoui, C. M. Jones, J. A. Villadangos, Y. Zhan, A. M. Lew, K. Shortman, W. R. Heath, F. R. Carbone, Migratory Dendritic Cells Transfer Antigen to a Lymph Node-Resident Dendritic Cell Population for Efficient CTL Priming. *Immunity*. **25**, 153–162 (2006).

37. B. Li, C. Lu, S. Oveissi, J. Song, K. Xiao, D. Zanker, M. Duan, J. Chen, H. Xu, Q. Zou, C. Wu, J. W. Yewdell, W. Chen, Host CD8α + and CD103 + dendritic cells prime transplant antigen-specific CD8 + T cells via cross-dressing. *Immunol. Cell Biol.* **98**, 563–576 (2020).

38. D. Roggenbuck, M. G. Mytilinaiou, S. V Lapin, D. Reinhold, K. Conrad, Asialoglycoprotein receptor (ASGPR): A peculiar target of liver-specific autoimmunity. *Autoimmun. Highlights*. **3** (2012), pp. 119–125.

39. S. J. Berendam, A. F. Koeppel, N. R. Godfrey, S. J. Rouhani, A. N. Woods, A. B. Rodriguez, J. D. Peske, K. L. Cummings, S. D. Turner, V. H. Engelhard, Comparative Transcriptomic Analysis Identifies a Range of Immunologically Related Functional Elaborations of Lymph Node Associated Lymphatic and Blood Endothelial Cells. *Front. Immunol.* **10**, 816 (2019).

40. L. Bonifaz, D. Bonnyay, K. Mahnke, M. Rivera, M. C. Nussenzweig, R. M. Steinman, Efficient Targeting of Protein Antigen to the Dendritic Cell Receptor DEC-205 in the Steady State Leads to Antigen Presentation on Major Histocompatibility Complex Class I Products and Peripheral CD8+ T Cell Tolerance. *J. Exp. Med.* **196**, 1627–1638 (2002).

41. G. Schreibelt, L. J. J. Klinkenberg, L. J. Cruz, P. J. Tacken, J. Tel, M. Kreutz, G. J. Adema, G. D. Brown, C. G. Figdor, I. J. M. De Vries, The C-type lectin receptor CLEC9A mediates antigen uptake and (cross-)presentation by human blood BDCA3+ myeloid dendritic cells. *Blood*. **119**, 2284–2292 (2012).

42. J.-H. Martens, J. Kzhyshkowska, M. Falkowski-Hansen, K. Schledzewski, A.

Gratchev, U. Mansmann, C. Schmuttermaier, E. Dippel, W. Koenen, F. Riedel, M. Sankala, K. Tryggvason, L. Kobzik, G. Moldenhauer, B. Arnold, S. Goerdt, Differential expression of a gene signature for scavenger/lectin receptors by endothelial cells and macrophages in human lymph node sinuses, the primary sites of regional metastasis. *J. Pathol.* **208**, 574–589 (2006).

43. J. Nadesalingam, A. W. Dodds, K. B. M. Reid, N. Palaniyar, Mannose-Binding Lectin Recognizes Peptidoglycan via the N -Acetyl Glucosamine Moiety, and Inhibits Ligand-Induced Proinflammatory Effect and Promotes Chemokine Production by Macrophages . *J. Immunol.* **175**, 1785–1794 (2005).

44. I. Mondor, M. Baratin, M. Lagueyrie, L. Saro, S. Henri, R. Gentek, D. Suerinck, W. Kastenmuller, J. X. Jiang, M. Bajénoff, Lymphatic Endothelial Cells Are Essential Components of the Subcapsular Sinus Macrophage Niche. *Immunity*. **0** (2019), doi:10.1016/j.immuni.2019.04.002.

45. C. Kurts, R. M. Sutherland, G. Davey, M. Li, A. M. Lew, E. Blanas, F. R. Carbone, J. F. A. P. Miller, W. R. Heath, CD8 T cell ignorance or tolerance to islet antigens depends on antigen dose. *Proc. Natl. Acad. Sci. U. S. A.* **96**, 12703–12707 (1999).

46. S. S. Tay, Y. C. Wong, D. M. McDonald, N. A. W. Wood, B. Roediger, F. Sierro, C. Mcguffog, I. E. Alexander, G. A. Bishop, J. R. Gamble, W. Weninger, G. W. McCaughan, P. Bertolino, D. G. Bowen, Antigen expression level threshold tunes the fate of CD8 T cells during primary hepatic immune responses. *Proc. Natl. Acad. Sci. U. S. A.* **111**, E2540–E2549 (2014).

47. S. E. Henrickson, T. R. Mempel, I. B. Mazo, B. Liu, M. N. Artyomov, H. Zheng, A. Peixoto, M. P. Flynn, B. Senman, T. Junt, H. C. Wong, A. K. Chakraborty, U. H. von Andrian, T cell sensing of antigen dose governs interactive behavior with dendritic cells and sets a threshold for T cell activation. *Nat. Immunol.* **9**, 282–291 (2008).

48. N. Chihara, A. Madi, T. Kondo, H. Zhang, N. Acharya, M. Singer, J. Nyman, N. D. Marjanovic, M. S. Kowalczyk, C. Wang, S. Kurtulus, T. Law, Y. Etminan, J. Nevin, C. D. Buckley, P. R. Burkett, J. D. Buenrostro, O. Rozenblatt-Rosen, A. C. Anderson, A. Regev, V. K. Kuchroo, Induction and transcriptional regulation of the co-inhibitory gene module in T cells. *Nature*. **558**, 454–459 (2018).

49. S. Schülke, Induction of Interleukin-10 Producing Dendritic Cells As a Tool to Suppress Allergen-Specific T Helper 2 Responses. *Front. Immunol.* **9** (2018), doi:10.3389/fimmu.2018.00455.

50. A. Sharma, D. Rudra, Emerging functions of regulatory T cells in tissue homeostasis. *Front. Immunol.* **9**, 1–26 (2018).

51. Q. Han, N. Bagheri, E. M. Bradshaw, D. A. Hafler, D. A. Lauffenburger, J. C. Love, Polyfunctional responses by human T cells result from sequential release of cytokines. *Proc. Natl. Acad. Sci. U. S. A.* **109**, 1607–1612 (2012).

52. P. Johansen, T. Storni, L. Rettig, Z. Qiu, A. Der-Sarkissian, K. a Smith, V. Manolova, K. S. Lang, G. Senti, B. Müllhaupt, T. Gerlach, R. F. Speck, A. Bot, T. M. Kündig, Antigen kinetics determines immune reactivity. *Proc. Natl. Acad. Sci. U. S. A.* **105**, 5189–94 (2008).

53. J. M. Gardner, J. J. DeVoss, R. S. Friedman, D. J. Wong, Y. X. Tan, X. Zhou, K. P. Johannes, M. A. Su, H. Y. Chang, M. F. Krummel, M. S. Anderson, Deletional tolerance mediated by extrathymic aire-expressing cells. *Science (80-.).* **321**, 843–847 (2008).

54. A. Mukhopadhaya, T. Hanafusa, I. Jarchum, Y. G. Chen, Y. Iwai, D. V. Serreze, R. M. Steinman, K. V. Tarbell, T. P. DiLorenzo, Selective delivery of β cell antigen to dendritic cells in vivo leads to deletion and tolerance of autoreactive CD8+ T cells in NOD mice. *Proc. Natl. Acad. Sci. U. S. A.* **105**, 6374–6379 (2008).

55. A. S. Krupnick, X. Lin, W. Li, R. Higashikubo, B. H. Zinselmeyer, H. Hartzler, K. Toth, J. H. Ritter, M. Y. Berezin, S. T. Wang, M. J. Miller, A. E. Gelman, D. Kreisel, Central memory CD8+ T lymphocytes mediate lung allograft acceptance. *J. Clin. Invest.* **124**, 1130–1143 (2014).

56. E. Wherry, T cell exhaustion. *Nat. Immunol.* (2011) (available at http://www.nature.com/ni/journal/v12/n6/abs/ni.2035.html).

57. A. C. Anderson, N. Joller, V. K. Kuchroo, Lag-3, Tim-3, and TIGIT: Co-inhibitory Receptors with Specialized Functions in Immune Regulation. *Immunity*. **44** (2016), pp. 989–1004.

58. E. Picarda, S. Bézie, L. Usero, J. Ossart, M. Besnard, H. Halim, K. Echasserieau, C. Usal, J. Rossjohn, K. Bernardeau, S. Gras, C. Guillonneau, Cross-Reactive Donor-Specific CD8+ Tregs Efficiently Prevent Transplant Rejection. *Cell Rep.* **29**, 4245-4255.e6 (2019).

59. B. Bisikirska, J. Colgan, J. Luban, J. A. Bluestone, K. C. Herold, TCR stimulation

with modified anti-CD3 mAb expands CD8+ T cell population and induces CD8+CD25+ Tregs. *J. Clin. Invest.* **115**, 2904–2913 (2005).

60. B. Beverly, S. mo Kang, M. J. Lenardo, R. H. Schwartz, Reversal of in vitro T cell clonal anergy by IL-2 stimulation. *Int. Immunol.* **4**, 661–671 (1992).

61. M. W. Webb, J. Sun, M. A. Sheard, W. Y. Liu, H. W. Wu, J. R. Jackson, J. Malvar, R. Sposto, D. Daniel, R. C. Seeger, Colony stimulating factor 1 receptor blockade improves the efficacy of chemotherapy against human neuroblastoma in the absence of T lymphocytes. *Int. J. Cancer*. **143**, 1483–1493 (2018).

62. K. Hildner, B. T. Edelson, W. E. Purtha, M. Diamond, H. Matsushita, M. Kohyama, B. Calderon, B. U. Schraml, E. R. Unanue, M. S. Diamond, R. D. Schreiber, T. L. Murphy, K. M. Murphy, Batf3 Deficiency Reveals a Critical Role for CD8 + Dendritic Cells in Cytotoxic T Cell Immunity. *Science (80-.).* **322**, 1097–1100 (2008).

63. J. Verdaguer, D. Schmidt, A. Amrani, B. Anderson, N. Averill, P. Santamaria, Spontaneous autoimmune diabetes in monoclonal T cell nonobese diabetic mice. *J. Exp. Med.* **186**, 1663–1676 (1997).

64. S. M. Lieberman, A. M. Evans, B. Han, T. Takaki, Y. Vinnitskaya, J. A. Caldwell, D. V Serreze, J. Shabanowitz, D. F. Hunt, S. G. Nathenson, P. Santamaria, T. P. DiLorenzo, Identification of the β cell antigen targeted by a prevalent population of pathogenic CD8+ T cells in autoimmune diabetes. *Proc. Natl. Acad. Sci. U. S. A.* **100**, 8384–8388 (2003).

65. S. Tsai, A. Shameli, P. Santamaria, in *Advances in Immunology* (Elsevier Inc.,

2008; http://dx.doi.org/10.1016/S0065-2776(08)00804-3), vol. 100, pp. 79–124.

66. A. Amranl, J. Verdaguer, P. Serra, S. Tafuro, R. Tan, P. Santamaria, Progression of autoimmune diabetes driven by avidity maturation of a T- cell population. *Nature*. **406**, 739–742 (2000).

67. M. Bao, Y. Yang, H.-S. Jun, J.-W. Yoon, Molecular Mechanisms for Gender Differences in Susceptibility to T Cell-Mediated Autoimmune Diabetes in Nonobese Diabetic Mice. *J. Immunol.* **168**, 5369–5375 (2002).

68. D. Daniel, R. G. Gill, N. Schloot, D. Wegmann, Epitope specificity, cytokine production profile and diabetogenic activity of insulin-specific T cell clones isolated from NOD mice. *Eur. J. Immunol.* **25**, 1056–1062 (1995).

69. B. D. Stadinski, L. Zhang, F. Crawford, P. Marrack, G. S. Eisenbarth, J. W. Kappler, Diabetogenic T cells recognize insulin bound to IAg7 in an unexpected, weakly binding register. *Proc. Natl. Acad. Sci. U. S. A.* **107**, 10978–10983 (2010).

70. J. W. McGinty, M. L. Marré, V. Bajzik, J. D. Piganelli, E. A. James, T Cell Epitopes and Post-Translationally Modified Epitopes in Type 1 Diabetes. *Curr. Diab. Rep.* **15** (2015), p. 90.

71. J. Sidney, J. L. Vela, D. Friedrich, R. Kolla, M. von Herrath, J. D. Wesley, A. Sette, Low HLA binding of diabetes-associated CD8+ T-cell epitopes is increased by post translational modifications. *BMC Immunol.* **19**, 12 (2018).

72. J. I. Andorko, K. L. Hess, C. M. Jewell, Harnessing Biomaterials to Engineer the Lymph Node Microenvironment for Immunity or Tolerance. *AAPS J.* **17**, 323–338

(2015).

73. J. a Hubbell, S. N. Thomas, M. a Swartz, Materials engineering for immunomodulation. *Nature*. **462**, 449–60 (2009).

74. H. Liu, K. D. Moynihan, Y. Zheng, G. L. Szeto, A. V. Li, B. Huang, D. S. Van Egeren, C. Park, D. J. Irvine, Structure-based programming of lymph-node targeting in molecular vaccines. *Nature*. **507**, 519–522 (2014).

75. L. Nuhn, N. Vanparijs, A. De Beuckelaer, L. Lybaert, G. Verstraete, K. Deswarte, S. Lienenklaus, N. M. Shukla, A. C. D. Salyer, B. N. Lambrecht, J. Grooten, S. A. David, S. De Koker, B. G. De Geest, pH-degradable imidazoquinoline-ligated nanogels for lymph node-focused immune activation. *Proc. Natl. Acad. Sci. U. S. A.* **113**, 8098–103 (2016).

76. P. Sagoo, N. Ali, G. Garg, F. O. Nestle, R. I. Lechler, G. Lombardi, Human regulatory T cells with alloantigen specificity are more potent inhibitors of alloimmune skin graft damage than polyclonal regulatory T cells. *Sci. Transl. Med.* **3** (2011), doi:10.1126/scitranslmed.3002076.

77. Q. Tang, J. Y. Adams, A. J. Tooley, M. Bi, B. T. Fife, P. Serra, P. Santamaria, R. M. Locksley, M. F. Krummel, J. A. Bluestone, Visualizing regulatory T cell control of autoimmune responses in nonobese diabetic mice. *Nat. Immunol.* **7**, 83–92 (2006).

78. B. Akkaya, Y. Oya, M. Akkaya, J. Al Souz, A. H. Holstein, O. Kamenyeva, J. Kabat, R. Matsumura, D. W. Dorward, D. D. Glass, E. M. Shevach, Regulatory T cells mediate specific suppression by depleting peptide–MHC class II from

dendritic cells. *Nat. Immunol.* **20**, 218–231 (2019).

79. E. Xystrakis, A. S. Dejean, I. Bernard, P. Druet, R. Liblau, D. Gonzalez-Dunia, A. Saoudi, Identification of a novel natural regulatory CD8 T-cell subset and analysis of its mechanism of regulation. *Blood*. **104**, 3294–3301 (2004).

80. S. Sugita, Y. Futagami, S. Horie, M. Mochizuki, Transforming growth factor β-producing Foxp3+CD8+CD25+ T cells induced by iris pigment epithelial cells display regulatory phenotype and acquire regulatory functions. *Exp. Eye Res.* **85**, 626–636 (2007).

81. H.-K. Kang, M. A. Michaels, B. R. Berner, S. K. Datta, Very Low-Dose Tolerance with Nucleosomal Peptides Controls Lupus and Induces Potent Regulatory T Cell Subsets. *J. Immunol.* **174**, 3247–3255 (2005).

82. S. Bézie, I. Anegon, C. Guillonneau, Advances on CD8+ Treg Cells and Their Potential in Transplantation. *Transplantation*. **102** (2018), pp. 1467–1478.

83. C. J. Workman, L. S. Cauley, I.-J. Kim, M. A. Blackman, D. L. Woodland, D. A. A. Vignali, Lymphocyte Activation Gene-3 (CD223) Regulates the Size of the Expanding T Cell Population Following Antigen Activation In Vivo. *J. Immunol.* **172**, 5450–5455 (2004).

84. C. J. Workman, D. A. A. Vignali, Negative Regulation of T Cell Homeostasis by Lymphocyte Activation Gene-3 (CD223). *J. Immunol.* **174**, 688–695 (2005).

85. S. Cemerski, S. Zhao, M. Chenard, J. Laskey, L. Cui, R. Shukla, B. Haines, E. Hsieh, M. Beaumont, J. Mattson, W. Blumenschein, H. Hirsch, L. Fayadat-Dilman,

L. Liang, R. De Waal Malefyt, T cell activation and anti-tumor efficacy of anti-LAG-3 antibodies is independent of LAG-3 – MHCII blocking capacity. *J. Immunother. Cancer*. **3**, P183 (2015).

86. J. Wang, M. F. Sanmamed, I. Datar, T. T. Su, L. Ji, J. Sun, L. Chen, Y. Chen, G. Zhu, W. Yin, L. Zheng, T. Zhou, T. Badri, S. Yao, S. Zhu, A. Boto, M. Sznol, I. Melero, D. A. A. Vignali, K. Schalper, L. Chen, Fibrinogen-like Protein 1 Is a Major Immune Inhibitory Ligand of LAG-3. *Cell*. **176**, 334-347.e12 (2019).

87. D. M. Francis, M. P. Manspeaker, A. Schudel, L. F. Sestito, M. J. O'Melia, H. T. Kissick, B. P. Pollack, E. K. Waller, S. N. Thomas, Blockade of immune checkpoints in lymph nodes through locoregional delivery augments cancer immunotherapy. *Sci. Transl. Med.* **12**, 1–12 (2020).

88. L. Kähäri, R. Fair-Mäkelä, K. Auvinen, P. Rantakari, S. Jalkanen, J. Ivaska, M. Salmi, Transcytosis route mediates rapid delivery of intact antibodies to draining lymph nodes. *J. Clin. Invest.* **129**, 3086–3102 (2019).

89. D. van Dinther, H. Veninga, S. Iborra, E. G. F. Borg, L. Hoogterp, K. Olesek, M. R. Beijer, S. T. T. Schetters, H. Kalay, J. J. Garcia-Vallejo, K. L. Franken, L. B. Cham, K. S. Lang, Y. van Kooyk, D. Sancho, P. R. Crocker, J. M. M. den Haan, Functional CD169 on Macrophages Mediates Interaction with Dendritic Cells for CD8+T Cell Cross-Priming. *Cell Rep.* **22**, 1484–1495 (2018).

90. R. Backer, T. Schwandt, M. Greuter, M. Oosting, F. Jüngerkes, T. Tüting, L. Boon, T. O'Toole, G. Kraal, A. Limmer, J. M. M. Den Haan, Effective collaboration between marginal metallophilic macrophages and CD8+ dendritic cells in the

generation of cytotoxic T cells. *Proc. Natl. Acad. Sci. U. S. A.* **107**, 216–221 (2010).

91. J. Dubrot, F. V Duraes, L. Potin, F. Capotosti, D. Brighouse, T. Suter, S. LeibundGut-Landmann, N. Garbi, W. Reith, M. a Swartz, S. Hugues, Lymph node stromal cells acquire peptide-MHCII complexes from dendritic cells and induce antigen-specific CD4+ T cell tolerance. *J. Exp. Med.* **211**, 1153–66 (2014).

92. M. K. Ruhland, E. W. Roberts, E. Cai, A. M. Mujal, K. Marchuk, C. Beppler, D. Nam, N. K. Serwas, M. Binnewies, M. F. Krummel, Visualizing Synaptic Transfer of Tumor Antigens among Dendritic Cells. *Cancer Cell*. **37**, 786-799.e5 (2020).

93. J. A. Villadangos, P. Schnorrer, Intrinsic and cooperative antigen-presenting functions of dendritic-cell subsets in vivo. *Nat. Rev. Immunol.* **7**, 543–555 (2007).

94. S. Burgdorf, A. Kautz, V. Böhnert, P. a Knolle, C. Kurts, Distinct Pathways of Antigen Uptake. *Science*. **612**, 612–616 (2007).

95. W. R. Heath, G. T. Belz, G. M. N. Behrens, C. M. Smith, S. P. Forehan, I. A. Parish, G. M. Davey, N. S. Wilson, F. R. Carbone, J. A. Villadangos, Cross-presentation, dendritic cell subsets, and the generation of immunity to cellular antigens. *Immunol. Rev.* **199**, 9–26 (2004).

96. D. Dudziak, A. O. Kamphorst, G. F. Heidkamp, V. R. Buchholz, C. Trumpfheller, S. Yamazaki, C. Cheong, K. Liu, H.-W. Lee, C. G. Park, R. M. Steinman, M. C. Nussenzweig, Differential Antigen Processing by Dendritic Cell Subsets in Vivo. *Science (80-.).* **315**, 107–111 (2007).

97. S. Manickasingham, C. Reis e Sousa, Microbial and T Cell-Derived Stimuli Regulate Antigen Presentation by Dendritic Cells In Vivo. *J. Immunol.* **165**, 5027–5034 (2000).

98. E. Segura, A. L. Albiston, I. P. Wicks, S. Y. Chai, J. A. Villadangos, Different cross-presentation pathways in steady-state and inflammatory dendritic cells. *Proc. Natl. Acad. Sci. U. S. A.* **106**, 20377–20381 (2009).

99. S. T. Nizza, J. J. Campbell, CD11b+ migratory dendritic cells mediate CD8 T cell cross-priming and cutaneous imprinting after topical immunization. *PLoS One*. **9**, 1–8 (2014).

100. M. H. Den Brok, C. Büll, M. Wassink, A. M. De Graaf, J. A. Wagenaars, M. Minderman, M. Thakur, S. Amigorena, E. O. Rijke, C. C. Schrier, G. J. Adema, Saponin-based adjuvants induce cross-presentation in dendritic cells by intracellular lipid body formation. *Nat. Commun.* **7** (2016), doi:10.1038/ncomms13324.

101. Y. Chung, J. H. Chang, M. N. Kweon, P. D. Rennert, C. Y. Kang, CD8α-11b+ dendritic cells but not CD8α+ dendritic cells mediate cross-tolerance toward intestinal antigens. *Blood*. **106**, 201–206 (2005).

102. N. S. Wilson, G. M. N. Behrens, R. J. Lundie, C. M. Smith, J. Waithman, L. Young, S. P. Forehan, A. Mount, R. J. Steptoe, K. D. Shortman, T. F. de Koning-Ward, G. T. Belz, F. R. Carbone, B. S. Crabb, W. R. Heath, J. A. Villadangos, Systemic activation of dendritic cells by Toll-like receptor ligands or malaria infection impairs cross-presentation and antiviral immunity. *Nat. Immunol.* **7**, 165–

172 (2006).

103. K. E. Foulds, L. A. Zenewicz, D. J. Shedlock, J. Jiang, A. E. Troy, H. Shen, Cutting Edge: CD4 and CD8 T Cells Are Intrinsically Different in Their Proliferative Responses. *J. Immunol.* **168**, 1528–1532 (2002).

104. H. Rabenstein, A. C. Behrendt, J. W. Ellwart, R. Naumann, M. Horsch, J. Beckers, R. Obst, Differential kinetics of antigen dependency of CD4+ and CD8+ T cells. *J. Immunol.* **192**, 3507–17 (2014).

105. M. Y. Gerner, K. A. Casey, W. Kastenmuller, R. N. Germain, Dendritic cell and antigen dispersal landscapes regulate T cell immunity. *J. Exp. Med.* **214**, 3105–3122 (2017).

106. J. M. Leal, J. Y. Huang, K. Kohli, C. Stoltzfus, M. R. Lyons-Cohen, B. E. Olin, M. Gale, M. Y. Gerner, Innate cell microenvironments in lymph nodes shape the generation of T cell responses during type I inflammation. *Sci. Immunol.* **6**, eabb9435 (2021).

107. L. Rapetti, S. Meunier, C. Pontoux, C. Tanchot, CD4 Help Regulates Expression of Crucial Genes Involved in CD8 T Cell Memory and Sensitivity to Regulatory Elements. *J. Immunol.* **181**, 299–308 (2008).

108. P. Novy, M. Quigley, X. Huang, Y. Yang, CD4 T Cells Are Required for CD8 T Cell Survival during Both Primary and Memory Recall Responses. *J. Immunol.* **179**, 8243–8251 (2007).

109. J. Kim, S. J. Ryu, K. Oh, J. M. Ju, J. Y. Jeon, G. Nam, D. S. Lee, H. R. Kim, J. Y.

Kim, J. Chang, T. Sproule, K. Choi, D. Roopenian, E. Y. Choi, Memory programming in CD8+T-cell differentiation is intrinsic and is not determined by CD4 help. *Nat. Commun.* **6**, 7994 (2015).

110. C. Kurts, F. R. Carbone, M. Barnden, E. Blanas, J. Allison, W. R. Heath, J. F. A. P. Miller, CD4+ T cell help impairs CD8+ T cell deletion induced by cross-presentation of self-antigens and favors autoimmunity. *J. Exp. Med.* **186**, 2057–2062 (1997).

111. J. Steitz, J. Brück, J. Lenz, S. Büchs, T. Tüting, Peripheral CD8+ T cell tolerance against melanocytic self-antigens in the skin is regulated in two steps by CD4+ T cells and local inflammation: Implications for the pathophysiology of vitiligo. *J. Invest. Dermatol.* **124**, 144–150 (2005).

112. Z. Ye, K. A. Ahmed, S. Hao, X. Zhang, Y. Xie, M. A. Munegowda, Q. Meng, R. Chibbar, J. Xiang, Active CD4+ helper T cells directly stimulate CD8+ cytotoxic T lymphocyte responses in wild-type and MHC II gene knockout C57BL/6 mice and transgenic RIP-mOVA mice expressing islet b-cell ovalbumin antigen leading to diabetes. *Autoimmunity*. **41**, 501–511 (2008).

113. S. Ghorashian, P. Veliça, I. Chua, A.-M. McNicol, B. Carpenter, A. Holler, E. Nicholson, M. Ahmadi, M. Zech, S.-A. Xue, W. Uckert, E. Morris, R. Chakraverty, H. J. Stauss, CD8 T Cell Tolerance to a Tumor-Associated Self-Antigen Is Reversed by CD4 T Cells Engineered To Express the Same T Cell Receptor. *J. Immunol.* **194**, 1080–1089 (2015).

114. H. Bashuda, K. Seino, C. Ra, H. Yagita, K. Okumura, Lack of cognate help by

CD4+ T cells and anergy of CD8+ T cells are the principal mechanisms for anti-leukocyte function-associated antigen- 1/intercellular adhesion molecule-1-induced cardiac allograft tolerance. *Transplantation*. **63**, 113–118 (1997).

115. J. T. Harty, V. P. Badovinac, Shaping and reshaping CD8+ T-cell memory. *Nat. Rev. Immunol.* **8**, 107–19 (2008).

116. T. Kurosaki, K. Kometani, W. Ise, Memory B cells. *Nat. Rev. Immunol.* **15**, 149–59 (2015).

117. A. Vatti, D. M. Monsalve, Y. Pacheco, C. Chang, J. M. Anaya, M. E. Gershwin, Original antigenic sin: A comprehensive review. *J. Autoimmun.* **83** (2017), pp. 12–21.

118. S. M. Kaech, W. Cui, Transcriptional control of effector and memory CD8+ T cell differentiation. *Nat. Rev. Immunol.* **12**, 749–761 (2012).

119. J. T. Chang, E. J. Wherry, A. W. Goldrath, Molecular regulation of effector and memory T cell differentiation. *Nat. Immunol.* **15** (2014), pp. 1104–1115.

120. L. Gattinoni, X.-S. Zhong, D. C. Palmer, Y. Ji, C. S. Hinrichs, Z. Yu, C. Wrzesinski, A. Boni, L. Cassard, L. M. Garvin, C. M. Paulos, P. Muranski, N. P. Restifo, Wnt signaling arrests effector T cell differentiation and generates CD8+ memory stem cells. *Nat. Med.* **15**, 808–13 (2009).

121. A. M. Intlekofer, N. Takemoto, E. J. Wherry, S. A. Longworth, J. T. Northrup, V. R. Palanivel, A. C. Mullen, C. R. Gasink, S. M. Kaech, J. D. Miller, L. Gapin, K. Ryan, A. P. Russ, T. Lindsten, J. S. Orange, A. W. Goldrath, R. Ahmed, S. L. Reiner,

Effector and memory CD8+T cell fate coupled by T-bet and eomesodermin. *Nat. Immunol.* **6**, 1236–1244 (2005).

122. N. S. Joshi, W. Cui, C. X. Dominguez, J. H. Chen, T. W. Hand, S. M. Kaech, Increased Numbers of Preexisting Memory CD8 T Cells and Decreased T-bet Expression Can Restrain Terminal Differentiation of Secondary Effector and Memory CD8 T Cells. *J. Immunol.* **187**, 4068–4076 (2011).

123. L. M. McLane, P. P. Banerjee, G. L. Cosma, G. Makedonas, E. J. Wherry, J. S. Orange, M. R. Betts, Differential Localization of T-bet and Eomes in CD8 T Cell Memory Populations. *J. Immunol.* **190**, 3207–3215 (2013).

124. S. M. Kaech, J. T. Tan, E. J. Wherry, B. T. Konieczny, C. D. Surh, R. Ahmed, Selective expression of the interleukin 7 receptor identifies effector CD8 T cells that give rise to long-lived memory cells. *Nat. Immunol.* **4**, 1191–8 (2003).

125. D. Herndler-Brandstetter, H. Ishigame, R. Shinnakasu, V. Plajer, C. Stecher, J. Zhao, M. Lietzenmayer, L. Kroehling, A. Takumi, K. Kometani, T. Inoue, Y. Kluger, S. M. Kaech, T. Kurosaki, T. Okada, R. A. Flavell, KLRG1+Effector CD8+T Cells Lose KLRG1, Differentiate into All Memory T Cell Lineages, and Convey Enhanced Protective Immunity. *Immunity*. **48**, 716-729.e8 (2018).

126. M. Polonsky, J. Rimer, A. Kern-Perets, I. Zaretsky, S. Miller, C. Bornstein, E. David, N. M. Kopelman, G. Stelzer, Z. Porat, B. Chain, N. Friedman, Induction of CD4 T cell memory by local cellular collectivity. *Science (80-.).* **360**, eaaj1853 (2018).

127. B. Youngblood, J. S. Hale, H. T. Kissick, E. Ahn, X. Xu, A. Wieland, K. Araki, E. E.

West, H. E. Ghoneim, Y. Fan, P. Dogra, C. W. Davis, B. T. Konieczny, R. Antia, X. Cheng, R. Ahmed, Effector CD8 T cells dedifferentiate into long-lived memory cells. *Nature*. **552**, 404–409 (2017).

128. R. S. Akondy, M. Fitch, S. Edupuganti, S. Yang, H. T. Kissick, K. W. Li, B. A. Youngblood, H. A. Abdelsamed, D. J. McGuire, K. W. Cohen, G. Alexe, S. Nagar, M. M. McCausland, S. Gupta, P. Tata, W. N. Haining, M. J. McElrath, D. Zhang, B. Hu, W. J. Greenleaf, J. J. Goronzy, M. J. Mulligan, M. Hellerstein, R. Ahmed, Origin and differentiation of human memory CD8 T cells after vaccination. *Nature*. **552**, 362–367 (2017).

129. J. T. Chang, V. R. Palanivel, I. Kinjyo, F. Schambach, A. M. Intlekofer, A. Banerjee, S. A. Longworth, K. E. Vinup, P. Mrass, J. Oliaro, N. Killeen, J. S. Orange, S. M. Russell, W. Weninger, S. L. Reiner, Asymmetric T lymphocyte division in the initiation of adaptive immune responses. *Science (80-.).* **315**, 1687–1691 (2007).

130. M. Borsa, I. Barnstorf, N. S. Baumann, K. Pallmer, A. Yermanos, F. Gräbnitz, N. Barandun, A. Hausmann, I. Sandu, Y. Barral, A. Oxenius, Modulation of asymmetric cell division as a mechanism to boost CD8 + T cell memory. *Sci. Immunol.* **4**, eaav1730 (2019).

131. C. Touvrey, L. Derré, E. Devevre, P. Corthesy, P. Romero, N. Rufer, D. E. Speiser, Dominant human CD8 T cell clonotypes persist simultaneously as memory and effector cells in memory phase. *J. Immunol.* **182**, 6718–26 (2009).

132. D. T. Utzschneider, M. Charmoy, V. Chennupati, L. Pousse, D. P. Ferreira, S.

Calderon-Copete, M. Danilo, F. Alfei, M. Hofmann, D. Wieland, S. Pradervand, R. Thimme, D. Zehn, W. Held, T Cell Factor 1-Expressing Memory-like CD8+ T Cells Sustain the Immune Response to Chronic Viral Infections. *Immunity*. **45**, 415–427 (2016).

133. R. Kratchmarov, A. M. Magun, S. L. Reiner, TCF1 expression marks self-renewing human CD8 + memory T cells. *Blood Adv.* **2**, 1–13 (2018).

134. J. Klarquist, A. Chitrakar, N. D. Pennock, A. M. Kilgore, T. Blain, C. Zheng, T. Danhorn, K. Walton, L. Jiang, J. Sun, C. A. Hunter, A. D'Alessandro, R. M. Kedl, Clonal expansion of vaccine-elicited T cells is independent of aerobic glycolysis. *Sci. Immunol.* **3**, eaas9822 (2018).

135. M. D. Martin, V. P. Badovinac, Defining Memory CD8 T Cell. *Front. Immunol.* **9**, 2692 (2018).

136. S. C. Jameson, D. Masopust, Understanding Subset Diversity in T Cell Memory. *Immunity*. **48** (2018), pp. 214–226.

137. J. M. Schenkel, D. Masopust, Tissue-resident memory T cells. *Immunity*. **41** (2014), pp. 886–897.

138. S. N. Mueller, L. K. Mackay, Tissue-resident memory T cells: Local specialists in immune defence. *Nat. Rev. Immunol.* **16** (2016), pp. 79–89.

139. N. S. Kurd, Z. He, T. L. Louis, J. J. Milner, K. D. Omilusik, W. Jin, M. S. Tsai, C. E. Widjaja, J. N. Kanbar, J. G. Olvera, T. Tysl, L. K. Quezada, B. S. Boland, W. J. Huang, C. Murre, A. W. Goldrath, G. W. Yeo, J. T. Chang, Early precursors and

molecular determinants of tissue-resident memory CD8+ T lymphocytes revealed by single-cell RNA sequencing. *Sci. Immunol.* **5** (2020), doi:10.1126/SCIIMMUNOL.AAZ6894.

140. P. C. Rosato, S. Wijeyesinghe, J. M. Stolley, D. Masopust, Integrating resident memory into T cell differentiation models. *Curr. Opin. Immunol.* **63** (2020), pp. 35–42.

141. S. Ariotti, M. A. Hogenbirk, F. E. Dijkgraaf, L. L. Visser, M. E. Hoekstra, J.-Y. Song, H. Jacobs, J. B. Haanen, T. N. Schumacher, S. Ariotti, J. B. Haanen, T. N. Schumacher, D. Masopust, V. Vezys, E. J. Wherry, D. L. Barber, R. Ahmed, T. Gebhardt, L. M. Wakim, L. Eidsmo, P. C. Reading, W. R. Heath, F. R. Carbone, L. M. Wakim, A. Woodward-Davis, M. J. Bevan, T. Gebhardt, P. G. Whitney, A. Zaid, L. K. Mackay, A. G. Brooks, W. R. Heath, F. R. Carbone, S. N. Mueller, M. Hofmann, H. Pircher, X. Jiang, R. A. Clark, L. Liu, A. J. Wagers, R. C. Fuhlbrigge, T. S. Kupper, H. Shin, A. Iwasaki, S. Ariotti, J. B. Beltman, G. Chodaczek, M. E. Hoekstra, A. E. van Beek, R. Gomez-Eerland, L. Ritsma, J. van Rheenen, A. F. Marée, T. Zal, R. J. de Boer, J. B. Haanen, T. N. Schumacher, N. Çuburu, B. S. Graham, C. B. Buck, R. C. Kines, Y. Y. Pang, P. M. Day, D. R. Lowy, J. T. Schiller, M. Hofmann, A. Oschowitzer, S. R. Kurzhals, C. C. Krüger, H. Pircher, K. E. Mark, A. Wald, A. S. Magaret, S. Selke, L. Olin, M. L. Huang, L. Corey, J. T. Schiffer, L. Abu-Raddad, K. E. Mark, J. Zhu, S. Selke, D. M. Koelle, A. Wald, L. Corey, J. T. Schiffer, L. Corey, J. T. Schiffer, D. Swan, R. Al Sallaq, A. Magaret, C. Johnston, K. E. Mark, S. Selke, N. Ocbamichael, S. Kuntz, J. Zhu, B. Robinson, M. L. Huang, K. R. Jerome, A. Wald, L. Corey, B. Breart, F. Lemaître,

S. Celli, P. Bousso, J. M. Schenkel, K. A. Fraser, V. Vezys, D. Masopust, M. D. Young, M. J. Wakefield, G. K. Smyth, A. Oshlack, N. Yan, Z. J. Chen, A. J. Müller, O. Filipe-Santos, G. Eberl, T. Aebischer, G. F. Späth, P. Bousso, S. G. Hansen, J. C. Ford, M. S. Lewis, A. B. Ventura, C. M. Hughes, L. Coyne-Johnson, N. Whizin, K. Oswald, R. Shoemaker, T. Swanson, A. W. Legasse, M. J. Chiuchiolo, C. L. Parks, M. K. Axthelm, J. A. Nelson, M. A. Jarvis, M. Piatak, J. D. Lifson, L. J. Picker, L. K. Mackay, A. T. Stock, J. Z. Ma, C. M. Jones, S. J. Kent, S. N. Mueller, W. R. Heath, F. R. Carbone, T. Gebhardt, M. D. Robinson, D. J. McCarthy, G. K. Smyth, T cell memory. Skin-resident memory $CD8^+$ T cells trigger a state of tissue-wide pathogen alert. *Science*. **346**, 101–5 (2014).

142. N. Dumauthioz, S. Labiano, P. Romero, Tumor Resident Memory T Cells: New Players in Immune Surveillance and Therapy. *Front. Immunol.* **9**, 2076 (2018).

143. R. Fonseca, L. K. Beura, C. F. Quarnstrom, H. E. Ghoneim, Y. Fan, C. C. Zebley, M. C. Scott, N. J. Fares-Frederickson, S. Wijeyesinghe, E. A. Thompson, H. Borges da Silva, V. Vezys, B. Youngblood, D. Masopust, Developmental plasticity allows outside-in immune responses by resident memory T cells. *Nat. Immunol.*, 1–10 (2020).

144. L. K. Beura, S. Wijeyesinghe, E. A. Thompson, M. G. Macchietto, P. C. Rosato, M. J. Pierson, J. M. Schenkel, J. S. Mitchell, V. Vezys, B. T. Fife, S. Shen, D. Masopust, T Cells in Nonlymphoid Tissues Give Rise to Lymph-Node-Resident Memory T Cells. *Immunity*. **48**, 327-338.e5 (2018).

145. T. M. Olsen, B. C. Stone, V. Chuenchob, S. C. Murphy, Prime-and-Trap Malaria

Vaccination To Generate Protective CD8 + Liver-Resident Memory T Cells. *J. Immunol.*, ji1800740 (2018).

146. N. Çuburu, R. Kim, G. C. Guittard, C. D. Thompson, P. M. Day, D. E. Hamm, Y.-Y. S. Pang, B. S. Graham, D. R. Lowy, J. T. Schiller, A Prime-Pull-Amplify Vaccination Strategy To Maximize Induction of Circulating and Genital-Resident Intraepithelial CD8+ Memory T Cells. *J. Immunol.*, ji1800219 (2019).

147. D. M. Mitchell, E. V Ravkov, M. A. Williams, Distinct roles for IL-2 and IL-15 in the differentiation and survival of CD8+ effector and memory T cells. *J. Immunol.* **184**, 6719–30 (2010).

148. H. A. Abdelsamed, C. C. Zebley, B. Youngblood, Epigenetic maintenance of acquired gene expression programs during memory CD8 T cell homeostasis. *Front. Immunol.* **9** (2018), p. 6.

149. J. P. Snook, C. Kim, M. A. Williams, TCR signal strength controls the differentiation of CD4 + effector and memory T cells. *Sci. Immunol.* **3**, eaas9103 (2018).

150. J. K. Fiege, I. A. Stone, E. J. Fay, M. W. Markman, S. Wijeyesinghe, M. G. Macchietto, S. Shen, D. Masopust, R. A. Langlois, The Impact of TCR Signal Strength on Resident Memory T Cell Formation during Influenza Virus Infection. *J. Immunol.*, ji1900093 (2019).

151. H. H. Tam, M. B. Melo, M. Kang, J. M. Pelet, V. M. Ruda, M. H. Foley, J. K. Hu, S. Kumari, J. Crampton, A. D. Baldeon, R. W. Sanders, J. P. Moore, S. Crotty, R. Langer, D. G. Anderson, A. K. Chakraborty, D. J. Irvine, Sustained antigen

availability during germinal center initiation enhances antibody responses to vaccination. *Proc. Natl. Acad. Sci.* **113**, E6639–E6648 (2016).

152. D. a Blair, D. L. Turner, T. O. Bose, Q.-M. Pham, K. R. Bouchard, K. J. Williams, J. P. McAleer, L. S. Cauley, A. T. Vella, L. Lefrancois, Duration of Antigen Availability Influences the Expansion and Memory Differentiation of T Cells. *J. Immunol.* **187**, 2310–2321 (2011).

153. R. N. Germain, Ligand-dependent regulation of T cell development and activation. *Immunol. Res.* **27** (2003), pp. 277–286.

154. C. M. Card, S. S. Yu, M. a. Swartz, Emerging roles of lymphatic endothelium in regulating adaptive immunity. *J. Clin. Invest.* **124**, 943–952 (2014).

155. G. J. Randolph, S. Ivanov, B. H. Zinselmeyer, J. P. Scallan, *Annu. Rev. Immunol.*, in press, doi:10.1146/annurev-immunol-041015-055354.

156. K. Maisel, M. S. Sasso, L. Potin, M. A. Swartz, Exploiting lymphatic vessels for immunomodulation: Rationale, opportunities, and challenges. *Adv. Drug Deliv. Rev.* **114** (2017), pp. 43–59.

157. E. Brakenhielm, K. Alitalo, Cardiac lymphatics in health and disease. *Nat. Rev. Cardiol.*, 1 (2018).

158. A. Louveau, J. Herz, M. N. Alme, A. F. Salvador, M. Q. Dong, K. E. Viar, S. G. Herod, J. Knopp, J. C. Setliff, A. L. Lupi, S. Da Mesquita, E. L. Frost, A. Gaultier, T. H. Harris, R. Cao, S. Hu, J. R. Lukens, I. Smirnov, C. C. Overall, G. Oliver, J. Kipnis, CNS lymphatic drainage and neuroinflammation are regulated by

meningeal lymphatic vasculature. *Nat. Neurosci.*, 1 (2018).

159. B. A. J. Tamburini, J. M. Finlon, A. E. Gillen, M. S. Kriss, K. A. Riemondy, R. Fu, R. P. Schuyler, J. R. Hesselberth, H. R. Rosen, M. A. Burchill, Chronic Liver Disease in Humans Causes Expansion and Differentiation of Liver Lymphatic Endothelial Cells. *Front. Immunol.* **10**, 1036 (2019).

160. M. a. Swartz, A. W. Lund, Lymphatic and interstitial flow in the tumour microenvironment: linking mechanobiology with immunity. *Nat. Rev. Cancer*. **12**, 210–219 (2012).

161. S. J. Rouhani, J. D. Eccles, P. Riccardi, J. D. Peske, E. F. Tewalt, J. N. Cohen, R. Liblau, T. Mäkinen, V. H. Engelhard, Roles of lymphatic endothelial cells expressing peripheral tissue antigens in CD4 T-cell tolerance induction. *Nat. Commun.* **6**, 6771 (2015).

162. E. D. Reynoso, J.-W. Lee, S. J. Turley*, in *Advances in Experimental Medicine and Biology*, S. P. Schoenberger, P. D. Katsikis, B. Pulendran, Eds. (Springer New York, New York, NY, 2009; http://www.embase.com/search/results?subaction=viewrecord&from=export&id=L354529509%5Cnhttp://sfx.library.uu.nl/utrecht?sid=EMBASE&issn=00652598&id=doi:&atitle=Crossroads+between+Innate+and+Adaptive+Immunity+II:+Preface&stitle=Adv.+Exp.+Med.+Biol.&title=A), vol. 633 of *Advances in Experimental Medicine and Biology*, pp. 113–127.

163. R. Nadafi, C. Gago de Graça, E. D. Keuning, J. J. Koning, S. de Kivit, T. Konijn, S. Henri, J. Borst, R. M. Reijmers, L. G. M. van Baarsen, R. E. Mebius, Lymph

Node Stromal Cells Generate Antigen-Specific Regulatory T Cells and Control Autoreactive T and B Cell Responses. *Cell Rep.* **30**, 4110-4123.e4 (2020).

164. S. Hirosue, E. Vokali, V. R. Raghavan, M. Rincon-Restrepo, A. W. Lund, P. Corthesy-Henrioud, F. Capotosti, C. Halin Winter, S. Hugues, M. A. Swartz, Steady-State Antigen Scavenging, Cross-Presentation, and CD8+ T Cell Priming: A New Role for Lymphatic Endothelial Cells. *J. Immunol.* **192**, 5002–5011 (2014).

165. A. W. Lund, F. V. Duraes, S. Hirosue, V. R. Raghavan, C. Nembrini, S. N. Thomas, A. Issa, S. Hugues, M. A. Swartz, VEGF-C Promotes Immune Tolerance in B16 Melanomas and Cross-Presentation of Tumor Antigen by Lymph Node Lymphatics. *Cell Rep.* **1**, 191–199 (2012).

166. B. A. Tamburini, M. A. Burchill, R. M. Kedl, Antigen capture and archiving by lymphatic endothelial cells following vaccination or viral infection. *Nat. Commun.* **5**, 3989 (2014).

167. R. M. Kedl, R. S. Lindsay, J. M. Finlon, E. D. Lucas, R. S. Friedman, B. A. J. Tamburini, Migratory dendritic cells acquire and present lymphatic endothelial cell-archived antigens during lymph node contraction. *Nat. Commun.* **8**, 2034 (2017).

168. C. V Carman, R. Martinelli, T Lymphocyte–Endothelial Interactions: Emerging Understanding of Trafficking and Antigen-Specific Immunity. *Front. Immunol.* **6** (2015), doi:10.3389/fimmu.2015.00603.

169. J. Dubrot, F. V Duraes, G. Harlé, A. Schlaeppi, D. Brighouse, N. Madelon, C. Göpfert, N. Stokar-Regenscheit, H. Acha-Orbea, W. Reith, M. Gannagé, S.

Hugues, Absence of MHC-II expression by lymph node stromal cells results in autoimmunity. *Life Sci. Alliance*. **1**, e201800164 (2018).

170. D. Malhotra, A. L. Fletcher, J. Astarita, V. Lukacs-Kornek, P. Tayalia, S. F. Gonzalez, K. G. Elpek, S. K. Chang, K. Knoblich, M. E. Hemler, M. B. Brenner, M. C. Carroll, D. J. Mooney, S. J. Turley, Transcriptional profiling of stroma from inflamed and resting lymph nodes defines immunological hallmarks. *Nat. Immunol.* **13**, 499–510 (2012).

171. A. Takeda, M. Hollmén, D. Dermadi, J. Pan, K. F. Brulois, R. Kaukonen, T. Lönnberg, P. Boström, I. Koskivuo, H. Irjala, M. Miyasaka, M. Salmi, E. C. Butcher, S. Jalkanen, Single-Cell Survey of Human Lymphatics Unveils Marked Endothelial Cell Heterogeneity and Mechanisms of Homing for Neutrophils. *Immunity*. **51**, 561-572.e5 (2019).

172. N. Fujimoto, Y. He, M. D'Addio, C. Tacconi, M. Detmar, L. C. Dieterich, Single-cell mapping reveals new markers and functions of lymphatic endothelial cells in lymph nodes. *PLoS Biol.* **18**, e3000704 (2020).

173. M. Xiang, R. A. Grosso, A. Takeda, J. Pan, T. Bekkhus, K. Brulois, D. Dermadi, S. Nordling, M. Vanlandewijck, S. Jalkanen, M. H. Ulvmar, E. C. Butcher, A Single-Cell Transcriptional Roadmap of the Mouse and Human Lymph Node Lymphatic Vasculature. *Front. Cardiovasc. Med.* **7** (2020), doi:10.3389/fcvm.2020.00052.

174. E. D. Lucas, B. A. J. Tamburini, Lymph Node Lymphatic Endothelial Cell Expansion and Contraction and the Programming of the Immune Response. *Front. Immunol.* **10**, 36 (2019).

175. E. Vokali, S. S. Yu, S. Hirosue, M. Rinçon-Restrepo, F. V. Duraes, S. Scherer, P. Corthésy-Henrioud, W. W. Kilarski, A. Mondino, D. Zehn, S. Hugues, M. A. Swartz, Lymphatic endothelial cells prime naïve CD8+ T cells into memory cells under steady-state conditions. *Nat. Commun.* **11**, 538 (2020).

176. T. Hara, S. Shitara, K. Imai, H. Miyachi, S. Kitano, H. Yao, S. Tani-ichi, K. Ikuta, Identification of IL-7–Producing Cells in Primary and Secondary Lymphoid Organs Using IL-7–GFP Knock-In Mice. *J. Immunol.* **189**, 1577–1584 (2012).

177. G. Cui, T. Hara, S. Simmons, K. Wagatsuma, A. Abe, H. Miyachi, S. Kitano, M. Ishii, S. Tani-ichi, K. Ikuta, Characterization of the IL-15 niche in primary and secondary lymphoid organs in vivo. *Proc. Natl. Acad. Sci.* **111**, 1915–1920 (2014).

178. A. Mendoza, V. Fang, C. Chen, M. Serasinghe, A. Verma, J. Muller, V. S. Chaluvadi, M. L. Dustin, T. Hla, O. Elemento, J. E. Chipuk, S. R. Schwab, Lymphatic endothelial S1P promotes mitochondrial function and survival in naive T cells. *Nature*. **546**, 158–161 (2017).

179. D. A. P. Louie, S. Liao, Lymp node subcapsular sinus macrophages as the frontline of lymphatic immune defense. *Front. Immunol.* **10**, 347 (2019).

180. S. Hirosue, J. Dubrot, Modes of Antigen Presentation by Lymph Node Stromal Cells and Their Immunological Implications. *Front. Immunol.* **6** (2015), doi:10.3389/fimmu.2015.00446.

181. D. J. Irvine, M. A. Swartz, G. L. Szeto, Engineering synthetic vaccines using cues from natural immunity. *Nat. Mater.* **12** (2013), pp. 978–990.

182. C. T. Mayer, P. Ghorbani, A. Nandan, M. Dudek, C. Arnold-Schrauf, C. Hesse, L. Berod, P. Stüve, F. Puttur, M. Merad, T. Sparwasser, Selective and efficient generation of functional Batf3-dependent CD103+ dendritic cells from mouse bone marrow. *Blood*. **124**, 3081–91 (2014).

183. R. Bianchi, A. Teijeira, S. T. Proulx, A. J. Christiansen, C. D. Seidel, T. Rülicke, T. Mäkinen, R. Hägerling, C. Halin, M. Detmar, A transgenic Prox1-Cre-tdTomato reporter mouse for lymphatic vessel research. *PLoS One*. **10**, e0122976 (2015).

184. O. J. Harrison, J. L. Linehan, H.-Y. Shih, N. Bouladoux, S.-J. Han, M. Smelkinson, S. K. Sen, A. L. Byrd, M. Enamorado, C. Yao, S. Tamoutounour, F. Van Laethem, C. Hurabielle, N. Collins, A. Paun, R. Salcedo, J. J. O'Shea, Y. Belkaid, Commensal-specific T cell plasticity promotes rapid tissue adaptation to injury. *Science (80-.).* **363**, eaat6280 (2019).

185. S. N. Thomas, J. M. Rutkowski, M. Pasquier, E. L. Kuan, K. Alitalo, G. J. Randolph, M. A. Swartz, Impaired Humoral Immunity and Tolerance in K14-VEGFR-3-Ig Mice That Lack Dermal Lymphatic Drainage. *J. Immunol.* **189**, 2181–2190 (2012).

186. S. Ciré, S. Da Rocha, M. Ferrand, M. K. Collins, A. Galy, In Vivo Gene Delivery to Lymph Node Stromal Cells Leads to Transgene-specific CD8+ T Cell Anergy in Mice. *Mol. Ther.* **24**, 1965–1973 (2016).

187. A. L. Fletcher, V. Lukacs-Kornek, E. D. Reynoso, S. E. Pinner, A. Bellemare-Pelletier, M. S. Curry, A.-R. Collier, R. L. Boyd, S. J. Turley, Lymph node fibroblastic reticular cells directly present peripheral tissue antigen under steady-

state and inflammatory conditions. *J. Exp. Med.* **207**, 689–97 (2010).

188. J. P. Böttcher, O. Schanz, D. Wohlleber, Z. Abdullah, S. Debey-Pascher, A. Staratschek-Jox, B. Höchst, S. Hegenbarth, J. Grell, A. Limmer, I. Atreya, M. F. Neurath, D. H. Busch, E. Schmitt, P. van Endert, W. Kolanus, C. Kurts, J. L. Schultze, L. Diehl, P. A. Knolle, Liver-primed memory T cells generated under noninflammatory conditions provide anti-infectious immunity. *Cell Rep.* **3**, 779–95 (2013).

189. M. L. Miller, C. M. McIntosh, Y. Wang, L. Chen, P. Wang, Y. M. Lei, M. D. Daniels, E. Watkins, C. M. Solano, A. S. Chong, M. L. Alegre, Resilience of T cell-intrinsic dysfunction in transplantation tolerance. *Proc. Natl. Acad. Sci. U. S. A.* **116**, 23682–23690 (2019).

190. B. E. Anderson, P. A. Taylor, J. M. McNiff, D. Jain, A. J. Demetris, A. Panoskaltsis-Mortari, A. Ager, B. R. Blazar, W. D. Shlomchik, M. J. Shlomchik, Effects of donor T-cell trafficking and priming site on graft-versus-host disease induction by naive and memory phenotype CD4 T cells. *Blood*. **111**, 5242–5251 (2008).

191. S. Tsai, A. Shameli, J. Yamanouchi, X. Clemente-Casares, J. Wang, P. Serra, Y. Yang, Z. Medarova, A. Moore, P. Santamaria, Reversal of Autoimmunity by Boosting Memory-like Autoregulatory T Cells. *Immunity*. **32**, 568–580 (2010).

192. D. Homann, L. Teyton, M. B. A. Oldstone, Differential regulation of antiviral T-cell immunity results in stable CD8+ but declining CD4+ T-cell memory. *Nat. Med.* **7**, 913–919 (2001).

193. D. S. Wilson, S. Hirosue, M. M. Raczy, L. Bonilla-Ramirez, L. Jeanbart, R. Wang, M. Kwissa, J. F. Franetich, M. A. S. Broggi, G. Diaceri, X. Quaglia-Thermes, D. Mazier, M. A. Swartz, J. A. Hubbell, Antigens reversibly conjugated to a polymeric glyco-adjuvant induce protective humoral and cellular immunity. *Nat. Mater.* **18**, 175–185 (2019).

194. E. Garrafa, L. Imberti, G. Tiberio, A. Prandini, S. M. Giulini, L. Caimi, Heterogeneous expression of toll-like receptors in lymphatic endothelial cells derived from different tissues. *Immunol. Cell Biol.* **89**, 475–481 (2011).

195. Y. Zhou, M. Guo, X. Wang, J. Li, Y. Wang, L. Ye, M. Dai, L. Zhou, Y. Persidsky, W. Ho, TLR3 activation efficiency by high or low molecular mass poly I:C. *Innate Immun.* **19**, 184–192 (2013).

196. N. K. Mehta, R. V. Pradhan, A. P. Soleimany, K. D. Moynihan, A. M. Rothschilds, N. Momin, K. Rakhra, J. Mata-Fink, S. N. Bhatia, K. D. Wittrup, D. J. Irvine, Pharmacokinetic tuning of protein–antigen fusions enhances the immunogenicity of T-cell vaccines. *Nat. Biomed. Eng.* **4**, 636–648 (2020).